Mode Identification from Combination Frequency Amplitudes in Pulsating White Dwarf Stars

by

Celeste Marie Yeates

A dissertation submitted to the faculty of the University of North Carolina at Chapel Hill in partial fulfillment of the requirements for the degree of Doctor of Philosophy in the Department of Physics & Astronomy.

Chapel Hill

2006

Approved by:

J. Christopher Clemens, Advisor
Bruce W. Carney, Reader
Charles R. Evans, Reader
Christian G. Iliadis, Reader
Robert K. McMahan, Reader
Daniel E. Reichart, Reader

ABSTRACT

Celeste Marie Yeates: Mode Identification from Combination Frequency Amplitudes in Pulsating White Dwarf Stars
(Under the Direction of J. Christopher Clemens)

The lightcurves of variable DA and DB white dwarf stars are usually multi-periodic and non-sinusoidal, so that their Fourier transforms show peaks at eigenfrequencies of the pulsation modes and at sums and differences of these frequencies. These combination frequencies provide extra information about the pulsations, both physical and geometrical, that is lost unless they are analyzed. Several theories provide a context for this analysis by predicting combination frequency amplitudes. In these theories, the combination frequencies arise from nonlinear mixing of oscillation modes in the outer layers of the white dwarf, so their analysis cannot yield direct information on the global structure of the star as eigenmodes provide. However, their sensitivity to mode geometry does make them a useful tool for identifying the spherical degree of the modes that mix to produce them. In this dissertation, we analyze data from eight hot, low-amplitude DAV white dwarfs and measure the amplitudes of combination frequencies present. By comparing these amplitudes to the predictions of the theory of Goldreich and Wu, we have verified that the theory is crudely consistent with the measurements. We have also investigated to what extent the combination frequencies can be used to measure the spherical degree (ℓ) of the modes that produce them. We find that modes with $\ell > 2$ are easily identifiable as high ℓ based on their combination frequencies alone. Distinguishing between $\ell = 1$ and 2 is also possible using harmonics. These results will be useful for conducting seismological analyses of large ensembles of ZZ Ceti stars, such as those being discovered using the Sloan Digital Sky Survey. Because this method relies only on photometry at optical wavelengths, it can be applied to faint stars

using 4 m class telescopes. We present new data from the 4.1 m Southern Astrophysical Research Telescope for the ZZ Ceti star L19-2. We use these data to determine the limits for application of this theory on data from a 4 m class telescope. We also analyze data for the hot, low-amplitude DBV EC 20058-5234 and demonstrate that the theory is applicable to both DAV and DBV white dwarf stars.

Dedicated to: Owen, Hyrum, and Claire

ACKNOWLEDGMENTS

Getting a Ph.D. has turned out to be hard work. I have wanted to give up my pursuit of a Ph.D. in Physics and Astronomy several times in the last six years. Although receiving a Ph.D. was one of my dearest goals, I sometimes lacked the immediate desire and often doubted my abilities. However, around the time of my first written exams (when I was ready to give up), my husband Owen told me that I needed to decide then and there whether or not I wanted to complete my degree — whether this was something that I was willing to put forth all of my effort to finish. I made the decision to continue to the end. Since then, there have been several times when I felt like I could not do it anymore and that my tasks were unachievable. At those times, Owen would remind me of my decision and assure me of my intelligence and capacity to accomplish my tasks. I am certain that without the continual, unwavering support of Owen, I would not have been able to achieve my goal of earning a Ph.D. in Physics and Astronomy. Many people ask me, "How can you be a graduate student and a mother of two children at the same time?" I simply tell them that I have an extremely supportive husband. For these reasons and more, I have dedicated this dissertation to Owen.

However, it is because of my Dad and Mom that I got started on this path to begin with. Setting aside the fact that they helped finance my undergraduate education at BYU, they instilled in me the faith, diligence, and determination necessary to reach this point. My parents taught me values that embrace knowledge as essential for this life. My Dad helped me with my homework and projects throughout high school. He has always been genuinely interested in what I am

studying and always made me feel very smart. While growing up, my Dad provided bookshelves full of interesting books on math, astronomy, airplanes, rockets, missiles, and every other fascinating topic. He taught me that there is nothing wrong with being interested in everything. My Mom is my number-one-fan. She has sacrificed and worked so hard to make sure that I have always had everything I need. She remembers everything I tell her and worries about everything that worries me. She sends me notes several times a week to remind me that she loves me. She is patient, loving, thoughtful, and kind. I am unable to communicate how it feels to know that no matter what, there is at least one person who completely understands me. My parents think I am funny, intelligent, hard working, ...and a bunch of other good qualities. It is good to be loved by them.

My five sisters are my best friends. I can go for a couple of months without talking to them, but then when we talk it is as if no time has passed. My sisters are my connection to the outside (non-academic) world. They have provided a supplement to my non-academic life that would have otherwise suffered without their help.

My thesis advisor, Chris Clemens, is the best advisor I could have picked. He is the most intelligent and motivated scientist I have ever met, but he is also humble, kind, and patient. Chris understands the most difficult concepts and can explain them in ways that I can understand. Even then, he never seems to mind that I ask him to repeat the same concept over and over again. Chris is also an optimist. There were several times when I went into his office with results that I was sure were going to ruin my project, but by the conclusion of our meeting, I would feel refreshed and ready to look at the problem in a new way. He taught me to be the kind of scientist who always questions conclusions and receives satisfaction from considering new ideas and possibilities. Also, I always appreciated having Chris along on observing runs; he made them much more fun with his ability to recite Star Wars from start to finish.

Most importantly, Chris not only advised me in scientific matters, but has given me guidance on parenting, marriage, and spiritual matters, to name a few. He has never complained that I like to work at home as much as possible so that I can be with my children when they need me. In fact, he has gone out of his way to accommodate my schedule and made himself available to meet with me whenever I could. Without Chris's support, I would not have completed my Ph.D. requirements.

While we were observing at SOAR, Kepler Oliveira sat down and patiently and carefully shared with me his wealth of knowledge about data reduction. Then, when I was at home trying to reconstruct the data reductions that he taught me, he patiently responded to all of my many emailed questions and guided me through the difficult process without ever complaining. Kepler probably has no idea how grateful I am for his help.

I would like to acknowledge the help of Dr. Boka Wesley Hadzija, who funds the Linda Dykstra Science Dissertation Fellowship. Additionally, I am grateful to the North Carolina Space Grant Consortium, which funded my research with fellowships for two consecutive summers.

Fellow graduate students are the greatest invention ever. You can rely on them and ask them for help without worrying that they will think you are stupid. I do not think that any of us could survive without each other — I certainly could not have survived without them. First and foremost, I must acknowledge Dr. Susan Thompson. She is my friend and mentor. If ever I run into astronomy problems, I think, "What would Susan do?" Fergal Mullally is another graduate student who is always ready with answers and computer programs when I ask him for help with data reduction, observing, and anything else. Melissa Nysewander, Jane Moran, and I were the only astronomers who came to UNC in August 2000. Not only did we help each other through coursework and exciting adventures in Arizona, they are my resident experts in IRAF, and they always know the answers to my (sometimes-stupid) questions. I am also grateful to Rachel Rosen

and Jennifer Weinberg-Wolf, who have always cheerfully helped me whenever I asked them.

Hyrum and Claire are my two babies that were born while I was a graduate student. They are so fabulous (not to mention strong-willed and determined). They bring the joy and happiness into our home that we need to get through the sometimes-arduous tasks of being graduate students. It is such a relief to have them to love and spend time with as an escape from work. I acknowledge them here as motivation to complete my dissertation as quickly as possible, and I dedicate this work to them.

Finally, I should mention the perpetual support of my Father in Heaven. I have great faith that He helps me daily. Let me give an example. Claire was born in September 2005 (which, in and of itself, was a miraculous experience). By that point, I had completed only two, albeit the largest two, chapters of my dissertation. Then, in little more than one semester, I was able to write four chapters of my dissertation, reduce new data from the SOAR Telescope, adjust to having a newborn baby, adequately take care of my husband and son, and defend my dissertation. Through it all, I was happy and only minimally stressed. I could not have accomplished all this, while remaining the cheerful individual that you know and love today, without Spiritual guidance.

Celeste Marie Yeates

July 6, 2006

CONTENTS

LIST OF TABLES

LIST OF FIGURES

LIST OF ABBREVIATIONS

AAS	American Astronomical Society
AGB	Asymptotic giant branch
BFW95	Brassard et al. (1995)
DAV	Hydrogen atmosphere variable white dwarf star (ZZ Ceti)
DBV	Helium atmosphere variable white dwarf star
DOV	He II atmosphere variable white dwarf star
FT	Fourier transform
H-R	Hertzsprung-Russell
HST	Hubble Space Telescope
PN	Planetary nebula
PNN	Planetary nebula nuclei
PNNV	Planetary nebula nuclei variable star
SDSS	Sloan Digital Sky Survey
S/N	Signal to Noise ratio
SOAR	Southern Astrophysical Research Telescope
UV	Ultraviolet
WET	Whole Earth Telescope

LIST OF SYMBOLS

a_i	Amplitude coefficient for pulsation modes
α_λ	Bolometric correction
$2\beta + \gamma$	Fixed parameterization of the radiative region overlying the convection zone in a white dwarf star
$(\delta f/f)$	Observable flux change in a white dwarf star
$\mathcal{F}$	Term containing the physics of the model of Wu (2001)
$\mathcal{G}$	Geometrical term of the model of Wu (2001)
g	Gravity
k	Radial overtone number
ℓ	Spherical degree associated with the spherical harmonic
m	Azimuthal order associated with the spherical harmonic
N_ℓ^m	Normalization factor of the spherical harmonic
$\langle P \rangle$	Average power over a given region of a Fourier transform
Θ_0	Inclination of a star's pulsation axis to the observer's line of sight
ρ_ℓ^m	Legendre Polynomials
τ_{c_0}	Convective timescale
T_{eff}	Effective temperature
ω_i	Pulsation frequency
ψ_i	Phase for pulsation modes
Y_ℓ^m	Spherical harmonics

Chapter 1

Introduction

Dana Barrett:	*You know, you don't act like a scientist.*
Dr. Peter Venkman:	*They're usually pretty stiff.*
Dana Barrett:	*You're more like a game show host.*
	— Ghostbusters

In 1862, while testing his new telescope on the bright star Sirius, Alvin Graham Clark noticed its dim companion, Sirius B, thereby discovering the first known white dwarf star. Sirius B is an extremely dense object with $R = 0.0084 \pm 0.00025 R_\odot$ ($\sim 0.9 R_\oplus$) and $M = 1.034 \pm 0.026 M_\odot$ (Holberg et al., 1998). The discovery of Sirius B marked the beginning of the study of a fascinating new kind of star. White dwarf stars typically have $\log g \sim 8$ with a narrow mass distribution centered on $\sim 0.56 M_\odot$ (Koester et al., 1979; Bergeron et al., 1992), with the bulk of the mass primarily in the carbon-oxygen core. Due to the high-gravity environment, the heavy elements settle to the center of the star, as confirmed by the purity of the observed atmospheres. In extreme cases, low mass white dwarf stars ($\leq 0.4 M_\odot$) have helium cores and high mass white dwarf stars ($\geq 1.05 M_\odot$) have oxygen-neon cores (Isern et al., 1998). For those white dwarf stars with typical mass, a thin layer of pure helium surrounds the carbon-oxygen core, and, for 75 percent of white dwarf stars, a thinner layer of pure hydrogen surrounds the helium. The exact ratio of carbon to oxygen in the core

is unsettled primarily because of the uncertainties in the rate of the $^{12}C(\alpha,\gamma)^{16}O$ reaction during the asymptotic giant branch (AGB) phase of stellar evolution. A high rate for this nuclear reaction means a greater abundance of oxygen in the center then in the outer layers (Isern et al., 1998).

White dwarf stars are the end-product of all but the most massive stars. As a consequence, understanding the origin and structure of white dwarf stars helps us better understand the preceding stages of stellar evolution for low mass stars (those $\leq 10 \pm 2M_{\odot}$; see Isern et al., 1998). Indeed, white dwarf stars provide a laboratory for understanding much of astrophysics. The compact interiors of these stars supply a testing ground for extreme conditions of temperature and pressure, while their surface temperatures unlock independent scales for the age and history of galaxies.

As white dwarf stars thermally radiate their reservoir of energy into the interstellar medium, they reach a temperature range in which certain conditions trigger driven pulsations from deep within their interiors. These pulsations, which we measure as surface temperature variations, equip us with a means of delving in to the unseen interiors of white dwarf stars, similar to the seismologists who use earthquakes to understand the internal layers of the Earth. This dissertation describes an important step forward for asteroseismologists, presenting a simplified method for identifying individual pulsation modes in these stars that utilizes the size of the nonlinearities present in the lightcurves of pulsating white dwarf stars.

1.1 White Dwarf Stars

White dwarf stars evolve from low mass stars. Theories for the stellar evolution of a main sequence star into a white dwarf star are well known (see Mazzitelli & D'Antona, 1986; D'Antona, 1989; Wood, 1990). In summary, following core H-burning, the star ascends the giant branch, enters the core He-burning phase, and

then the double-shell-burning phase on the AGB. In a process that is not well-understood (Mazzitelli & D'Antona, 1986), the planetary nebula (PN) is formed. The nuclei (central stars) of the planetary nebulae (PNN) are the forerunners of the white dwarf stars. After the nebula has been dispersed, the central star is called a pre-white dwarf star and it descends onto the constant-radius cooling track. Figure 1.1 contains a theoretical H-R Diagram emphasizing the white dwarf cooling track.

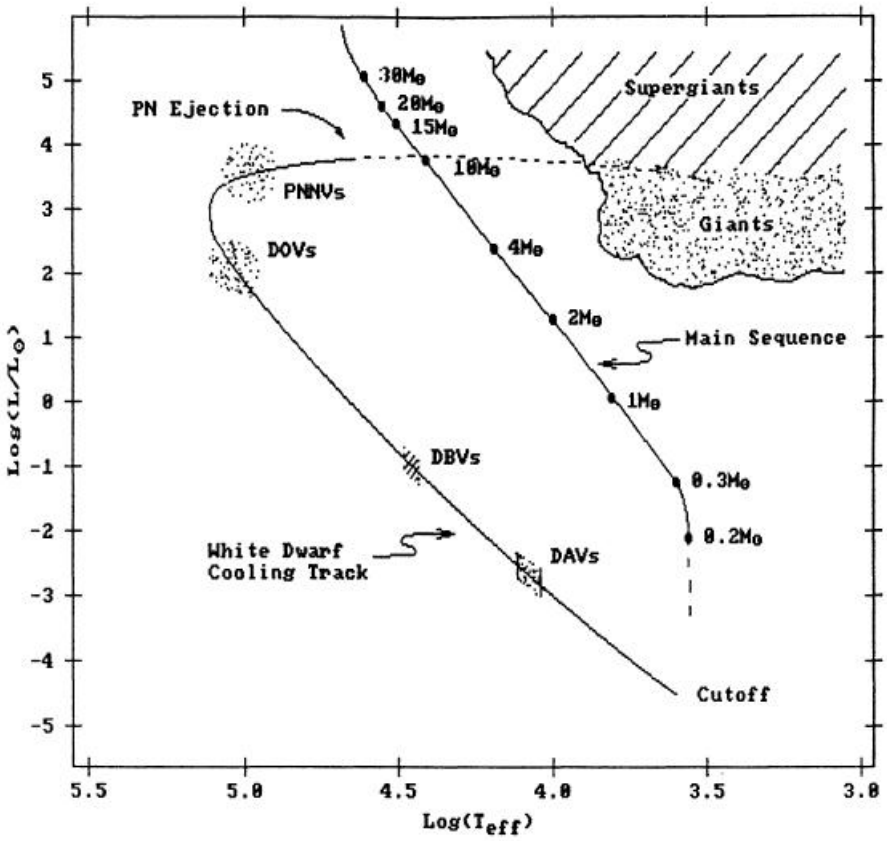

Figure 1.1: Theoretical H-R Diagram emphasizing white dwarf cooling-track. The PNNV and DOV instability strips are possibly joined together into one strip. In this dissertation, we analyze stars within the DBV and DAV instability strips. We reproduce this figure by permission of the Journal of the Royal Astronomical Society of Canada (see Fig. 1 of Wood, 1990).

White dwarf stars fall into several spectroscopic groups, based on the com-

position of the outermost layer. The most common type of white dwarf stars, classified as the DA group, shows only hydrogen lines. The DB group contains white dwarf stars with mainly helium lines and the DO white dwarf stars show strong He II lines. Other less common groups include DQ (with carbon features), DZ (with metal lines), and DC (showing only continuum).

Fowler (1926) used electron degeneracy pressure to explain the high densities in white dwarf stars. Immediately after, Chandrasekhar (1931, 1934a,b) began evaluating stellar structure in white dwarf stars. He calculated gas pressures for electrons at relativistic speeds and thereby determined the exact mass-radius relation for degenerate, relativistic stars, finding a critical mass (the Chandrasekhar limit) for the formation of white dwarf stars. Mestel (1952) proceeded to explain the cooling theory of white dwarf stars and to describe their lifetimes based on the latent heat. At the birth of a white dwarf star, the temperature and pressure in the white dwarf is no longer adequate to produce the energy required for the next phase of thermonuclear reactions. The compact core of the star is degenerate, with electrons providing the pressure support, and is an isothermal reservoir of heat energy that is transferred by conduction. Energetic electrons have a long mean free path because of the filled Fermi sea, providing the high thermal conductivity. Non-degenerate surface layers surround the degenerate core, controlling the outflow of the energy with high opacity. The high opacity results in a lower mean free path for the photons, reducing the energy outflow. The energy transport in the outer layers is dominated by radiation, then by convection resulting from the high opacity introduced by partial ionization regions.

1.1.1 White Dwarf Pulsations

After PNN stars evolve onto the constant-radius cooling track appropriate for their degenerate masses, they become the cool white dwarf stars that we observe (Mazzitelli & D'Antona, 1986). As they do so, they pass through three to four instability strips (see Figure 1.1). Despite the differences in temperature and

surface composition, the pulsation periods and the appearance of the lightcurves of these stars in the separate instability strips are similar. The pulsation periods for these stars range from 100 to 1500 s, with different periods favored depending on temperature. The Planetary Nebula Nuclei variable (PNNV) stars, the first instability region, have spectra dominated by He II and C IV, temperatures greater than 100,000 K, and pulsation periods greater than 1000 s. These pre-white dwarf stars provide the only way to study the production rate of plasmon neutrinos (Winget, 1998). The DOV (pulsating PG 1159) stars have temperatures greater than 100,000 K and have periods ranging from 300 to 850 s. These stars have passed the effective temperature turning point in the H-R Diagram (see Figure 1.1). Vauclair et al. (2002) call DOV stars direct descendants of PNN stars. However, the PNNV and DOV stars are often grouped together since the discovery of the hot pulsating PG 1159 star RXJ 2117.1 + 3412 (Vauclair et al., 1993). The DBV and DAV stars are much cooler than the PNNV and DOV stars and are similar to each other in temperature and mass. The DBV stars have temperatures near 25,000 K and pulsation periods between 100 and 1000 s. The PNNV and DOV stars (Grauer & Bond, 1984) and the DAV stars (Greenstein, 1976, 1982) were noted to contain similar group spectroscopic properties after discovery. However, Winget et al. (1982a) theoretically predicted the existence of pulsating DB stars prior to the discovery of the first DBV GD 358 by Winget et al. (1982b).

Although the DAV stars (also known as ZZ Ceti stars) are a continuous group with no temperature gap, they are subdivided into the HDAV (hot) stars and CDAV (cool) stars centered around 12,000 and 11,000 K. The HDAV pulsation periods are shorter (less than 500 s) than those of CDAV stars (200 to 1500 s). Although the pulsations of the HDAV stars are smaller in amplitude than those of the CDAV stars, the HDAV pulsations are stable in both period and amplitude (Winget & Fontaine, 1982; Clemens, 1994) such that we can measure the change in their period when we monitor the stars over several decades. In this

dissertation, we focus primarily on the HDAV stars because of their pulsation stability. However, the method for mode identification described in this work readily applies to all pulsating white dwarf stars. Indeed, we have applied the method to the DBV EC 20058-5234 in Chapter 5.

The variations we observe arise from the temperature changes associated with non-radial gravity-mode pulsations (Robinson et al., 1982). Theoretical tests performed by Kepler (1984) exclude r-modes (toroidal non-radial pulsations where the Coriolis force is the restoring force) in favor of g-mode pulsations. These g-modes, where gravity is the restoring force, have timescales coincident with the observed periods of pulsating white dwarf stars. The motions are largely horizontal on the surface of the star.

1.1.2 Driving Mechanisms

There are at least two competing views on the theoretical source of the driving mechanisms for pulsating white dwarf stars, most notably the κ-γ mechanism and convection. When astronomers discovered pulsations in white dwarf stars, many theorists determined that the κ-γ mechanism, which drives the radial pulsations of Cepheid variables, can be applied to explain the non-radial pulsations of the DAV and DBV stars (Winget et al., 1981; Dolez & Vauclair, 1981; Dziembowski & Koester, 1981; Winget et al., 1982a). The κ-γ mechanism allows the driving to be caused by the hydrogen (for DAV) and helium (for DBV) partial ionization zones. These theoretical analyses all individually argue that the g-modes can be excited by this κ-γ mechanism.

However, Brickhill (1983) points out that the perturbation to the convective flux is neglected in the theoretical models mentioned above. He writes that neglecting the perturbation to the convective flux inevitably results in strong driving. In the models of Brickhill (1983), the ionization zone only excites pulsations when convection carries most of the flux. Because the time-scale of the convective motions is much less than that of the oscillations, the efficiency of

convection could damp out any excitation due to the κ-γ mechanism. In fact, his models show that many g-mode pulsations will be excited in stars where convection carries all of the flux to the surface. The convection zone is able to adjust instantaneously to the changing thermal structure (the time-scale is approximately one second), more swiftly than the oscillation time-scale (Brickhill, 1990). These driven pulsations are much stronger than those predicted by the κ-γ mechanism when the convective perturbations are included, hence the term "convective driving" (Brickhill, 1991a)[1].

1.1.3 Asteroseismology

Asteroseismology is the study of the interiors of stars using their stellar pulsations. Because of its proximity, helioseismologists have comprehensively examined the oscillations of the Sun for the last fifty years. Christensen-Dalsgaard (2002) describes measurements of the large-scale structure and rotation of the solar interior, which is known to a precision that rivals our knowledge of the interior of the Earth.

Winget (1998) reviews the asteroseismology of white dwarf stars. The "forward technique" of asteroseismology is to perform a normal-mode analysis by matching all observed frequencies to theoretical models for white dwarf interiors and determine which model best fits the observed periods. Instability is believed to be an evolutionary stage for white dwarf stars (cf. Fontaine et al., 1982; Mukadam et al., 2004a). The information gleaned from an asteroseismological analysis of a white dwarf star is therefore applicable to all non-pulsating white dwarf stars with the same mass.

The g-mode pulsation frequencies, ω, of pulsating white dwarf stars satisfy

[1]Pesnell (1987) also recognized that the convection zone had been neglected in the κ-γ mechanism scenario. He introduced a driving mechanism called "convective blocking" as a modification of the ionization driving mechanism. However, Brickhill (1991b) argues that the ZZ Ceti pulsations are much more powerful than the convective blocking scenario allows.

the conditions of the dispersion relation,

$$\omega^2 \ll N^2, L_\ell^2, \tag{1.1}$$

where N is the Brunt-Väisälä frequency and L_ℓ is the Lamb, or acoustic, frequency:

$$N^2 = -g\left[\frac{d\ln\rho}{dr} - \frac{1}{\Gamma_1}\frac{d\ln P}{dr}\right] \tag{1.2}$$

and

$$L_\ell^2 \equiv \frac{\ell(\ell+1)}{r^2}\frac{\Gamma_1 P}{\rho} = \frac{\ell(\ell+1)}{r^2}c_s^2, \tag{1.3}$$

where c_s^2 is the speed of sound. For further description of these frequencies, refer to Winget (1998). Figure 1.2, a propagation diagram, is a plot of N^2 and L_ℓ^2 through the interior of a white dwarf star. The propagation diagram in Figure 1.2 is a theoretical model of a white dwarf star at $T_{eff} = 12,000$ K, as calculated by P. A. Bradley. From the dispersion relation in equation 1.1, we see that the region of propagation for the g-modes in a white dwarf star is under the two solid lines in Figure 1.2. This propagation diagram shows that the pulsations are global oscillations that reveal information about both the surface layers of the star and the deep interiors. Also, Figure 1.2 shows that the periods we should expect from g-mode oscillations range between about 100 and 1000 s.

Using the dispersion relation in equation 1.1, integration over the surface of a white dwarf star yields an expression for g-mode frequencies,

$$\omega_{k,\ell,m} \approx \left\langle \frac{N^2\ell(\ell+1)}{k^2r^2}\right\rangle^{1/2} + \left(1 - \frac{C_k}{\ell(\ell+1)}\right)m\Omega, \tag{1.4}$$

where ℓ and m are the spherical and azimuthal quantum numbers associated with spherical harmonics, k is the radial overtone number, and r is the radius of the star. The second term on the right-hand side of the expression describes the effects of rotation on the g-mode frequencies, namely the non-degeneracy of m

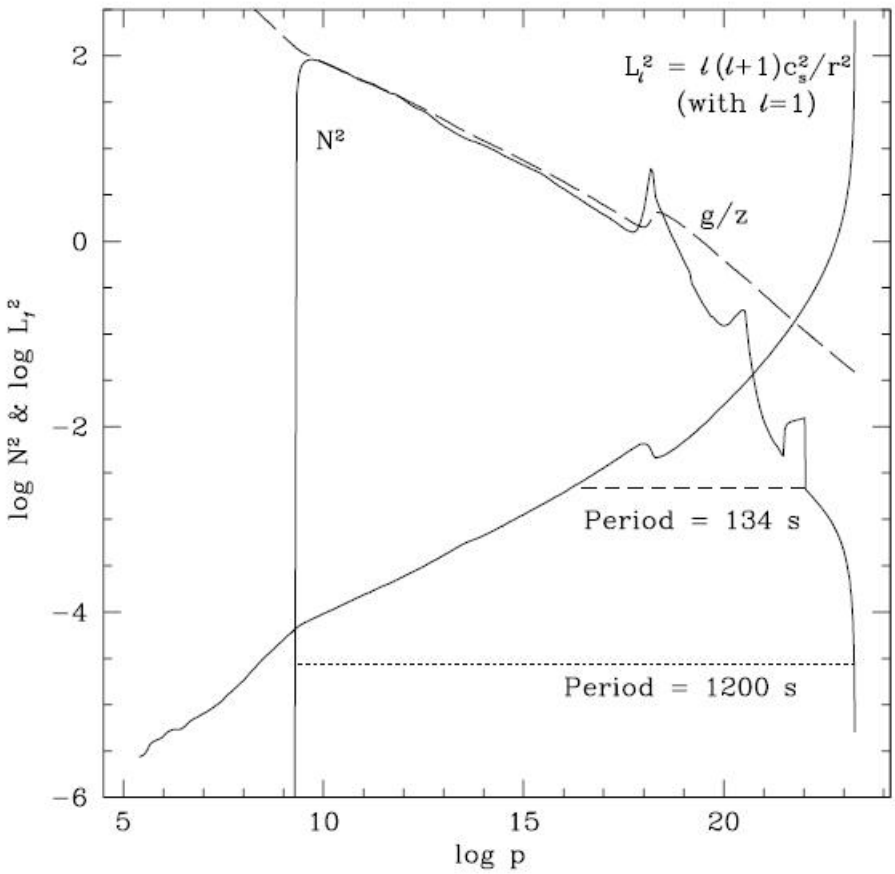

Figure 1.2: Theoretical propagation diagram for white dwarf star with $T_{eff} = 12,000$ K. The solid lines represent the squares of the Brunt-Väisälä frequency, N^2, and the Lamb frequency, L_ℓ^2, in s^{-2}. The horizontal axis is pressure in dynes cm^{-2}, with the center of the star on the right. Gravity modes with frequency ω propagate with periods found in the region below the curves for N^2 and L_ℓ^2. These regions are marked with horizontal dashed lines for two $\ell = 1$ modes with periods of 134 and 1200 s, where $\omega = L_\ell$ and $\omega = N$, respectively. The long-dashed line, $N^2 \sim g/z$, is an analytic approximation of Goldreich & Wu (1999). We reproduce this figure by permission of the American Astronomical Society (AAS) (see Fig. 1 of Goldreich & Wu, 1999).

producing $2\ell+1$ components for each pulsation mode. The term Ω is the rotation frequency and the constant C_k is approximately one in most cases.

For the slow-rotation limit, the case for most white dwarf stars, the first term in equation 1.4 dominates for the frequency. In a compositionally homogenous white dwarf star, we can learn many things about the stellar interior by comparing the observed pulsation properties of the star to the first term in equation 1.4. The spacing of consecutive radial overtone g-modes for a given ℓ is uniform in period, allowing identification of ℓ for each mode. This mean spacing in period also depends on N^2, and therefore gives the mass of the star. Deviations from the mean spacing between modes provide information about "compositional stratification," allowing the measurement of the mass of surface and internal layers of the star.

Identification of k, ℓ, and m for each pulsation mode is essential for asteroseismological analyses of white dwarf stars. Historically, there are very few white dwarf stars with complete seismological studies. Without correct identification of ℓ for pulsation modes, there are too many theoretical models to fit to the observed period spectra of white dwarf stars. Current methods for mode identification require the Hubble Space Telescope (HST) or large optical telescopes like Keck. These methods are extremely expensive and time consuming and work for only a limited number of stars. However, this dissertation provides a fast and inexpensive method for the determination of the ℓ and m of these pulsation modes for large quantities of white dwarf stars.

1.1.4 Nonlinear Pulsations

Linearly independent pulsation modes are an assumption of the asteroseismological models. The DAV and DBV stars have distinctive non-sinusoidal variations at large amplitude, and more linear behavior at small amplitude (McGraw, 1980). Consequently, the Fourier transforms (FTs) of DAV and DBV lightcurves generally show power at harmonics and at sum and difference frequencies. These

"combination frequencies" are not in general the result of independent pulsation eigenmodes, but rather of frequency mixing between eigenmodes in the outermost layers (Brickhill, 1992b; Goldreich & Wu, 1999; Ising & Koester, 2001; Brassard et al., 1995, hereafter BFW95), implying that the assumption of independent modes is not unjustified. At some amplitude, the pulsations will appear non-sinusoidal because of the T^4 dependence of the measured flux. The combination frequencies that we measure in the white dwarf stars are larger than those expected from the T^4 nonlinearity, and require an additional nonlinear process in the surface layers of the white dwarf.

The first attempt to identify the nonlinear process was Brickhill (1983, 1990, 1991a,b, 1992a,b), who explored the time dependent properties of the surface convection zone. Using a numerical model of the surface convection zone, Brickhill (1992a) calculated the first non-sinusoidal theoretical shapes of ZZ Ceti lightcurves. In his model, the nearly isentropic surface convection zone adjusts its entropy on short timescales, attenuating and delaying any flux changes that originate at its base. As the base of the convection zone is heated and it absorbs more energy, it absorbs more mass and consequently grows deeper. At the top of the sinusoidal flux variation, the convection zone is thin. Therefore, the thin convection zone introduces very little delay into the sinusoidal signal. However, at the bottom of the sinusoidal flux variation, the convection zone is cool and deep. The deep convection zone introduces a greater delay at the bottom of the sinusoidal variation as compared with the delay introduced at the top. This causes the flux variation at the surface of the convection zone to have the non-sinusoidal appearance that we observe in the lightcurves of ZZ Ceti stars. This effect is more dramatic as the amplitude of the signal is increased. As the convection zone changes thickness during a single pulsation cycle, the amount of attenuation and delay changes as well, distorting sinusoidal input variations and creating combination frequencies in the Fourier spectrum of the output signal.

Goldreich & Wu (1999) repeated and expanded Brickhill's work using an

analytic approach. Wu (2001) was able to derive approximate expressions for the size of combination frequencies that depend upon the frequency, amplitude, and spherical harmonic indices of the parent modes,[2] and upon the inclination of the star's pulsation axis to our line of sight. Her solutions yield physical insight into the problem, and make predictions for individual stars straightforward to calculate. Wu (2001) herself compared her calculations to measured combination frequencies in the DBV GD 358 and the large-amplitude ZZ Ceti, G29-38, finding good correspondence.

1.2 Mode Identification

In §1.1.3, we discussed that the uniform spacing of consecutive radial overtone g-modes allows identification of ℓ for each mode. This is true only when large numbers of observed modes are available and does not insure that each mode in a pattern of evenly spaced modes is the same ℓ. For stars with few observed modes, the case for many HDAVs, other methods can be applied to the data. The ℓ-identification of single modes requires either using the HST (Robinson et al., 1995) or time-resolved spectroscopy with very large optical telescopes (Clemens et al., 2000). The HST method was pioneered by Robinson et al. (1995) using observations in the UV. The method uses the large limb-darkening in the UV to determine different ℓ values for modes by examining the behavior of amplitude as a function of wavelength. Another method, ensemble asteroseismology (Clemens, 1994), combines modes from many individual HDAVs (correcting for differing mass) to make it look like the mode distribution of one star. Kleinman et al. (1998) (see also Kleinman, 1995) apply this method to the unstable CDAV G29-38, combining modes that appear from season to season to find a large set of modes for seismological analysis.

[2]The spherical harmonics describe the displacements of the atmosphere and the temperature distribution over the stellar surface.

The method for mode identification that we introduce here is based on using the nonlinearities present in the lightcurves. The nonlinearities arise from the mixing of oscillation modes in the outer layers of the white dwarf, so their analysis cannot yield direct information on the global structure of the star as eigenmodes provide. However, their sensitivity to mode geometry does make them a useful tool for identifying the spherical degree of the modes that mix to produce them.

1.2.1 Mode Identification from Combination Frequencies

We commenced this work after noticing a curious difference between two otherwise similar stars, L19-2 and G185-32. Both stars are hot, low-amplitude ZZ Ceti stars with nearly identical effective temperature and mass. They exhibit pulsations at similar periodicities. However, whereas G185-32 has two detected combination frequencies, L19-2 has none. What could cause G185-32 to excite nonlinear pulsations and L19-2 to excite none? Is it a geometrical effect due to the inclination of the star's pulsation axis relative to the observer's line of sight? Alternatively, is there a more interesting cause — are the daughter combination frequencies affected by the ℓ and m spherical harmonic indices of their parent modes? Consequently, can we learn anything interesting about the ℓ and m of the parent modes from their daughter combination frequencies? The answer is a resounding "yes."

Brickhill (1992b) first suggested that a reliable theory that could reproduce combination frequency amplitudes would allow pulsation mode identification based on combination frequency amplitudes alone. The purpose of this work is to test the theory of Wu (2001) as a mode identification method. We will show that the theory of Wu (2001), suitably calibrated, serves as a crude mode identification method that works most of the time. Because this is a simple method requiring straightforward calculations, it can easily be applied to each pulsating white dwarf and depends only upon photometric measurements that are easy to make.

1.2.2 Overview

This work serves as an evaluation of the theory of Wu (2001) as a mode identification method. We provide a detailed explanation of the analytical calculations of Wu (2001) in Chapter 2. We discuss our method for estimating the inclination of the stars' pulsation axes to the observer's line of sight. In Chapters 3 through 5, we have applied this theory to observations of pulsating white dwarf stars. We present the data for each star individually and compare predictions based on Wu's equations with the observed amplitudes.

In Chapter 3, we examine a sample of eight hot, low-amplitude ZZ Ceti stars. Of the stars that we studied, four exhibit detectable combination frequencies: GD 66, GD 244, G117-B15A, and G185-32. The remainder, L19-2, GD 165, R548, and G226-29, do not show combination frequencies. The data that we present in Chapter 3 are a combination of published Fourier spectra, new reductions of archival Whole Earth Telescope (WET) data, and original data obtained with the McDonald Observatory 2.1 m Struve Telescope.

Chapter 4 contains our analysis of new observations of L19-2 with the 4.1 m Southern Astrophysical Research (SOAR) Telescope. The purpose of this chapter is twofold. First, we test our hypothesis that larger telescope data on this star might be useful as a further test of the reliability of the theory of Wu (2001) for mode identification. Second, we gain further observational experience for the author. In this chapter, we present the new L19-2 data and submit our analysis of the pulsation modes.

In Chapter 5, we include an additional analysis of the DBV star EC 20058-5234 to demonstrate that the method is both easy to use and applicable to DBV stars.

Chapter 6 summarizes the results of this analysis and provides directions and motivation for further application. We discuss future application of the technique, emphasizing a prescription for applying the theory of Wu (2001) to large samples of ZZ Ceti stars. We have also provided tabulated matrices of

combination frequency integrals for $\ell \leq 4$ in Appendix A.

As discussed in §1.1.3, pulsation mode identification is integral to asteroseismology. Existing methods of mode identification require time-resolved spectroscopy using either very large optical telescopes or the HST. However, the follow-up photometry of ZZ Ceti candidates from the Sloan Digital Sky Survey (SDSS) is finding large numbers of these pulsators that will be too faint for practical time-resolved spectroscopic methods (see Mukadam et al., 2004b; Mullally et al., 2005). Determining a quick and inexpensive method for confidently assigning values of the spherical degree (ℓ) and azimuthal order (m) to individual eigenfrequencies is therefore a crucial requirement in asteroseismology today. The photometric mode identification method discussed in this dissertation can be quickly applied to large samples of stars and provide the results necessary for asteroseismological analysis.

Chapter 2

Analytical Amplitudes for Combination Frequencies in the Theory of Yanqin Wu

Dr. Peter Venkman: *You're always so concerned about your reputation. Einstein did his best stuff when he was working as a patent clerk!*

Dr. Ray Stantz: *Do you know how much a patent clerk earns?*

— Ghostbusters

2.1 Introduction

There are three known classes of pulsating white dwarf stars in three different instability strips: the pulsating PG 1159 stars at about 100,000 K, the DBV (He I spectrum, variable) stars at 25,000 K, and the DAV (H) stars at 12,000 K.[3] In spite of the differences in temperature and surface composition, the pulsation periods and the appearance of the lightcurves are similar. The DAV and

[3]This chapter is an expanded version of sections 1, 2, and 4 of Yeates et al. (2005) and is reproduced by permission of the AAS.

DBV stars in particular (with periods between 100 and 1000 s), have distinctive non-sinusoidal variations at large amplitude, and more linear behavior at small amplitude (McGraw, 1980). Consequently, the Fourier transforms (FTs) of DAV and DBV lightcurves generally show power at harmonics and at sum and difference frequencies. These "combination frequencies" are not in general the result of independent pulsation eigenmodes, but rather of frequency mixing between eigenmodes (Brickhill, 1992b; Goldreich & Wu, 1999; Ising & Koester, 2001, BFW95). In this chapter, we discuss how the amplitudes of combination frequencies can help identify the spherical harmonic indices of their parent modes.

As discussed in §1.1.1, the variations we observe arise from the temperature changes associated with non-radial gravity-mode pulsations (Robinson et al., 1982). At some amplitude, these pulsations will appear non-sinusoidal because of the T^4 dependence of the measured flux. The combination frequencies that we measure in even low amplitude DAV white dwarfs are larger than those expected from the T^4 nonlinearity, and require an additional nonlinear process in the surface layers of the white dwarf.

The first attempt to identify the nonlinear process was Brickhill (1983, 1990, 1991a,b, 1992a,b), who explored the time dependent properties of the surface convection zone. Using a numerical model of the surface convection zone, Brickhill (1992a) calculated the first non-sinusoidal theoretical shapes of ZZ Ceti lightcurves. In his model, the nearly isentropic surface convection zone adjusts its entropy on short timescales, attenuating and delaying any flux changes that originate at its base. As the convection zone changes thickness during a single pulsation cycle, the amount of attenuation and delay changes as well, distorting sinusoidal input variations and creating combination frequencies in the Fourier spectrum of the output signal.

Goldreich & Wu (1999) repeated and expanded Brickhill's work using an analytic approach. Wu (2001) was able to derive approximate expressions for

the size of combination frequencies that depend upon the frequency, amplitude, and spherical harmonic indices of the parent modes, and upon the inclination of the star's pulsation axis to our line of sight. Her solutions yield physical insight into the problem, and make predictions for individual stars straightforward to calculate. Wu (2001) herself compared her calculations to measured combination frequencies in the DBV GD 358 and the large-amplitude ZZ Ceti, G29-38, finding good correspondence.

Subsequently, Ising & Koester (2001) extended the numerical simulations of lightcurves of Brickhill (1992a,b), showing that for large amplitude pulsations ($\delta P/P > 5\%$) the numerical models must incorporate the time-dependence of quantities that are held constant in the method of Brickhill (e.g., heat capacities). In these full time-dependent calculations, the large amplitude variations begin to show maxima in locations different from those described by the low-order spherical harmonics. However, for the small amplitude variations we consider in this dissertation, this effect is negligible, and the numerical results of Ising & Koester (2001) are in agreement with Brickhill (1992a,b) and Wu (2001).

An entirely different model for explaining combination frequencies was proposed by BFW95. Instead of changes in the convection zone, BFW95 invoke the nonlinear response of the radiative atmosphere, ignoring the changes to the surface convection zone. These radiative nonlinearities can be larger than expected from the T^4 dependence of flux because of the sensitivity of the H absorption lines to temperature. Vuille & Brassard (2000) compared the predictions of this theory to those of Brickhill for the large amplitude pulsator G29-38, and found that the combination frequencies in that star are too large to be explained by the BFW95 theory. This does not necessarily invalidate the theory, but suggests that some other mechanism is at work, at least in G29-38. Vuille & Brassard (2000) left open the question of low amplitude pulsators, which have much smaller combination frequencies. In one case at least (G117-B15A), the BFW95 theory was able to account for the amplitude of the combination frequencies (Brassard et al.,

1993). However, this success relied on an exact match between the spectroscopic temperature of the star and a narrow maximum in the theoretical predictions. Using more recent spectroscopic temperature estimates for G117-B15A, which differ from the old by only 850 K (see Bergeron et al., 2004), the theory underestimates the combination frequency amplitudes by more than an order of magnitude. In general, even for the low amplitude pulsators, the BFW95 theory underestimates the sizes of combination frequencies by an order of magnitude or more.

We begin in §2.2 by summarizing the analytical expressions of Wu (2001) necessary for predicting the amplitudes of combination frequencies. We also discuss our method for estimating the inclination of the stars' pulsation axes to the observer's line of sight, and show that our result is insensitive to error in this estimate. In §2.3, we discuss the sensitivity of this method to errors and provide a prescription for applying the theory of Wu (2001) to large samples of ZZ Ceti stars.

2.2 Theoretical Review

In this section, we will summarize the analytic model of Wu (2001) and explain how we apply her theory, along with an independent estimation of the stellar inclination angle, to predict the amplitudes of combination frequencies. The models of Wu (2001) rely upon an attenuation and a delay of the perturbed flux within the convection zone to produce non-sinusoidal photospheric flux variations. The differential equation describing these effects (Wu, 2001) is:

$$\left(\frac{\delta F}{F}\right)_b = X + \tau_{c_0}[1 + (2\beta + \gamma)X]\frac{dX}{dt}, \tag{2.1}$$

where $(\delta F/F)_b$ is the assumed sinusoidal flux perturbation at the base of the convection zone, $X \equiv (\delta F/F)_{ph}$ is the flux variation at the photosphere and is related to the photometric variations we observe, and τ_{c_0} is the time delay

introduced by the convection zone. Physically it represents the timescale over which the convection zone can absorb a flux change (by adjusting its entropy) instead of communicating it to the surface. In this dissertation, we approximate τ_{c_0} by setting it equal to the longest observed mode period. This is a lower limit, because modes with periods longer than τ_{c_0} cannot be driven, but the longest observed period might not be quite as large as τ_{c_0}. Parameters β and γ are fixed parameterizations of the radiative region overlying the convection zone, and represent an attenuation of the flux. The mixing length models of Wu & Goldreich (1999) yield $\beta \sim 1.2$ and $\gamma \sim -15$ in the temperature range of ZZ Ceti stars (see their Figure 1).

The solution to equation 2.1 represents the detectable flux variation at the photosphere, and has the assumed form:

$$\begin{aligned}\left(\frac{\delta F}{F}\right)_{ph} &= a_i \cos(\omega_i t + \psi_i) + a_{2i} \cos(2\omega_i t + \psi_{2i}) \\ &+ a_j \cos(\omega_j t + \psi_j) + a_{2j} \cos(2\omega_j t + \psi_{2j}) \\ &+ a_{i-j} \cos[(\omega_i - \omega_j)t + \psi_{i-j}] \\ &+ a_{i+j} \cos[(\omega_i + \omega_j)t + \psi_{i+j}] + ... \end{aligned} \tag{2.2}$$

Solving equation 2.1 yields expressions for the amplitude coefficients ($a_{i\pm j}$) and the phases ($\psi_{i\pm j}$) at each combination frequency ($\omega_i \pm \omega_j$). In this dissertation we do not consider phases because they are impossible to recover from some of the published data, and difficult to measure in the presence of noise. Thus, we focus on the amplitudes represented by:

$$a_{i\pm j} = \frac{n_{ij}}{2} \frac{a_i a_j}{2} \frac{\mid 2\beta + \gamma \mid (\omega_i \pm \omega_j)\tau_{c_0}}{\sqrt{1 + [(\omega_i \pm \omega_j)\tau_{c_0}]^2}}, \tag{2.3}$$

where $n_{ij} = 2$ for $i \neq j$ and 1 otherwise.

These $a_{i\pm j}$ represent total flux amplitudes for the combination frequencies and are given in terms of the total flux amplitudes of the parent modes (a_i,

a_j). Because we measure an integrated flux in a restricted wavelength range, these amplitudes are not analogous to the ones we measure. However, they can be transformed into quantities like those we measure by integrating over the appropriate spherical harmonic viewed at some inclination (Θ_0) in the presence of an Eddington limb-darkening law, and then applying a bolometric correction (α_λ) appropriate for the detector and filter combination.

Calculating the integrated amplitude requires an expression for the flux in the presence of limb darkening. For a parent mode, which is assumed to have the angular dependence of a spherical harmonic, Wu (2001) gives:

$$g_\ell^m(\Theta_0) \equiv \frac{1}{2\pi} \oint_0^{2\pi} d\phi \int_{\pi/2}^{0} Re[Y_\ell^m(\Theta, \Phi)] \left(1 + \frac{3}{2}\cos(\theta)\right) \cos(\theta) d\cos(\theta), \quad (2.4)$$

where (θ, ϕ) are in the coordinate system defined by the observer's line of sight, and (Θ, Φ) are aligned to the pulsation axis of the star. These two coordinate systems are separated by the angle Θ_0, which is the inclination of the star. Evaluating this integral requires estimating this inclination, and applying the appropriate coordinate transformation (see Appendix A of Wu (2001)).

For the combination frequencies, the integrated flux depends on the product of the spherical harmonics of the parent modes:

$$G_{\ell_i\ \ell_j}^{m_i \pm m_j}(\Theta_0) \equiv \frac{N_{\ell_i}^{m_i} N_{\ell_j}^{m_j}}{2\pi} \oint_0^{2\pi} d\phi \int_{\pi/2}^{0} \rho_{\ell_i}^{m_i}(\Theta) \rho_{\ell_j}^{m_j}(\Theta) \cos\left((m_i \pm m_j)\Phi\right) \times \left(1 + \frac{3}{2}\cos(\theta)\right) \cos(\theta) d\cos(\theta), \quad (2.5)$$

where the $\rho_\ell^m(\Theta)$ are Legendre Polynomials, and the N_ℓ^m are the normalization factors for the parent mode spherical harmonics. Our expression differs from that of Wu (2001) slightly, in that we explicitly retain these normalization factors.

The bolometric correction is simpler, since it is only a numeric factor expressing the ratio of the amplitudes measured by the detector to the bolometric

variations given by the theory. We calculated this factor using model atmospheres of different temperatures provided by D. Koester (discussed in Finley et al., 1997). The observations we analyze in the following chapters are either white light measurement using a bi-alkali photocathode or CCD measurements with a red cutoff filter (BG40). We applied the known sensitivity curves of these systems and the UV cutoff of the Earth's atmosphere to the model spectra. In Figure 2.1, we show the sensitivity of α_λ to stellar T_{eff} and $\log g$ values and to the assumed ℓ value of the pulsation modes for the bi-alkali photocathode detector.[4] The bolometric correction is approximately constant over the ranges of T_{eff} and $\log g$ that we consider (i.e., in the instability strip). Because of the wavelength dependence of limb darkening these corrections depend upon the value of ℓ assumed for the modes, but this dependence is weak at optical wavelengths for low ℓ. The correction is roughly constant for low ℓ ($\ell \leq 2$), but decreases by approximately a factor of 2 for $\ell = 3$.

The sample of stars we consider in Chapter 3 are centered on $T_{eff} = 12,000$ K and their $\log g$ range between ~ 8.00 and 8.25. We averaged the bolometric correction that we calculated for these values of $\log g$ at 12,000 K and found $\alpha_\lambda = 0.46$ and 0.42 for the bi-alkali photocathode and CCD, respectively. Our values are calculated assuming $\ell = 1$. They are so close to the value that Wu (2001) used (0.4) that we have decided to retain her value of 0.4 to make our results directly comparable to hers.

Now we can write the observable flux change at the photosphere in terms of

$$\left(\frac{\delta f}{f}\right)_i = \alpha_\lambda a_i g_{\ell_i}^{m_i}(\Theta_0) \tag{2.6}$$

$$\left(\frac{\delta f}{f}\right)_{i\pm j} = \alpha_\lambda a_{i\pm j} G_{\ell_i\ \ell_j}^{m_i \pm m_j}(\Theta_0) \tag{2.7}$$

[4]The plot of the CCD plus filter bolometric correction is nearly identical to the bi-alkali plot, with a slight downward shift.

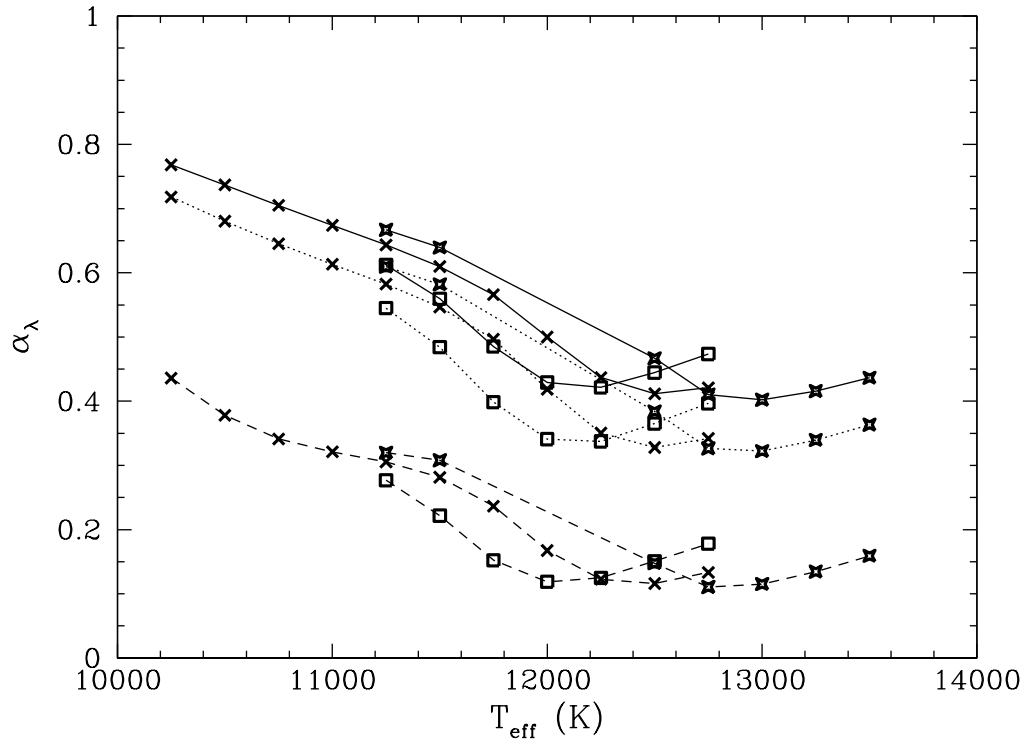

Figure 2.1: Bolometric correction as a function of T_{eff}, $\log g$, and ℓ for bi-alkali photocathode. Each data point represents a discrete value of $\log g$ and the ℓ assumed for the modes. The stars represent $\log g = 8.50$, the crosses represent $\log g = 8.25$, and the open squares represent $\log g = 8.00$. Each of these groups of stars, crosses, and open squares are connected point-to-point by a line representing ℓ. The solid lines are $\ell = 1$, the dotted lines are $\ell = 2$, and the dashed lines are $\ell = 3$. The plot of the CCD plus filter bolometric correction is nearly identical to the bi-alkali plot, with a slight downward shift.

so the predicted combination amplitude is:

$$\left(\frac{\delta f}{f}\right)_{i\pm j} = \frac{n_{ij}}{2}\frac{\left(\frac{\delta f}{f}\right)_i\left(\frac{\delta f}{f}\right)_j}{2\alpha_\lambda}\frac{\mid 2\beta+\gamma \mid (\omega_i \pm \omega_j)\tau_{c0}}{\sqrt{1+[(\omega_i \pm \omega_j)\tau_{c0}]^2}}\frac{G_{\ell_i\ \ell_j}^{m_i \pm m_j}(\Theta_0)}{g_{\ell_i}^{m_i}(\Theta_0)g_{\ell_j}^{m_j}(\Theta_0)}. \tag{2.8}$$

Equation 2.8 is the expression we use to calculate the predicted combination frequency amplitudes for various assumptions of ℓ and m for the parent modes.

We reiterate that the bolometric corrections of the two parent modes are really only equal if they are modes of the same ℓ. Moreover, the value for α_λ for the combination frequency amplitude in equation 2.7 will be a linear combination

of the bolometric corrections of the two parent modes. Consequently, the $1/\alpha_\lambda$ dependence of $(\delta f/f)_{i\pm j}$ in equation 2.8 (and of R_c in equation 2.9) is only an approximation.

In addition to α_λ, calculating a prediction for the combination frequency amplitudes requires six additional quantities, $(\delta f/f)_i$, ω_i, β, γ, τ_{c_0}, and Θ_0. The first two are the parent mode amplitude and frequency measured from the FT, β and γ are theoretical atmospheric parameters defined by Wu (2001), and τ_{c_0} is the convective timescale estimated from the longest period mode. The final quantity, Θ_0, is the inclination, which we discuss later.

Physically, it is useful to rearrange equation 2.8 into the form:

$$\begin{aligned} R_c &\equiv \frac{\left(\frac{\delta f}{f}\right)_{i\pm j}}{n_{ij}\left(\frac{\delta f}{f}\right)_i\left(\frac{\delta f}{f}\right)_j} \\ &= \left[\frac{\mid 2\beta+\gamma \mid (\omega_i \pm \omega_j)\tau_{c_0}}{4\alpha_\lambda\sqrt{1+[(\omega_i \pm \omega_j)\tau_{c_0}]^2}}\right]\frac{G_{\ell_i\ \ell_j}^{m_i\pm m_j}(\Theta_0)}{g_{\ell_i}^{m_i}(\Theta_0)g_{\ell_j}^{m_j}(\Theta_0)} \\ &= F(\omega_i,\omega_j,\tau_{c_0},2\beta+\gamma)\frac{G_{\ell_i\ \ell_j}^{m_i\pm m_j}(\Theta_0)}{g_{\ell_i}^{m_i}(\Theta_0)g_{\ell_j}^{m_j}(\Theta_0)} \\ &= \mathcal{F}\ \mathcal{G}. \end{aligned} \tag{2.9}$$

The ratio R_c is a dimensionless ratio between the combination frequency and the product of its parents, as introduced by van Kerkwijk et al. (2000). It is instructive to consider the two terms on the right hand side of equation 2.9 separately. The first term ($\mathcal{F}$) incorporates the physics particular to this model, i.e., the thermal properties of the convection zone, while the second term ($\mathcal{G}$) is geometric, and will be present in any theory that accounts for combination frequencies using nonlinear mixing. In the theory of Wu (2001), the ℓ and m dependence is entirely contained within this geometric term (except for the ℓ dependence of the bolometric correction discussed before). Thus mode identification is possible

if changes in $\mathcal{G}$ with ℓ are large compared to the natural variations in $\mathcal{F}$.

In this respect, the theory of Wu (2001) is promising. For any individual star with multiple pulsation modes, the only parameter in $\mathcal{F}$ that changes from one mode to another is ω. Moreover, the functional dependence on ω is such that for typical ZZ Ceti *sum* frequencies the variations in $\mathcal{F}$ are so small that $\mathcal{F} \sim$ constant (see Figure 2.2). The same is not true for difference frequencies, which lie at low frequencies and are therefore suppressed. For comparison between modes in two different stars, the other parameters in $\mathcal{F}$ change slowly, so that small adjustments to $\mathcal{F}$ should be able to reproduce a variety of stars with similar temperature and mean pulsation period, such as the ensemble we consider in this chapter.

The theory of BFW95 can be expressed in the same form as equation 2.9 by replacing $\mathcal{F}$ with their tabulated atmospheric model parameters. However the BFW95 $\mathcal{F}$ is independent of pulsation frequency for different modes in any single star, so low frequency difference modes are not suppressed. For comparisons between modes in different stars, the BFW95 theory is radically different from that of Wu (2001). The BFW95 $\mathcal{F}$ term, which is normally an order of magnitude smaller than in the Wu (2001) theory, grows to comparable size for a narrow range of temperature that depends sensitively on stellar mass. Thus the expectation of the BFW95 theory is that combination frequencies in *most* ZZ Ceti stars will be smaller than in the theory of Wu (2001) (for the same ℓ). Moreover, the temperature sensitivity of $\mathcal{F}$ makes mode identification more problematic if the BFW95 theory is correct. Without very precise temperature measurements, it is impossible to distinguish between large differences in $\mathcal{F}$ arising from temperature differences, and large changes in $\mathcal{G}$, the geometric term, arising from differences in ℓ or Θ_0.

For either theory, the calculation of $\mathcal{G}$ in equation 2.9 requires assigning a value to the inclination of the pulsation axis to our line of sight. Following Pesnell (1985), we can estimate the inclination for each star by comparing finely split

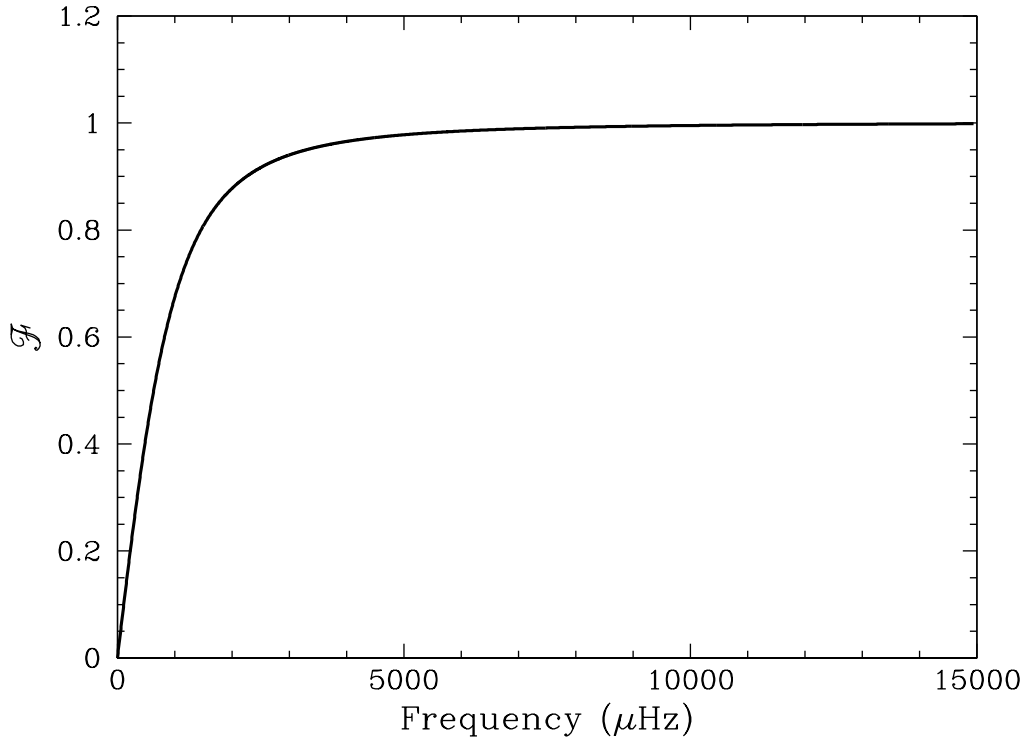

Figure 2.2: Typical $\mathcal{F}$ dependence on frequency, normalized to one. $\mathcal{F}$ incorporates the physics of the model of Wu (2001) (see equation 2.9). For a given star, it is only dependent on the frequency of the combination or harmonic. The only parameter in $\mathcal{F}$ whose value varies across stars is τ_{c_0}, which affects the location of the low frequency roll-off. The other component of R_c, $\mathcal{G}$, depends upon ℓ, m, and Θ_0 (see Figure 2.3).

modes of different m. This requires that we make potentially dubious assumptions about the relative intrinsic sizes of pulsation modes, but the final result is not very sensitive to the assumptions. Figures 2.3 and 2.4 show why. Figure 2.3 shows the dependence of the geometric factor on inclination for $m = 0$ modes. It varies very slowly over a large range, and then changes rapidly when we look directly down upon a nodal line. For $\ell = 1$, this occurs near $\Theta_0 = 90°$, because the parent modes are totally geometrically cancelled and the combination frequencies are not. However, the apparent size of these modes, as opposed to the ratio of their sizes, diminishes rapidly near 90°, and they eventually fall below the noise threshold of the FT. At the same viewing angle, if any $m \neq 0$ modes

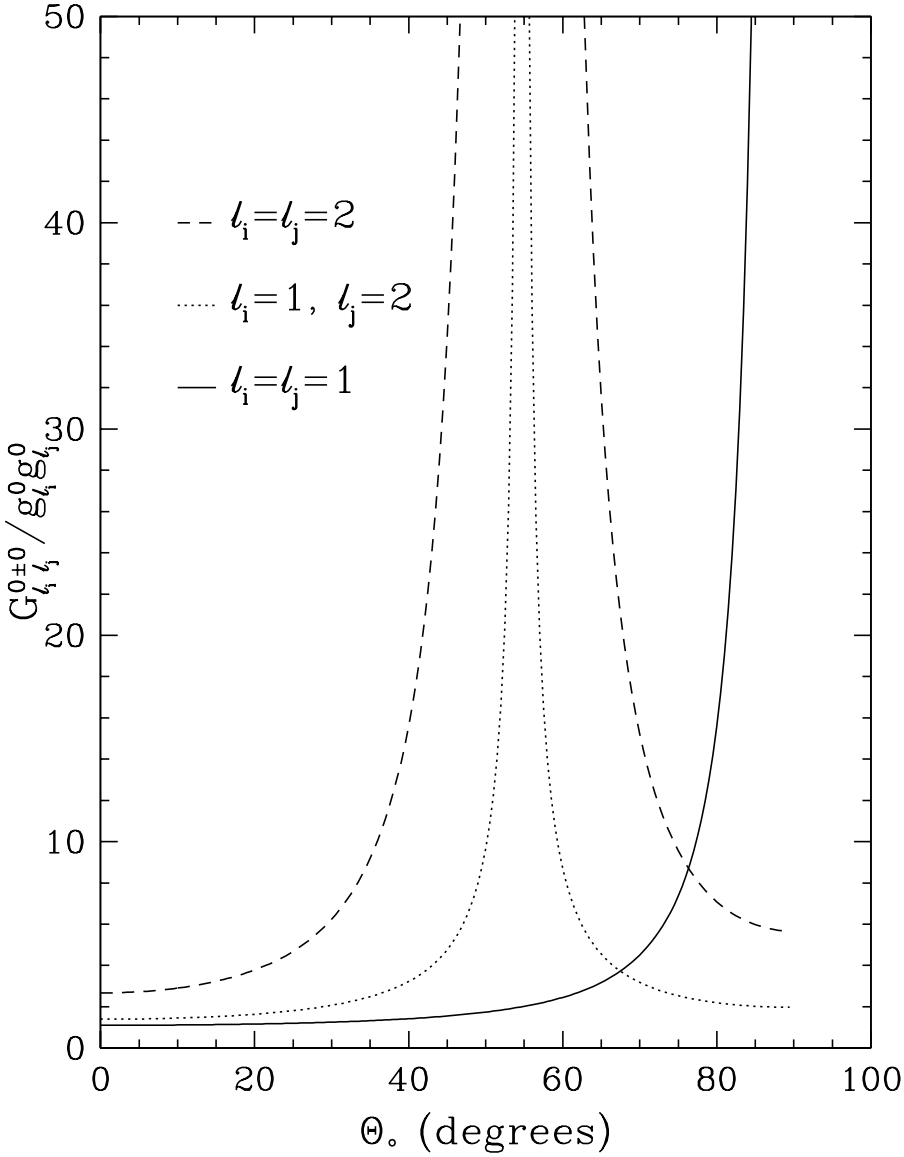

Figure 2.3: $\mathcal{G}$ with $m_i = m_j = 0$ (see equation 2.9) plotted as a function of inclination angle (Θ_0). For low inclinations ($\Theta_0 \leq 25°$), the predicted amplitudes of the combination frequencies show only a gradual increase with $\ell_i = \ell_j = 1$ (solid line), $\ell_i = \ell_j = 2$ (dashed line), and $\ell_i = 1$, $\ell_j = 2$ (dotted line).

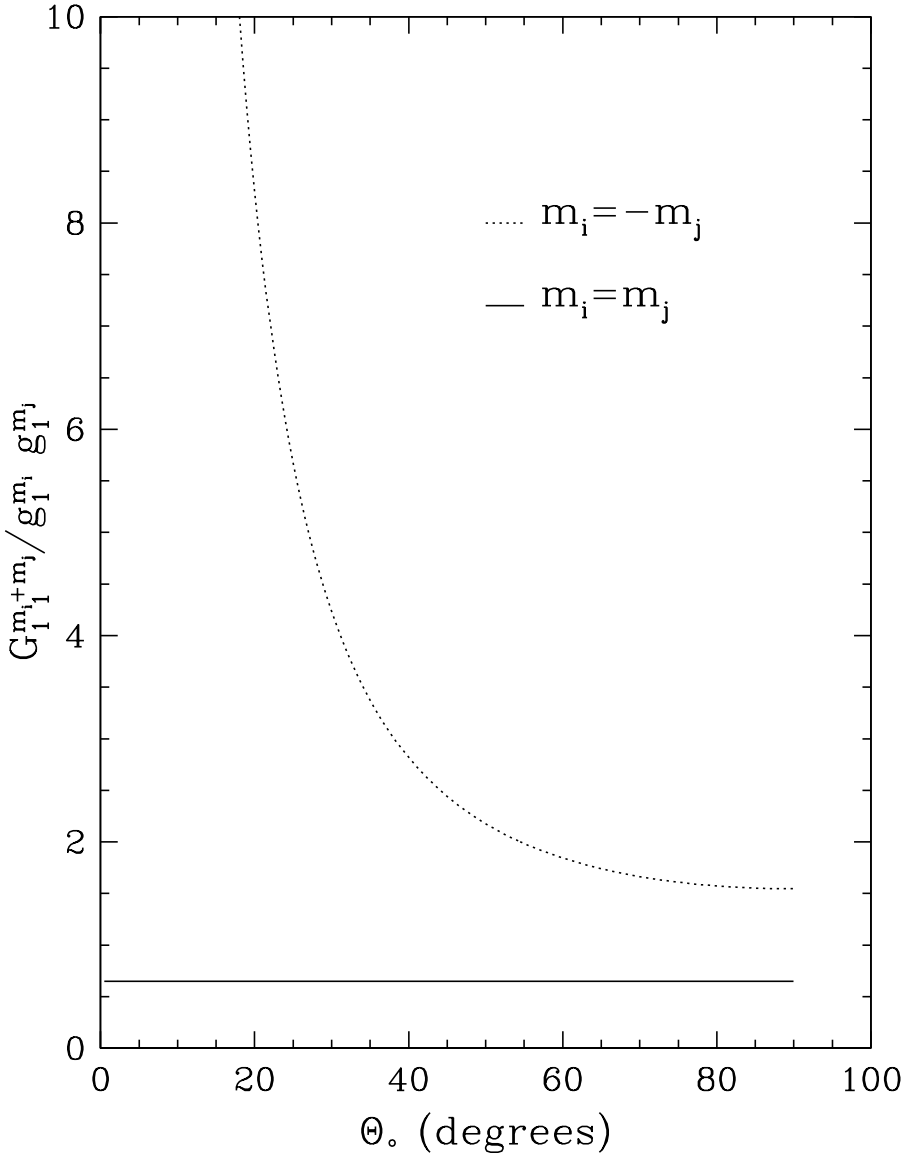

Figure 2.4: $\mathcal{G}$ with $\ell_i = \ell_j = 1$ and $m_i + m_j$ (see equation 2.9) plotted as a function of inclination angle (Θ_0). The amplitude of the combination frequencies is insensitive to inclination when $\Theta_0 \geq 60°$ for $m_i = -m_j$ (dotted line). When both parent modes have the same m (solid line), the combination amplitude is *always* independent of inclination. $\mathcal{G}$ with $m_i - m_j$ can be obtained by letting the dotted line represent $m_i = m_j$ and the solid line represent $m_i = -m_j$.

are present, they will dominate the power spectrum and so will their combination frequencies. As Figure 2.4 shows, these combinations are not very sensitive to inclination for Θ_0 near 90°. In other words, the analysis of combination frequencies requires that they be detectable. At low inclination, only $m = 0$ combination frequencies are detectable and at low inclination these are insensitive to Θ_0, and at high inclinations only $m \neq 0$ modes are detectable and at high inclination these are insensitive to Θ_0. For higher ℓ the situation is more complicated, because there are more nodal lines, but the basic argument still applies.

With this in mind, following Pesnell (1985), we have assumed that the intrinsic mode amplitudes are the same for all the modes within a multiplet. When modes of a specific ℓ value are rotationally split into $2\ell + 1$ modes (as described by the second term in equation 1.4), the inclination of a star can be found by equating the amplitude ratio of the $m = 0$ peak and an $m \neq 0$ peak with the corresponding ratio of $N_\ell^m \rho_\ell^m(\Theta_0)$ for both values of m. The N_ℓ^m are the coefficients of the spherical harmonic, $Y_\ell^m(\Theta, \Phi)$, and the $\rho_\ell^m(\Theta_0)$ are the Legendre Polynomials. For an $\ell = 1$ triplet, this ratio is:

$$\frac{\left(\frac{\delta f}{f}\right)_1^0}{\left\langle\left(\frac{\delta f}{f}\right)\right\rangle_1^{\pm 1}} = \frac{N_1^0 \rho_1^0(\Theta_0)}{N_1^1 \rho_1^1(\Theta_0)} = \sqrt{2}\frac{\cos(\Theta_0)}{\sin(\Theta_0)}. \tag{2.10}$$

We estimated the inclination for each star by averaging the amplitudes of the $m = \pm 1$ members of the largest amplitude $\ell = 1$ multiplets in each star.

There are four stars in Chapter 3 with detected combination frequencies. For three of these, the Pesnell (1985) method yields low inclination ($\Theta_0 < 20°$). The only combination frequencies detected in these stars are combinations of $m = 0$ parent modes, as established by their singlet nature or by their central location in a frequency symmetric triplet. Figure 2.3 shows that except for at large inclination, the amplitudes of the combination frequencies are not very sensitive to inclination for the central, $m = 0$, parent modes. The fourth star (GD 244) has a high inclination ($\Theta_0 \geq 80°$), and shows only combinations of $m \neq 0$ parent

modes. Figure 2.4 shows that at high inclinations the amplitudes of combination frequencies are not very sensitive to inclination when the parent modes are $m = \pm 1$ members of an $\ell = 1$ triplet. In fact, for certain m combinations, the amplitudes of combination frequencies are measured *independent* of inclination. Therefore, for all stars that we analyze, the amplitudes of the combination frequencies are at most weakly dependent on the inclination, as long as the value of ℓ is small. Hence, the approximation of inclination is a small source of error in our analysis.

With independent estimates of inclination, the only factor that remains unknown in the factor $\mathcal{G}$ of the theory of Wu (2001) is the value of ℓ for each mode. Thus we can compare the measured combination frequencies in the data, if any, to the predicted amplitudes of combination frequencies under various assumptions for the ℓ value of the parent modes. In this way we can hope to constrain or actually measure the value of ℓ. We will see that harmonics of a single mode are more valuable in this enterprise than combinations between two different modes. This is because there is a greater contrast in the theory between same-ℓ combinations, and for harmonics there is only one parent, and therefore only one ℓ involved. In the following chapter, we apply the theory to eight hot, low-amplitude ZZ Ceti stars, and show that it is possible to establish the values of ℓ for most modes in these stars.

2.3 Conclusions

The main result of this chapter is that combination frequencies, particularly harmonics, in the lightcurves of white dwarf stars can be used along with the theory of Wu (2001) to constrain and in many cases to determine uniquely the spherical harmonic index (ℓ) of the modes that produced them. We will show in Chapter 3 that this mode identification method is a quick and easy diagnostic tool that frequently yields definitive results.

The method we describe requires only time-series photometry and simple calculations as presented in §2.2. The essential part of these calculations is the evaluation of the geometric term in the theory of Wu (2001), which we have named $\mathcal{G}$. Calculating $\mathcal{G}$ requires the evaluation of integrals of spherical harmonics in the presence of a limb darkening law. To assist others in application of this technique, we have included tabulated matrices of combination frequency integrals for $\ell \leq 4$ in Appendix A. Applying these requires a straightforward estimation of the inclination, which we do using multiplet amplitudes, where detected, and limits on the sizes of multiplet members where not detected. This requires that we assume that modes of every m are excited to the same amplitude in every mode, and that rotation always removes the frequency degeneracy of multiplet members. Fortunately, our results are not highly sensitive to these assumptions.

Both the observational and the calculated values of R_c (see equation 2.9) contain parameters with varying levels of sensitivity to error. The observational parameters are the measured amplitudes of the combination frequencies and their parent modes from the FT of the data.[5] The quantitative error associated with these measured amplitudes are the formal errors of the least squares fit used to calculate the frequency, amplitude, and phase for each pulsation mode. The error bars in the figures depicting R_c in Chapters 3 through 5 contain these formal errors of the measured amplitudes. These formal errors are often regarded as underestimates (Winget et al., 1991), but our calculations for the reduced χ^2 suggest that instead they are a slight overestimate of the amplitude errors in some cases. These errors are generally small compared with the measured amplitudes, but the errors grow as the peak amplitude decreases to the level of the noise. This is often the case for detected combination frequencies. Therefore, the sensitivity of the observed R_c to the formal amplitude errors increases with decreasing combination frequency amplitude.

[5]There is also the parameter n_{ij}, which is 1 for harmonics and 2 otherwise.

The predictions for R_c are dependent upon the physical and geometrical parameters contained in $\mathcal{F}$ and $\mathcal{G}$ (see equation 2.9). The function $\mathcal{F}$ consists of the parameters $2\beta+\gamma$, ω, τ_{c_0}, and α_λ. The parameters β and γ are coupled as $2\beta+\gamma$ in our evaluation of the theory. In Chapter 3, we will show that this parameter, which describes the radiative region overlying the convection zone, can be measured using combination frequencies. The value that we found for $2\beta+\gamma$ is consistent with the theoretical values from Wu & Goldreich (1999) and the value that Wu (2001) used to compare the theory to observations. The calculated R_c is not very sensitive to the error in this parameter because when we normalize the value of $2\beta+\gamma$ using the star in our sample with the most detected combination frequencies, GD 66, the theory reproduces all the observed values of R_c to better than a factor of two. The parameter ω is the measured combination frequency from the FT of the data and the errors are the formal errors for the least squares fit as discussed for the amplitude in the previous paragraph. We estimate the thermal time constant, τ_{c_0}, with the longest period mode observed for a given star. This value only effects the location of the low-frequency roll-off for R_c (see Figure 2.2). It does not effect the predicted value of R_c in the region where we detect combination frequencies, therefore our predicted R_c is insensitive to the errors in τ_{c_0}. We discussed the error sensitivity of the bolometric constant, α_λ, in detail in the previous section. This parameter depends upon the T_{eff} and $\log g$ of the star and the ℓ values of the pulsation modes. The bolometric correction is approximately constant over the range of T_{eff} and $\log g$ that we consider (i.e., in the instability strip, see Figure 2.1). This correction is roughly steady for low ℓ ($\ell \leq 2$), but varies as ℓ increases. We use the α_λ for $\ell = 1$, which means that the sensitivity of R_c to the error in this parameter increases for high ℓ.

Finally, the function $\mathcal{G}$ contains the geometric parameters Θ_0 and Y_ℓ^m. Though our estimation of the inclination of the stellar pulsation axis, Θ_0, may not be exact, the analysis of combination frequencies requires that they be detectable. At low inclination, only $m = 0$ combination frequencies are detectable and at low

inclination these are insensitive to Θ_0, and at high inclinations only $m \neq 0$ modes are detectable and at high inclination these are insensitive to Θ_0. The sensitivity of the calculated R_c to Θ_0 is small, but grows for large ℓ because there are more nodal lines. The spherical harmonics, Y_ℓ^m, describe the displacements of the atmosphere and the temperature distribution over the stellar surface. Ising & Koester (2001) show that this approximation deteriorates as the amplitude of modes increase, but this approximation is appropriate for the low amplitude pulsation modes we consider in this work.

For convenience, we summarize application of the method as follows:

1. Calculate the inclination with the Pesnell (1985) method using the ratio of the observed amplitudes in a given multiplet. Consult the sensitivity of $\mathcal{G}$ to inclination (see Figures 2.3, 2.4, and A.1) to ensure that R_c is changing slowly with inclination near this value.

2. Calculate the theoretical R_c for both $\ell = 1$ and 2 by approximating τ_{c0} with the longest period mode and using the bolometric correction $\alpha_\lambda = 0.4$. We use $2\beta + \gamma = -9.35$ for hot, low-amplitude DA stars[6], while Wu (2001) uses $2\beta + \gamma = -10$ for the cool DA star G29-38.

3. Compare the calculated R_c with the measured value obtained with the amplitudes of the combinations and their parents.

[6]Please see the discussion of GD 66 in §3.2.2 for an explanation.

Chapter 3

Mode Identification from Combination Frequency Amplitudes in ZZ Ceti Stars

Dr. Peter Venkman: *Back off, man. I'm a scientist.*

— Ghostbusters

3.1 Introduction

The Fourier transforms (FTs) of non-sinusoidal DAV and DBV lightcurves generally show power at harmonics and at sum and difference frequencies.[7] These combination frequencies result from frequency mixing between eigenmodes (Brickhill, 1992b; Goldreich & Wu, 1999; Ising & Koester, 2001, BFW95). In the previous chapter, we have described a method for using the combination frequencies found in the Fourier spectra of pulsating white dwarfs to infer the spherical degree (ℓ) and azimuthal order (m) of the parent modes that mixed to produce them. In this chapter, we will explore combination frequencies in the small am-

[7]This chapter is an expanded version of sections 1, 3, and 4 of Yeates et al. (2005) and is reproduced by permission of the AAS.

plitude DAV (ZZ Ceti) white dwarf stars. The combination frequency peaks are smaller, and therefore harder to detect, than the combination frequencies in large amplitude pulsators like G29-38, but they are more stable, and therefore more likely to yield understandable and repeatable results. The small amplitude DAVs are also the pulsators in which the origin of the combination frequencies are most uncertain—they might arise from convective effects (Brickhill, 1992b) or from nonlinearities in the radiative flux alone, as proposed by BFW95.

In this chapter, we compare the analytic theory of Wu (2001) to observations of the hot, low-amplitude ZZ Ceti stars GD 66, GD 244, G117-B15A, G185-32, L19-2, GD 165, R548, and G226-29 to determine how well this theory reproduces the combination frequencies in hot DAV stars. If they correctly describe and predict the behavior of DAV pulsations, the analytical formulae of Wu (2001) will be an important tool for mode identification in ZZ Ceti stars. Confidently assigning values of the spherical degree (ℓ) and azimuthal order (m) to individual eigenfrequencies has heretofore required time-resolved spectroscopy using either very large optical telescopes (Clemens et al., 2000) or the HST (Robinson et al., 1995). As Brickhill (1992b) first proposed, and BFW95 reiterated, a reliable theory for combination frequency amplitudes allows pulsation mode identification based on measurements of combination frequencies alone. Thus, if we can verify that the predictions of Wu (2001) are consistent with observations, then they constitute an uncomplicated method of mode identification that relies only upon broadband photometry rather than spectroscopy. Moreover, the theory of Goldreich & Wu (and of Brickhill) implicitly contains a mode driving mechanism different from that originally proposed for the DAV stars. Verification of the analytical predictions of Wu (2001) will support this convective driving mechanism as the source of pulsations in DAV stars.

For this chapter, we have used published Fourier spectra, new reductions of archival WET data, and original data obtained with the McDonald Observatory 2.1 m Struve Telescope to measure combination frequency amplitudes or ampli-

tude limits for eight hot DAV stars. We have applied our best estimates of the inclination of the pulsation axis to the observer's line of sight and compared the amplitudes of the combination frequencies to the analytical calculations of Wu (2001). We find that the theory reproduces the relative amplitudes of combination frequencies in these stars very well, but over-predicts their absolute values by a factor of about 1.4. The calculations of Wu (2001) include an adjustable parameterization of the radiative atmosphere that can easily accommodate a factor this large. When we normalize its value using the star in our sample with the most detected combination frequencies, GD 66, the theory reproduces all the observed ratios of combination frequency to parent mode amplitudes to better than a factor of two. This is easily sufficient to verify the high ℓ identification for modes in G185-32, as established by Thompson et al. (2004) using time-resolved spectroscopy from Keck and the HST. It is also sufficient in many cases to distinguish between $\ell = 1$ and $\ell = 2$ by relying on mode harmonics. Based on these results, we conclude that the theory of Wu (2001), suitably calibrated, can function as a mode identification method for at least the hot ZZ Ceti stars. This conclusion is important because the follow-up photometry of ZZ Ceti candidates from the SDSS is finding large numbers of these pulsators that will be too faint for practical time-resolved spectroscopic methods (see Mukadam et al., 2004b; Mullally et al., 2005). Our results suggest that time-series photometry on 4 m class telescopes, augmented with multiplet splitting where available (e.g., Bradley, 2006), will be sufficient to classify modes in these stars.

In §3.2 we present the data for each of the eight stars individually and compare predictions based on the equations of Wu (2001) with the observed amplitudes. In §3.3 we summarize our results and discuss future application of the technique, emphasizing a prescription for applying the theory of Wu (2001) to large samples of ZZ Ceti stars.

3.2 Data Reduction and Analysis

The data we present in this section are a combination of published Fourier spectra, new reductions of archival WET data, and original data obtained with the McDonald Observatory 2.1 m Struve Telescope. They constitute all of the currently-available data with frequency resolution sufficient to measure amplitudes or amplitude limits for combination frequencies in hot DAV stars. The purpose of this section is to extract mode frequencies and amplitudes via Fourier methods. In principle, phase measurements are also possible, but in practice they are too noisy to be useful. In cases where combination frequencies are not sufficiently above the noise level to detect, we record the upper limit for comparison to theory.

3.2.1 Data Reduction

3.2.1.1 Published Data

The stars for which we use published data include G117-B15A, G185-32, GD 165, R548, and G226-29 (Kepler et al., 1995b; Castanheira et al., 2004; Bergeron et al., 1993; Mukadam et al., 2003; Kepler et al., 1995a). These stars were all included as secondary target stars in Whole Earth Telescope campaigns (WET; Nather et al., 1990) and the referenced papers present these WET data. Bergeron et al. (1993) (GD 165) and Mukadam et al. (2003) (R548) also include Canada-France-Hawaii Telescope (CFHT) observations, and Mukadam et al. (2003) includes supplemental McDonald Observatory observations. All of the published data we have analyzed for combination frequencies are found in these publications, along with explanations of the reduction and analysis procedures.

3.2.1.2 Unpublished Data and New Reductions

We obtained time-series photometry data on both GD 66 and GD 244 in 2003 and 2004 with the McDonald Observatory 2.1 m Struve Telescope using the

prime-focus ARGOS CCD photometer with a BG40 Schott glass filter (Nather & Mukadam, 2004). We observed GD 66 on fourteen nights during three observing runs totaling 155,130 s of data as indicated in the Journal of Observations, Table 3.1. We used two integrations times (10 s for the 2003 October run and 5 s for the 2003 November and 2004 January runs, see Table 3.1). To combine the runs into one lightcurve we binned the 5 s observations into 10 s bins. We observed GD 244 on ten nights during three observing runs totaling 124,500 s of data (see Table 3.1). We used an integration time of 5 s for all of our GD 244 observations. We performed a complete reduction of the original data for GD 66 and GD 244 using the methods described by Mukadam et al. (2004b).

The data for L19-2 were obtained as the secondary target for the WET campaign XCov 12 in 1995 April (see Sullivan, 1995). The observations of L19-2 that were included in this reduction are listed in the Journal of Observations, Table 3.2. The integration times of most runs were 10 s. We binned the 5 s Mt. John Observatory (MJUO) observations into 10 s bins. We performed a complete reduction of the original data using the methods described by Nather et al. (1990) and Kepler (1993).

3.2.2 Analysis

Of the stars that we studied, four exhibit detectable combination frequencies: GD 66, GD 244, G117-B15A, and G185-32. The remainder, L19-2, GD 165, R548, and G226-29, do not show combination frequencies, though we will show that the theory of Wu (2001) suggests that they must be just below the current noise limits. The temperature and $\log g$ for each star from Bergeron et al. (2004) are listed in Table 3.3. In §3.2.2.1 and §3.2.2.2, we will present the individual analyses. We will describe our calculations of the inclination of each star and compare the observed combination frequency amplitudes to the predictions of the theory of Wu (2001).

Table 3.1: Journal of Observations for GD 66 and GD 244

Run Name	Date (UT)	Start Time (UT)	Length (sec)	Integration Time (sec)
		GD 66		
A0726	2003 Oct 25	09:04:23	12750	10
A0729	2003 Oct 27	09:42:27	1870	10
A0730	2003 Oct 27	10:58:12	5420	10
A0733	2003 Oct 28	06:52:39	19530	10
A0738	2003 Oct 29	11:08:30	4560	10
A0742	2003 Oct 31	09:32:33	10720	10
A0746	2003 Nov 1	08:17:12	3970	10
A0755	2003 Nov 19	07:29:14	11475	5
A0767	2003 Nov 22	05:11:34	14785	5
A0789	2003 Nov 29	06:08:55	12045	5
A0793	2003 Nov 30	06:49:05	21585	5
A0795	2003 Dec 1	05:44:42	11940	5
A0835	2004 Jan 20	03:26:37	11715	5
A0838	2004 Jan 21	03:09:07	12765	5
		GD 244		
A0693	2003 Sep 2	08:42:35	10270	5
A0695	2003 Sep 3	04:21:55	7705	5
A0700	2003 Sep 4	05:23:28	9555	5
A0705	2003 Sep 5	04:50:31	15070	5
A0732	2003 Oct 28	01:30:10	18770	5
A0734	2003 Oct 29	00:53:42	12900	5
A0743	2003 Nov 1	00:58:45	10455	5
A0766	2003 Nov 22	00:54:49	14880	5
A0772	2003 Nov 24	00:58:49	12995	5
A0775	2003 Nov 25	01:10:11	11900	5

Note. − All observations were made with the McDonald Observatory 2.1 m Struve Telescope.

Table 3.2: Journal of Observations for L19-2 (WET Observations)

Run Name	Telescope	Date (UT)	Start Time (UT)	Length (sec)	Integration Time (sec)
S5843	SAAO 0.75 m	1995 Apr 25	17:53:00	5590	10
S5844	SAAO 0.75 m	1995 Apr 25	22:33:00	5040	10
RO064	Itajuba 1.60 m	1995 Apr 25	23:23:20	29080	10
AP2695-1	MJUO 1.0 m	1995 Apr 26	11:04:00	9245	5
AP2695-2	MJUO 1.0 m	1995 Apr 26	13:51:50	16135	5
RO065	Itajuba 1.60 m	1995 Apr 27	03:53:20	11810	10
S5845	SAAO 0.75 m	1995 Apr 27	17:23:00	31900	10
AP2895	MJUO 1.0 m	1995 Apr 28	11:38:20	18550	5
S5846	SAAO 0.75 m	1995 Apr 28	17:25:00	24360	10
RO066	Itajuba 1.60 m	1995 Apr 28	22:25:00	9410	10
RO067	Itajuba 1.60 m	1995 Apr 29	01:59:00	12600	10
AP2995	MJUO 1.0 m	1995 Apr 29	07:27:10	39270	5
S5847	SAAO 0.75 m	1995 Apr 29	17:20:00	31580	10
RO068	Itajuba 1.60 m	1995 Apr 29	22:26:40	33710	10
S5848	SAAO 0.75 m	1995 Apr 30	21:00:00	14340	10
RO069	Itajuba 1.60 m	1995 Apr 30	22:11:40	34560	10
MY0195	MJUO 1.0 m	1995 May 1	07:04:30	40660	5
S5849	SAAO 0.75 m	1995 May 1	23:41:00	7890	10
RO070	Itajuba 1.60 m	1995 May 2	01:27:50	9630	10
RO071	Itajuba 1.60 m	1995 May 2	05:02:20	10340	10
DB001	SAAO 0.75 m	1995 May 2	18:19:30	26990	10
DB002	SAAO 0.75 m	1995 May 3	02:38:40	5090	10
DB003	SAAO 0.75 m	1995 May 3	17:17:20	29990	10
RO073	Itajuba 1.60 m	1995 May 4	01:20:50	21510	10
DB004	SAAO 0.75 m	1995 May 4	01:47:20	8290	10
DB005	SAAO 0.75 m	1995 May 4	19:58:30	21150	10
DB006	SAAO 0.75 m	1995 May 5	02:02:40	3200	10

Note. − All data come from the WET campaign XCov12.

Table 3.3: Stellar Information

Star	T_{eff} (K)	$\log g$ (cgs)	Reference
GD 66	11,980	8.05	1
GD 244	11,680	8.08	1
G117-B15A	11,630	7.97	1
G185-32	12,130	8.05	1
L19-2	12,100	8.21	1
GD 165	11,980	8.06	1
R548	11,990	7.97	1
G226-29	12,460	8.28	1

References. – (1) Bergeron et al. (2004).

3.2.2.1 Stars With Detected Combination Frequencies

GD 66

Apart from an analysis by Fontaine et al. (1985), little progress toward understanding GD 66 has been made since Dolez et al. (1983) first reported its discovery. The relatively high number of combination frequencies identified in the FT of GD 66 makes it an ideal star to include in this dissertation.

To identify the pulsation modes and combination frequencies of GD 66, we computed an FT from the reduced and combined lightcurves listed in Table 3.1. We have included a sample lightcurve in Figure 3.1 and the FT of all GD 66 data in Figure 3.2. To identify closely spaced modes in the regions of obvious excess power, we utilized a prewhitening technique similar to that of O'Donoghue & Warner (1982) using an iterative nonlinear least squares procedure. For each peak, we fitted the frequency, amplitude, and phase and then subtracted the fit from the original lightcurve. We then fitted a second frequency to the altered data, choosing in every case the largest remaining peak, and used the result of this fit to conduct a simultaneous least squares fit to the original data. Thus at each step in the prewhitening, the frequencies removed are from a simultaneous fit to the original data.

The problems with applying such a procedure to a highly aliased data set are well known (Nather et al., 1990), and we have no illusions that we can successfully measure the correct frequencies of the smaller modes in the presence of the contaminating window function. Nonetheless, the exercise provides two pieces of information that are valuable and reliable. It tells us how many modes are required to model the data, and gives us crude amplitudes for the members of the multiplet that are useful in estimating inclination.

In Figure 3.3 we show the deconstruction of the 271 s pulsation mode (F1) by prewhitening. The FT of the reduced data in the region of F1 is shown in Figure 3.3a. The window function, in Figure 3.3b, is the FT of a lightcurve of

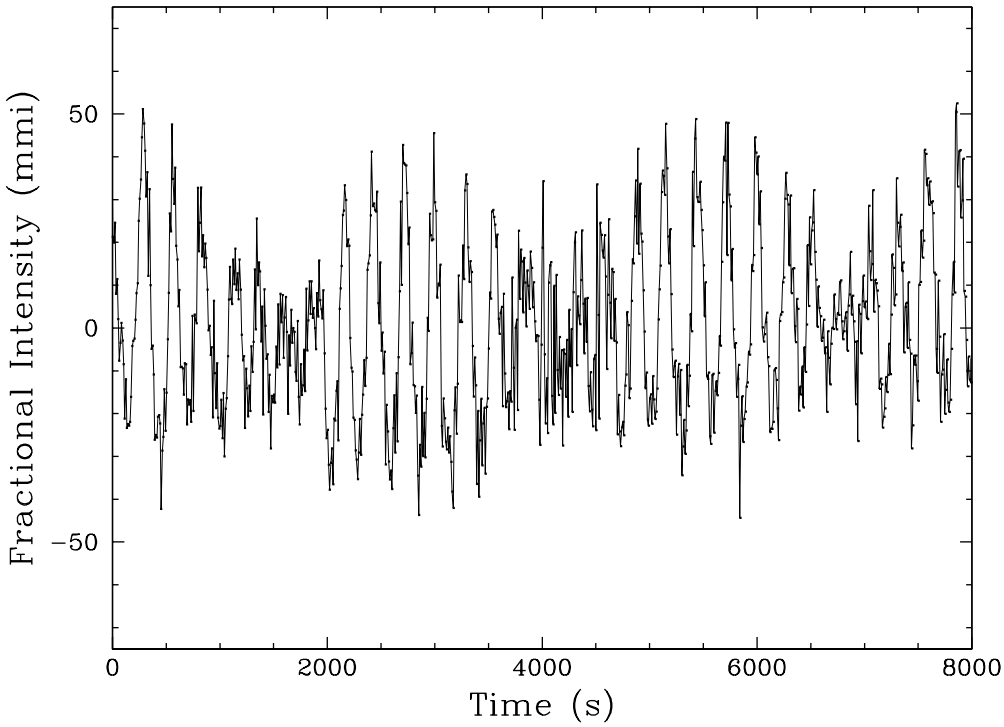

Figure 3.1: Lightcurve of GD 66. These data were acquired with the ARGOS CCD photometer on the McDonald Observatory 2.1 m Struve Telescope with an exposure time of 10 s.

a sinusoid with the same period, amplitude, and phase as the highest amplitude peak in the original FT that has been sampled in the same manner as the original data. Figure 3.3c shows the FT of the lightcurve with the largest peak removed. Figures 3.3c and 3.3d are prewhitened FTs that reveal additional low amplitude signals which were previously hidden in the window function of the highest amplitude peak. Figure 3.3e, in which there is no remaining signal, is an FT of a lightcurve with the three highest amplitude peaks fitted and removed from the original lightcurve. It is gratifying that the frequencies identified by this deconstruction form a frequency-symmetric triplet, but better sampling will be required to measure all three frequencies with confidence.

A similar procedure showed that F2 was consistent with a single frequency, to within the noise, and that F3 is a combination of at least three frequencies.

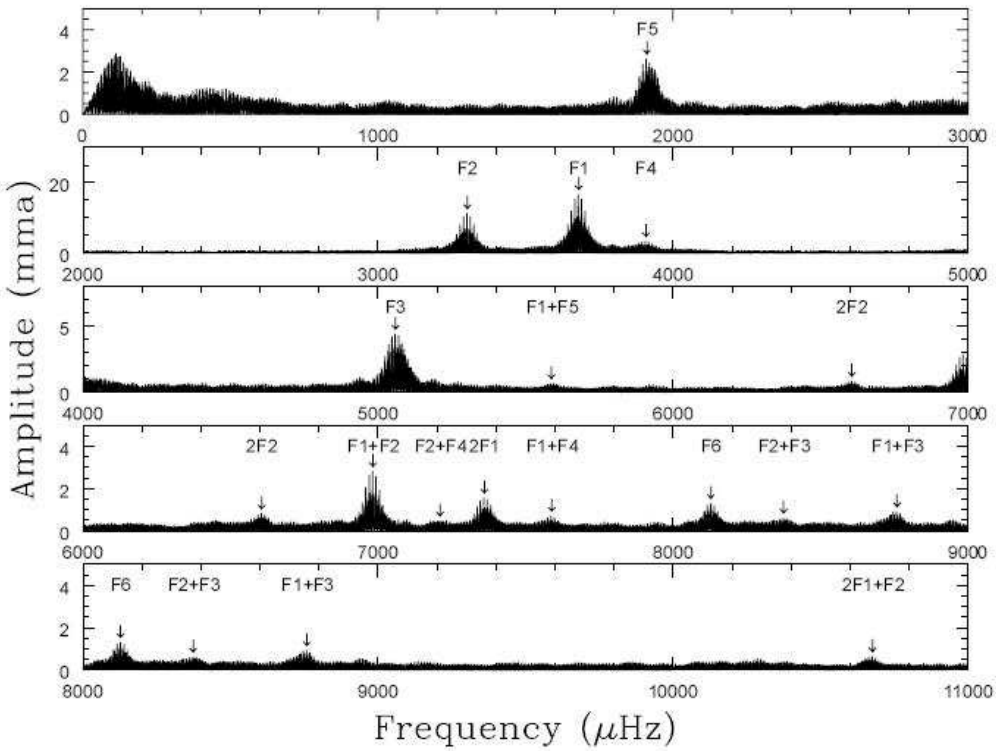

Figure 3.2: Fourier transform of GD 66. This FT includes all individual nights of the data that are listed in Table 3.1. We indicate the five pulsation modes and nine identified combination frequencies that we reference in Table 3.4. We believe the peak that we call F6 is due to the guide error of the telescope.

F4 and F5 both show residuals after prewhitening by one frequency, but they are too close to the noise level to deconstruct further. F6 is at the frequency expected from the drive of the telescope, and a peak at this location is present in all of the ARGOS data, so we do not interpret it as being astrophysically significant.

The five dominant pulsation modes (F1 - F5) and associated power derived from prewhitening are listed in Table 3.4 and presented visually in Figure 3.4. The amplitude of the smallest of our five modes is about three times above $\sqrt{\langle P \rangle}$, where $\langle P \rangle$ is the average power of the FT, yielding a false alarm probability (Horne & Baliunas, 1986) of about 20%. That is, there is a 20% chance that

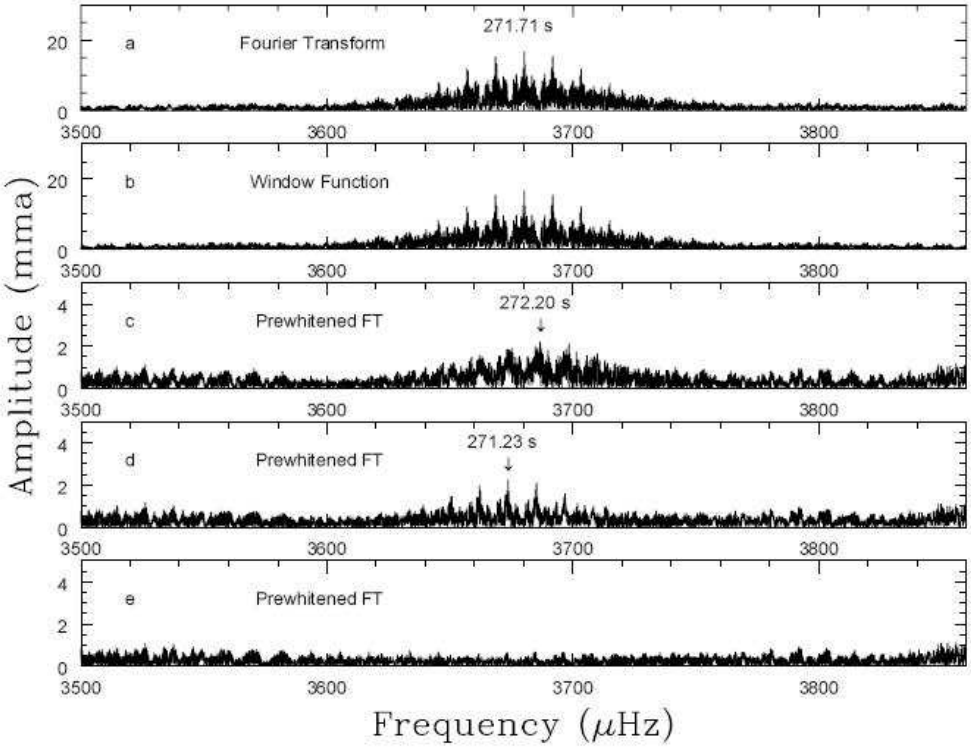

Figure 3.3: Deconstruction of F1 in GD 66. a: A Fourier transform of GD 66 near 271 s (F1). b: A window function obtained by taking an FT of a single sinusoid (with the same period and amplitude of the 271.71 s peak) that has been sampled in the same manner as the data. c: An FT near F1 with a period of 271.71 s removed. d: An FT near F1 with periods of 271.71 and 272.20 s removed. e: An FT near F1 with periods of 271.71, 272.20, and 271.23 s removed.

F5 is an artifact of noise. However, the existence of a combination frequency at F1+F5 adds confidence to this detection. All the pulsation modes except F5 were also identified by Fontaine et al. (2001). There is a large peak near the location of F5 in their data, but it was not formally significant against the noise level of their FT.

In addition to the five modes detected, we identified nine combination frequencies that were consistently present throughout the three month span of our GD 66 observations, with one exception (F1+F4 was not identified in the 2003 October data set). We verified our identification of combination frequencies with

a computer program inspired by Kleinman (1995). Our program allows a user to select pulsation modes in the data, calculates all possible combination frequencies of these modes, and then searches for significant combination frequencies in the data. The search is conducted over an estimated error range equal to the resolution of the FT. We consider this a better estimate of the frequency error than the smaller values from the least squares fit because the combination frequencies are usually low amplitude, i.e., only a few times as large as the background. The frequencies of such small signals are pulled by the presence of unresolved noise peaks, while the least squares fit formally assumes only a single unblended frequency is present. The program successfully identified all combination frequencies that we found by inspection in the data, and also found some combinations that we had missed in our visual search. In some cases, the highest amplitude peak among the combination frequency and its aliases did not fall within the error range we established. In these cases, prewhitening a forced fit of the expected combination frequency successfully removed the signal, and we have listed the amplitude from the forced frequency fit. Our listed period errors do not include the uncertainty in identifying the true peak among the alias peaks and these dominate the error for combination frequencies.

Having identified and measured the amplitudes of the combination frequencies allows us to calculate the ratio of combination to parent mode amplitudes (R_c, see equation 2.9) and compare it to the theoretical predictions. Figure 3.5 shows the observed R_c for all of the detected two-mode combination frequencies in GD 66. Where no combination was detected, we have plotted a limit equal to the 1 σ noise level in the FT. The observed R_c do not depend on any theory.

The theoretical calculations of R_c require that we supply an inclination estimate, an estimate of τ_{c_0}, and a value for the parameter $2\beta + \gamma$. For the first, a fit to the largest multiplet using the technique of Pesnell (1985) described in §2.2 yielded $\Theta_0 = 13°$, and we have used that value for all of the theoretical calculations. The result is not very sensitive to this parameter as long as $\Theta_0 \leq 25°$

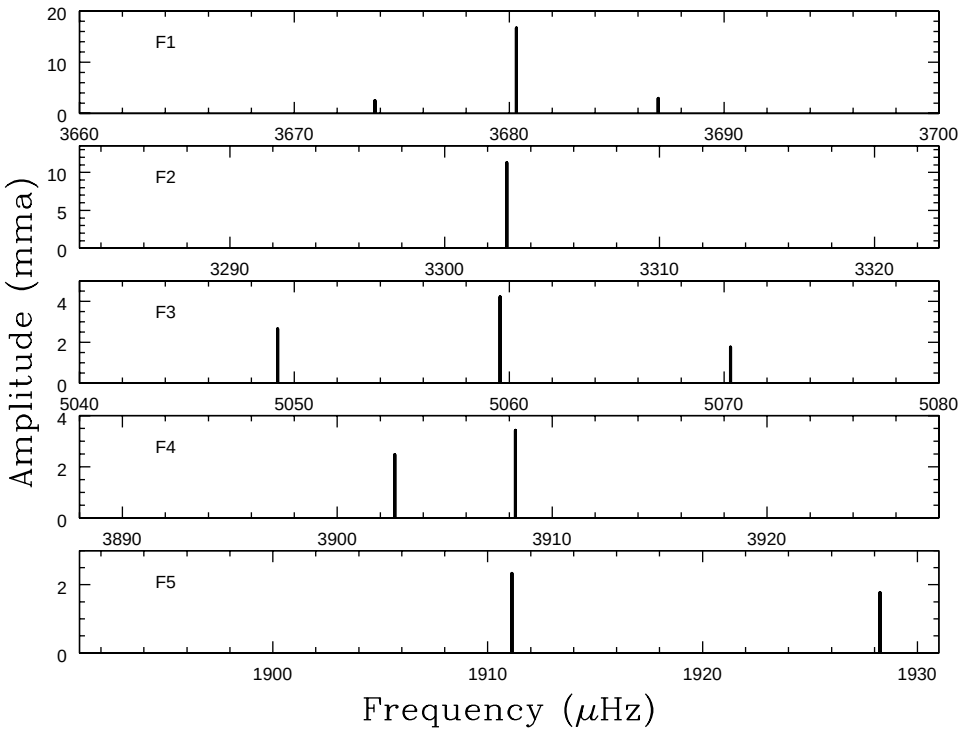

Figure 3.4: Prewhitened peaks of parent modes in GD 66 Fourier transform.

(see Figure 2.3). The inclination calculation requires an assumption for the ℓ identification of F1. However, this calculation is scarcely sensitive to our $\ell = 1$ assumption for F1. If F1 is actually an $\ell = 2$ mode, then the inclination of the star is 8°, and still in the range where our results are insensitive to inclination. For τ_{c_0}, we have used the value of 523 s, which is the longest period in GD 66, for reasons discussed in §2.2. This value only affects the location of the frequency roll-off, not the predicted combination frequency amplitudes in the high frequency limit. Finally, because the detected combinations have similar values of R_c, indicating similar ℓ, we decided to treat $2\beta + \gamma$ in this star as a free parameter.[8] The solid line in Figure 3.5 shows the best fit under the assumption that all modes are $\ell = 1$. The fitted value of $2\beta + \gamma$ is -9.35, very close to the value Wu (2001) herself used (-10) for her comparison to G29-38, and to her

[8]Please see §2.3 for a discussion of the sensitivity of R_c to errors.

theoretically calculated value (-12.6). Any other assumption for ℓ would yield values of $2\beta+\gamma$ different by a factor of ~ 3 or more, and we do not consider this a reasonable possibility. Using $\ell = 1$, the detected combination frequencies fit the model with a reduced χ^2 of 0.78, which may indicate that we have slightly overestimated our errors. We used the errors from the least square fits, which are often regarded as underestimates (Winget et al., 1991), but we see no evidence for that here.

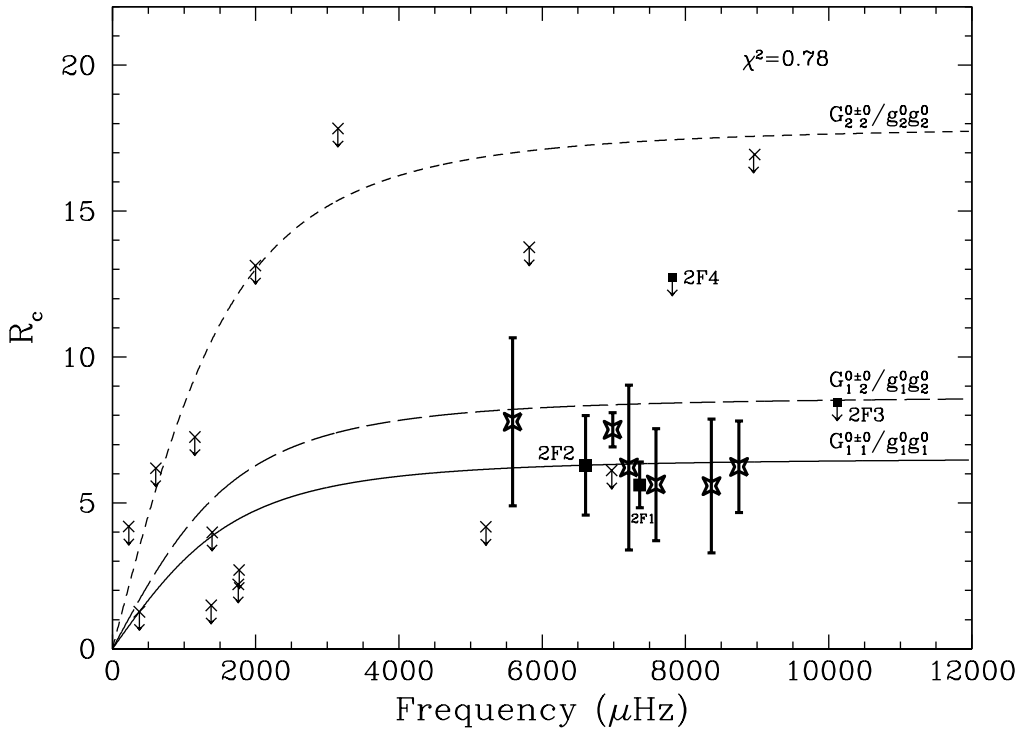

Figure 3.5: Ratio of combination to parent mode amplitudes (R_c) for GD 66. The lines are theoretical predictions for $G^{0+0}_{1\,1}/g^0_1g^0_1(\Theta_0 = 13°)$ (solid line), $G^{0+0}_{1\,2}/g^0_1g^0_2(\Theta_0 = 13°)$ (long-dashed line), and $G^{0+0}_{2\,2}/g^0_2g^0_2(\Theta_0 = 13°)$ (dashed line). The data points are the detected harmonics or limits (filled squares), detected cross combination frequencies (stars), and limits for the cross combinations (crosses). The downward arrows on the limits indicate that the points represent maximum values. The upper limit for R_c of 2F5 lies at 124 (not shown).

Even though the data show tight scatter about the line representing combinations between two $\ell = 1$ modes, we cannot conclude that all of the modes

are $\ell = 1$ on that basis alone. The line representing $\ell = 1, 2$ combinations (long dashes in Figure 3.5) is close to the $\ell = 1, 1$ line, and falls within the error bars for some combinations. Fortunately, the theoretical lines for same-ℓ combinations are well-separated, suggesting that harmonics, which are same-ℓ by definition, might be able to constrain ℓ when cross combinations (i.e., all combinations that are not harmonics) cannot. We have detected harmonics for F1 and F2, and measured limits for the harmonics of the remaining three modes. These are shown in Figure 3.5 as filled squares. The measured R_c for F1 and F2 and the limits for F3 and F4 are only consistent with $\ell = 1$, and so we identify all of those modes as $\ell = 1$, F4 somewhat tentatively because the limit is not very stringent. The limit for F5 is too large ($R_c = 124$) to fit on our plot and does not constrain ℓ uniquely. Though our identification relies primarily on harmonics, the cross combinations are all consistent with this conclusion. The m identifications we assigned in Table 3.4 arise from frequency splitting only, and are not derived from combination frequency amplitudes.

Finally, the R_c limits we have plotted at low frequency suggest that the roll-off expected from the theory actually occurs, which eliminates from consideration competing models, including the BFW95 theory, that predict no frequency dependence for R_c.

GD 244

Fontaine et al. (2001) first reported the detection of variability in the DAV white dwarf GD 244, but no subsequent observations have been published. The FTs of GD 244 and GD 66 both contain large pulsation modes near 200, 256, and 300 s. The similarity of GD 244 to GD 66, including its relatively high number of combination frequencies, makes it another ideal candidate to include in this study.

To identify the pulsation modes and combination frequencies of GD 244, we computed an FT from the reduced and combined lightcurves listed in Table 3.1.

We have included a sample lightcurve in Figure 3.6 and the FT of all GD 244 data in Figure 3.7. We used the prewhitening technique to identify pulsation modes and combination frequencies in GD 244, as with GD 66. We also used prewhitening to reveal the doublet structure in the two highest amplitude pulsation modes. As with GD 66, we do not expect that we have consistently measured the correct frequencies of the modes in these doublets in the presence of the contaminating window function. However, the amplitudes are useful in estimating the inclination.

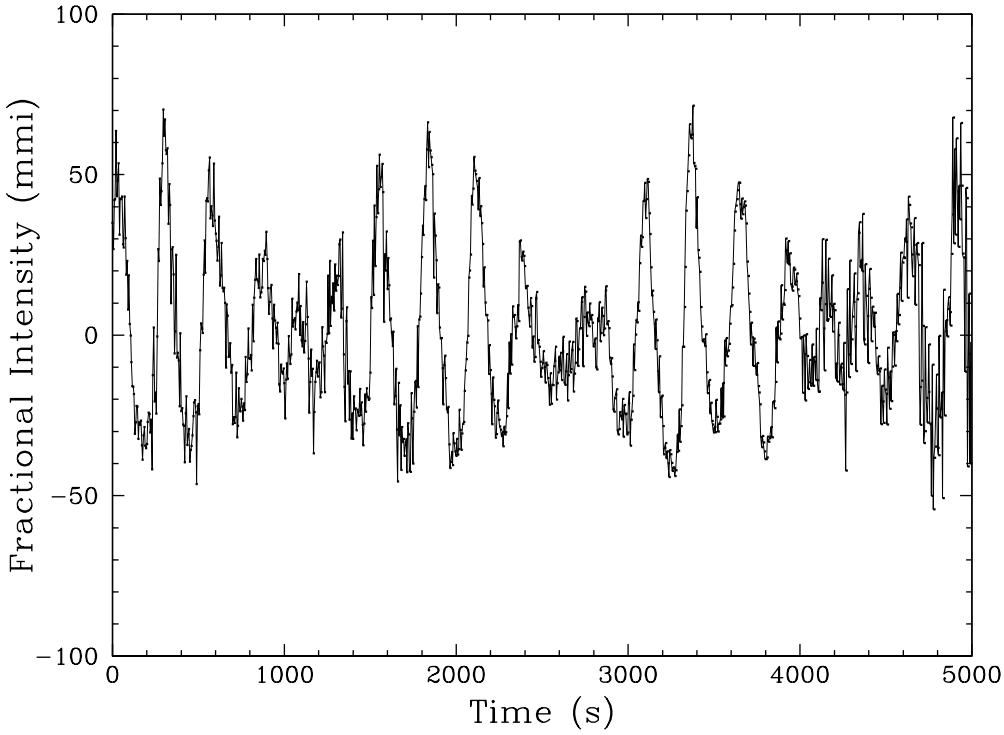

Figure 3.6: Lightcurve of GD 244. These data were acquired with the ARGOS CCD photometer on the McDonald Observatory 2.1 m Struve Telescope with an exposure time of 5 s.

In Figure 3.8 we show the deconstruction of the 256 s pulsation mode (F2) by prewhitening. The FT of the reduced data in the region of F2 is shown in Figure 3.8a. The window function for the GD 244 data set is in Figure 3.8b. Figure 3.8c shows the FT of the lightcurve with the largest peak removed. Panel c

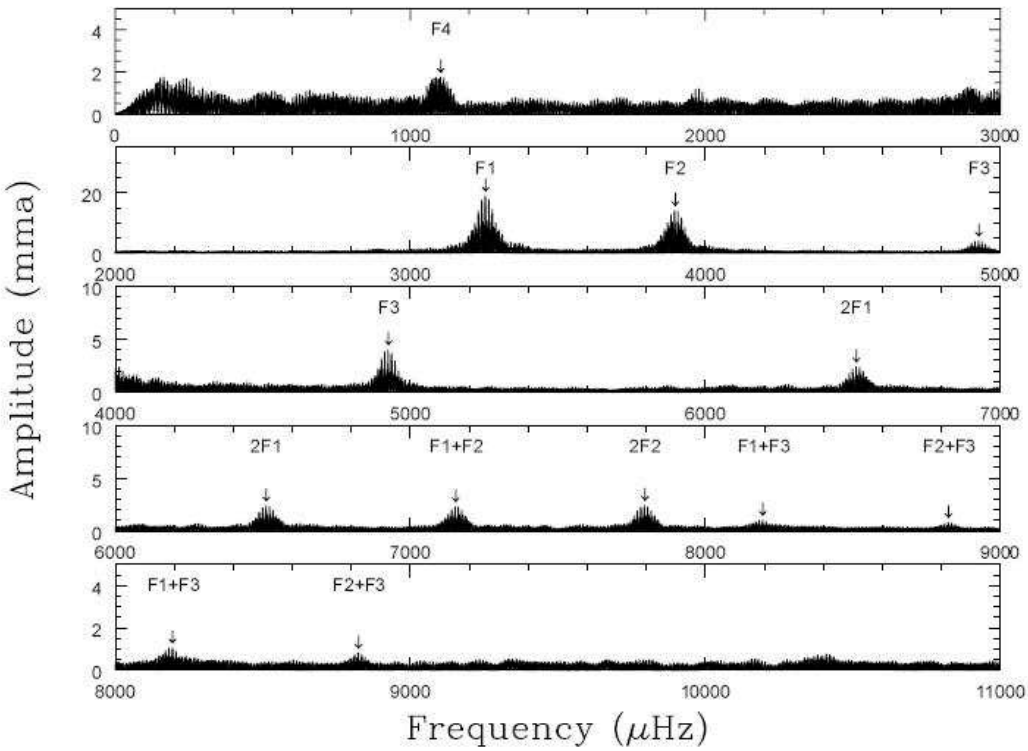

Figure 3.7: Fourier transform of GD 244. This FT includes all individual nights of data included in Table 3.1. We indicate the four pulsation modes and all combination frequencies that we reference in Table 3.5. F1+F3 is likely a blend with guide error.

is a prewhitened FT that reveals additional low amplitude signal that was previously hidden in the window function of the highest amplitude peak. Figure 3.8d is an FT of a lightcurve with the two highest amplitude peaks fitted and removed from the original lightcurve. We were unable to fit any other statistically significant signals from the FT in the bottom panel.

A similar procedure showed that F1 is also consistent with a doublet. F3, however, is consistent with a single frequency, although any putative companion peak would be in the noise if it scaled as the companions of F1 and F2. F4 is not formally significant, with a false alarm probability near 1 in the whole data set, but it appears above the noise at the same frequency in all three of the single

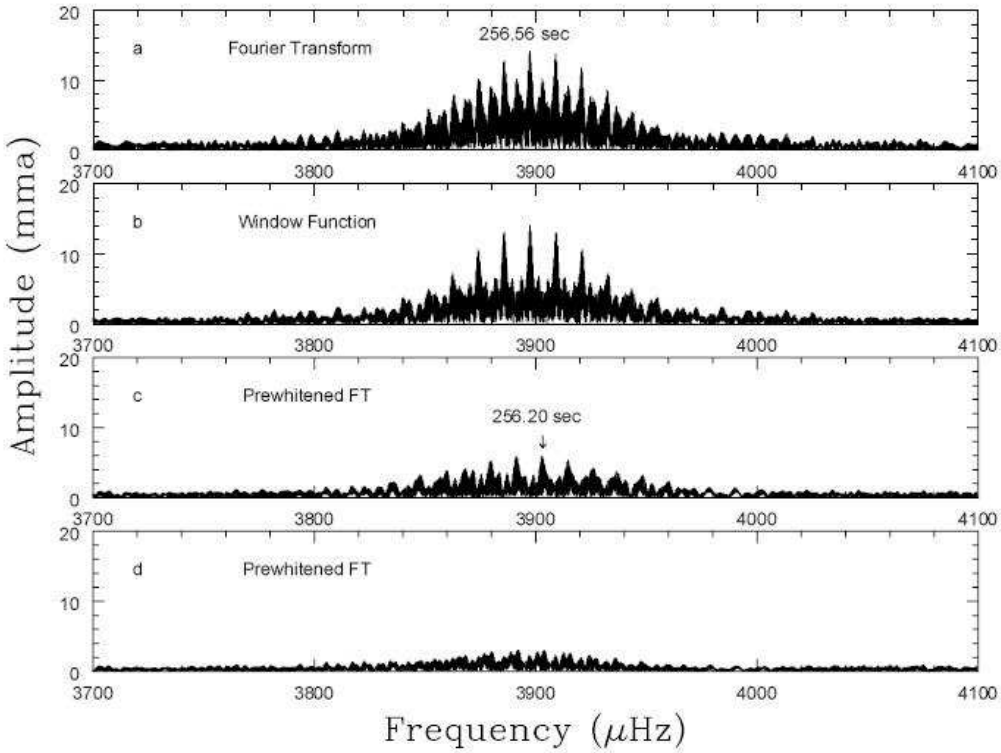

Figure 3.8: Deconstruction of F2 in GD 244. a: A Fourier transform of GD 244 near 256 s (F2). b: A window function obtained by taking an FT of a single sinusoid (with the same period and amplitude of the 256.56 s peak) that has been sampled in the same manner as the data. c: An FT near F2 with a period of 256.56 s removed. d: An FT near F2 with periods of 256.56 and 256.20 s removed. Fitting and removing further peaks did not reduce the noise level.

month FTs so we have included it in Table 3.5. It does not show any combination peaks and therefore does not enter our analysis. The complete list of pulsation modes is listed in Table 3.5 and presented visually in Figure 3.9. We did not detect the 294.6 s pulsation mode found by Fontaine et al. (2001) in GD 244. All other pulsation modes that we list, except F4, were identified by Fontaine et al. (2001). There are no formally significant peaks above the noise level in the low frequency region of their FT.

In addition to the four modes detected, we identified six combination frequencies that were consistently present throughout the observing run. In all cases,

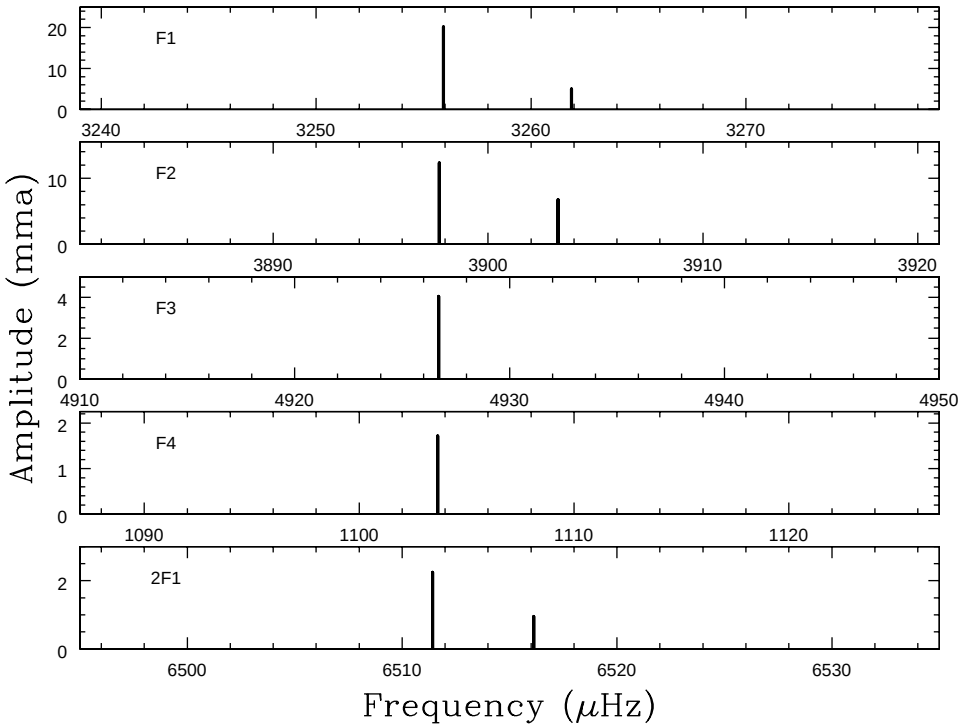

Figure 3.9: Prewhitened peaks in GD 244 Fourier transform. In addition to the parent modes, we include one combination frequency (2F1) in which we resolved fine structure.

the highest amplitude peak among the combination frequency and its aliases fell within the error of the expected frequency. We list the frequencies of the highest amplitude peaks in Table 3.5. The frequency errors were sufficiently small that there was no confusion between the harmonic of the largest component (presumed $m = -1$) and the sum of the $m = -1$ and $m = +1$ components.

We use the doublet structure at 307 s (F1) to estimate the inclination of the pulsation axis of GD 244. We assume that the doublet structure in these two pulsation modes results from viewing $\ell = 1$ modes at high inclination so that the third (central, $m = 0$) mode does not appear. As discussed previously, our results do not depend sensitively on this assumption. Using the maximum amplitude in the prewhitened FT of F1 as an estimate for the amplitude of the $m = 0$ peak, we apply the Pesnell (1985) method and find a minimum possible inclination of 80°. Recall that Figure 2.4 shows that at high inclination, the

amplitudes of combination frequencies with $\ell = 1$ and same-m parent modes have no dependence on inclination.

Figure 3.10 is a plot of the theoretical predictions for GD 244 (R_c with $\Theta_0 = 80°$) and the observed amplitudes of the six detected combination frequencies for comparison. We also include the observed noise limit (indicated by crosses for the same-m combinations and open squares for the different-m combinations) in cases where there was no combination frequency detected. The downward arrows imply an upper limit. When we apply the GD 66 calibration of $2\beta + \gamma = -9.35$ to GD 244 (in Figure 3.10), the predictions for the $\ell = 1, 1$ line resemble the observations for our detected combination frequencies except for the R_c of 2F2. The reduced χ^2 is 16.9 if all the modes are assumed to be $\ell = 1$, but 9.2 if we leave out the combinations of F2. Obviously we could reduce χ^2 further if we varied $2\beta + \gamma$ as before, but part of our exercise is to establish that we can conduct mode identification without fitting parameters, so that it is possible to measure the ℓ of hot ZZ Ceti stars with only a single detected combination frequency.

Turning to the harmonics, which are known to be same-ℓ and therefore to have well-separated predictions for R_c, 2F1 and the limit for 2F3 demand that F1 and F3 be $\ell = 1$ modes. The high measurement for 2F2 suggests that ℓ may not be 1. However, if we assume $\ell_{F2} = 2$, then $\chi^2 > 400$ because R_c for a harmonic of an $\ell = 2$, $m = 1$ mode is predicted to be near 90. Even if we relax the assumptions used to calculate inclination and adjust it to minimize χ^2 for the assumption of $\ell_{F2} = 2$, then at $\Theta_0 = 67°$, $\chi^2 = 17.3$. So even under the best assumptions, the identification of F2 as $\ell = 2$ would yield a worse fit than if we let it be $\ell = 1$. Moreover, its similar frequency splitting to F1 suggests that it is $\ell = 1$, but without better sampling with WET this is not a secure statement. Therefore, we have left question marks next to the identification of F2 in Table 3.5. It is possible that the harmonic of F2 is inflated by some independent unresolved pulsation mode, but our data are insufficient to test this possibility. Finally, for the smallest mode, F4, the limit on the harmonic constrains it to be $\ell \leq 3$, which

is not useful.

Because F1 and F2 are multiplets, we expect fine structure in their harmonics and combinations, and indeed we observe secondary peaks near both harmonics at the sum of the presumed $m = -1$ and $m = 1$ parent modes. Unfortunately, the theoretical lines for these cross terms in m are not well-separated from similar cross terms in an $\ell = 2$ mode (see Figure 3.10). Likewise, the F1+F2 peak shows multiplet structure, but we are unable to reliably dissect it into individual modes. The limits we have measured for the cross terms of different-ms are all consistent with the $\ell = 1$ identifications, but would not be sufficient alone to reach that conclusion.

G117-B15A

G117-B15A is one of the hottest known ZZ Ceti stars. McGraw & Robinson (1976) confirmed the star's variability and Kepler et al. (1982) found six pulsation modes. The dominant mode, at 215 s, is stable in amplitude and phase such that G117-B15A is the most precise optical clock known (Kepler et al., 2000a). We use published measurements for G117-B15A obtained from the WET campaign XCov 4 in 1990 May (Kepler et al., 1995b). They list the highest amplitude modes as $\ell = 1$.

The 215 s pulsation mode of G117-B15A has a large central peak and two possible adjacent peaks regarded by Kepler et al. (1995b) as "low probability" because they do not rise very far above the already low noise level. We have used the size of the adjacent peaks to constrain the inclination of this star, under the assumption that the central peak is an $\ell = 1$, $m = 0$ mode. We find that the star has a maximum inclination of 5° (nearly pole-on), and this result is not sensitive to the assumption of $\ell = 1$. In order to appear as a singlet, modes of any ℓ must be viewed at low inclination.

Figure 3.11 is a plot of the theoretical predictions for G117-B15A (R_c with $\Theta_0 = 5°$) and the observed amplitudes of the four detected combination frequen-

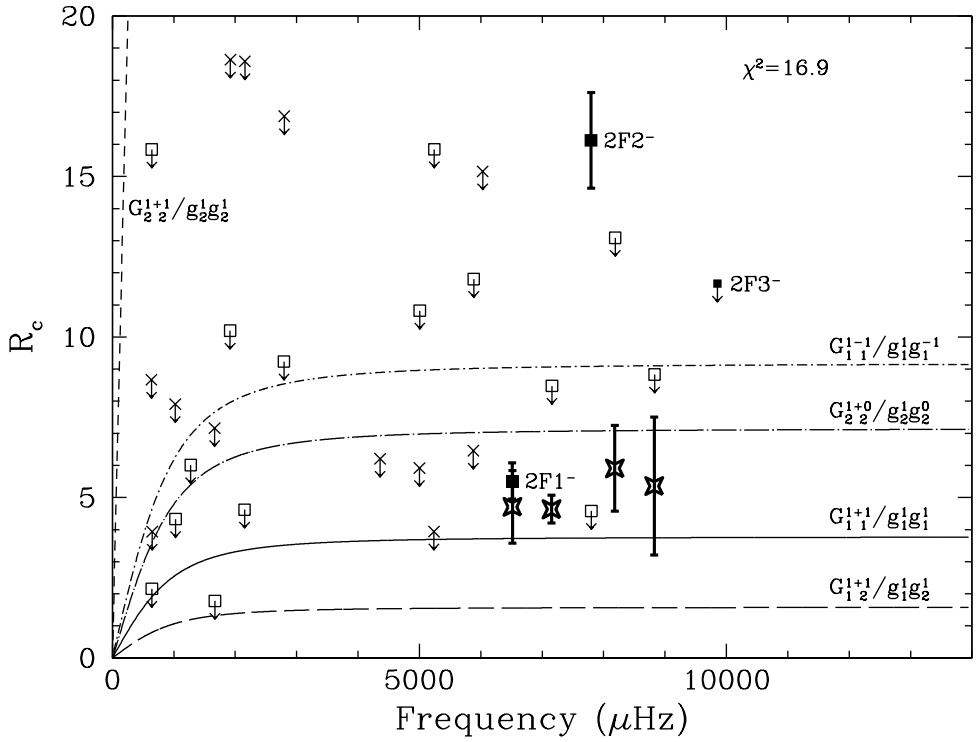

Figure 3.10: Ratio of combination to parent mode amplitudes (R_c) for GD 244. The lines are theoretical predictions for $G^{1+1}_{1\ 2}/g^1_1 g^1_2(\Theta_0 = 80°)$ (long-dashed line), $G^{1+1}_{1\ 1}/g^1_1 g^1_1(\Theta_0 = 80°)$ (solid line), $G^{1+0}_{2\ 2}/g^1_2 g^0_2(\Theta_0 = 80°)$ (dot-long-dashed line), $G^{1-1}_{1\ 1}/g^1_1 g^{-1}_1(\Theta_0 = 80°)$ (dot-dashed line), and $G^{1+1}_{2\ 2}/g^1_2 g^1_2(\Theta_0 = 80°)$ (dashed line). The data points are the detected harmonics or limits (filled squares), detected cross combination frequencies (stars), limits for the same-m cross combinations (crosses), and limits for the different-m cross combinations (open squares). The downward arrows on the limits indicate that the points represent maximum values.

cies for comparison. We also include the observed noise limit (indicated by the crosses) in cases where there was no combination frequency detected. The downward arrows below the crosses indicate an upper limit. Just as with GD 66, the theory of Wu (2001) predicts high amplitudes for all of the combination frequencies that we detect and low amplitudes for those we do not detect. When we apply the GD 66 calibration of $2\beta + \gamma = -9.35$ to G117-B15A (in Figure 3.11), the predictions are consistent with the observations for our detected combination frequencies, though the scatter is considerably worse than in GD 66. The

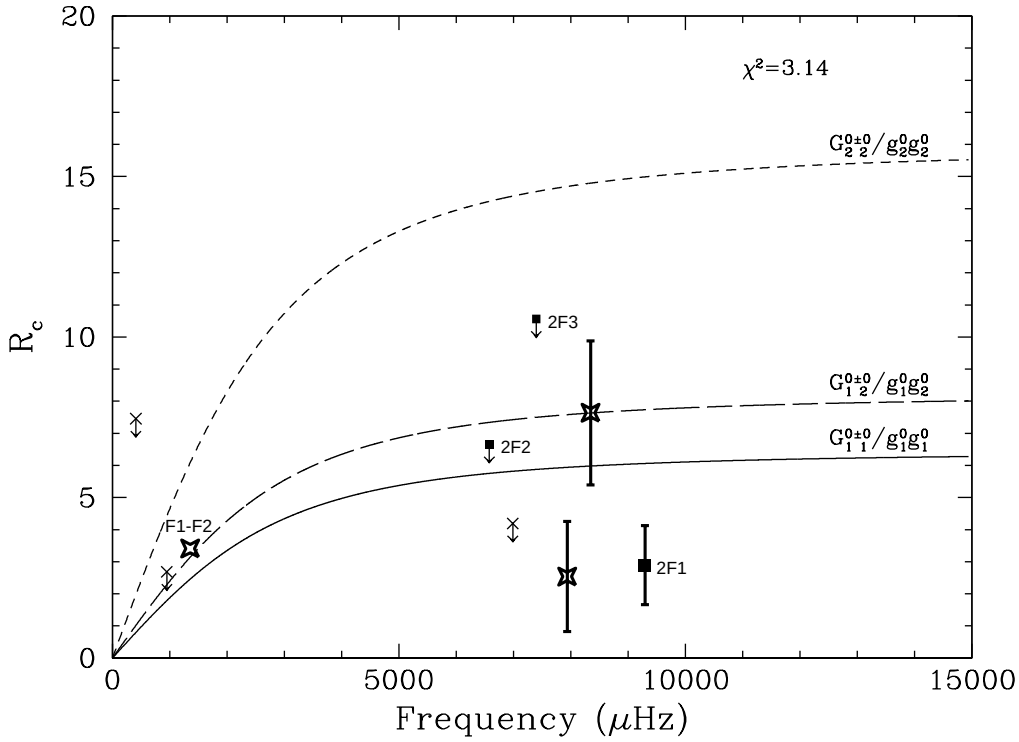

Figure 3.11: Ratio of combination to parent mode amplitudes (R_c) for G117-B15A. The lines are theoretical predictions for $G^{0+0}_{1\ 1}/g^0_1 g^0_1(\Theta_0 = 5°)$ (solid line), $G^{0+0}_{1\ 2}/g^0_1 g^0_2(\Theta_0 = 5°)$ (long-dashed line), and $G^{0+0}_{2\ 2}/g^0_2 g^0_2(\Theta_0 = 5°)$ (dashed line). The data points are the detected harmonics or limits (filled squares), detected cross combination frequencies (stars), and limits for the cross combinations (crosses). The downward arrows on the limits indicate that the points represent maximum values. There are no error bars for F1-F2 because there were none reported by Kepler et al. (1995b).

reduced χ^2 is 3.14 if all the modes are assumed to be $\ell = 1$. The combination F1-F2, located in the lower left quadrant of Figure 3.11, is not included in this χ^2, because no formal errors were reported by Kepler et al. (1995b). If we assume the error for the amplitude of this combination is greater than the largest errors in the plot, then it gives no information about the ℓ of its parents, but is consistent with the low frequency roll-off of the theory of Wu (2001).

Robinson et al. (1995) established that $\ell = 1$ for F1 by comparing time-series photometry observations in the UV and optical wavelengths. The amplitude

of the harmonic of this mode, combined with our analysis, confirms this $\ell = 1$ identification; the observed R_c for the harmonic of F1 is too small to be consistent with that for $\ell_i = \ell_j = 2$, which is 2.5 times greater than R_c for $\ell_i = \ell_j = 1$ and 5 greater than the R_c we observe. Likewise, the limit for the harmonic of F2 is sufficiently low to constrain this mode to be $\ell = 1$ with a 98.7 percent confidence level. The limit for 2F3 is more ambiguous, but clearly requires that $\ell \leq 2$ for F3. We list our mode identifications in Table 3.6. These results are consistent with the seismological analyses of both Bradley (1998) and Brassard et al. (1993), where the choice of $\ell = 1$ for these three peaks yielded reasonable physical parameters.

G185-32

McGraw et al. (1981) discovered the DA white dwarf G185-32 to be a relatively low amplitude multi-periodic ZZ Ceti star on the basis of its $(G - R)$ colors (see Greenstein, 1976). The largest amplitude peaks have periods of 71, 73, 142, 216, 301, and 370 s. G185-32 is unique among the ZZ Cetis in that it has a harmonic (at 71 s) that is sometimes measured to be larger than its parent frequency (at 142 s). This has led to disagreement over whether the harmonic is a pulse shape artifact, or whether there are resonances between real eigenmodes that happen to be harmonically related (Castanheira et al., 2004). Most recently, Thompson et al. (2004) has found that identifying the 142 s mode as high ℓ ($\ell = 4$) can explain all of the available observations, which include time-resolved UV spectroscopy from HST (Kepler et al., 2000b), time-resolved optical spectroscopy from Keck (Thompson et al., 2004), and time-series photometry from WET (Castanheira et al., 2004). An $\ell = 4$ mode cancels itself in the integration over the visible hemisphere for almost any value of inclination, but its harmonic may not, because it has a surface distribution with characteristics of lower ℓ. This allows a harmonic to appear larger than its fundamental. In our analysis, we apply the theory of Wu (2001) under the assumption that the peak

Table 3.4: GD 66 Periods and Mode Identifications

Mode Label	Frequency (μHz)	Period (sec)	σ_p (sec)	Amplitude (mma)	σ_{amp} (mma)	Δf^a (μHz)	ℓ	m^b
F1	3673.753	272.2012	0.0004	2.50	0.17	-6.582?	1	-1
	3680.335	271.7144	0.0001	16.70	0.16		1	0
	3686.927	271.2286	0.0004	2.93	0.17	6.592?	1	+1
F2	3302.889	302.7653	0.0001	11.29	0.19		1	0
F3	5049.227	198.0501	0.0002	2.65	0.21	-10.355?	1	-1
	5059.582	197.6448	0.0001	4.21	0.21		1	0
	5070.3[c]	197.23		1.77		10.7?	1	+1?
F4	3902.680	256.2341	0.0004	2.48	0.21	-5.603?	1?	-1?
	3908.283	255.8668	0.0003	3.43	0.21		1?	0?
F5	1911.121	523.2533	0.0016	2.33	0.22		1 or 2	?
	1928.257	518.6029	0.0021	1.77	0.22	17.136?	1 or 2	?
F6[d]	8127.845	123.0338	0.0002	1.30	0.22		guide	
2F1	7360.670	135.8572	0.0002	1.57	0.22	0.001		
F1+F2	6983.219	143.2004	0.0001	2.83	0.21	0.005		
F1+F3	8747.254	114.3216	0.0002	0.88	0.22	-7.336		
F1+F4	7588.604	131.7765	0.0004	0.64	0.22	0.015		
F1+F5	5587.599	178.9678	0.0007	0.61	0.22	3.857		
2F2	6605.802	151.3821	0.0004	0.80	0.22	-0.025		
F2+F3	8362.479	119.5818	0.0004	0.53	0.22	-0.009		
F2+F4	7210.499	138.6867	0.0006	0.48	0.22	0.672		
2F1+F2	10675.6	93.6720	0.0002	0.52	0.22	-11.994		

[a]For pulsation modes, Δf is the separation between the modes in the multiplets and the $m = 0$ member. For combination frequencies, Δf is the frequency difference between the calculated and observed combination frequency (i.e., $\Delta f = F1 + F2 - [F1 + F2]$).

[b]The m identifications in the table are based on the frequency splitting alone, not on the size of the combination peaks.

[c]We were unable to obtain a simultaneous fit with this frequency and the other two frequencies in the F3 triplet, though it does seem to be a significantly high amplitude peak above the noise.

[d]F6 is a formally significant peak that is due to the guide error of the telescope and probably does not represent a pulsation mode originating at the star.

Table 3.5: GD 244 Periods and Mode Identifications

Mode Label	Frequency (μHz)	Period (sec)	σ_p (sec)	Amplitude (mma)	σ_{amp} (mma)	Δf^a (μHz)	ℓ	m^b
F1	3255.919	307.1329	0.0001	20.18	0.17		1	-1
	3261.886	306.5712	0.0002	5.02	0.17	5.966?	1	+1
F2	3897.733	256.5594	0.0001	12.31	0.20		1?	-1?
	3903.255	256.1964	0.0001	6.73	0.20	5.522?	1?	+1?
F3	4926.697	202.9758	0.0001	4.04	0.21		1	-1?
F4	1103.656	906.0795	0.0056	1.72	0.21		≤ 3	?
$2F1^-$	6511.422	153.5763	0.0001	2.25	0.23	0.417		
$F1^-+F1^+$	6516.119	153.4656	0.0003	0.95	0.23	1.686		
$F1^-+F2^-$	7153.211	139.7974	0.0001	2.30	0.21	0.442		
$F1^-+F3^{-c}$	8182.615	122.2103	0.0002	0.96	0.21	0.001		
$2F2^-$	7795.472	128.2796	0.0001	2.44	0.21	-0.006		
$F2^-+F3^-$	8824.598	113.3196	0.0003	0.53	0.21	-0.168		

[a]For real pulsation modes, Δf is the separation between the modes in the doublets. For combination frequencies, Δf is the frequency difference between the calculated and observed combination frequency (i.e., $\Delta f = F1 + F2 - [F1 + F2]$).

[b]The m identifications in the table are based on frequency splitting alone, not on the size of the combination peaks.

[c]The period of $F1^-+F3^-$ in GD 244 is close to the period of F6 in GD 66 (see Table 3.4), so it is probable that the amplitude and frequency of this combination frequency are partially contaminated by the guide error of the telescope.

Table 3.6: Periods and Mode Identifications for Published Data with Combination Frequencies

Mode Label	Frequency (μHz)	Period (sec)	σ_p (sec)	Amplitude (mma)	σ_{amp} (mma)	Δf^a (μHz)	ℓ	m	Ref.
				G117-B15A					
F1	4646.909	215.1968	0.0007	19.15	0.39		1	0	1
F2	3288.91	304.052	0.004	6.89	0.44		1	0	1
F3	3697.47	270.455	0.004	5.47	0.45		1?	0	1
2F1	9293.68	107.600	0.004	1.06	0.45	0.14			1
F1+F2	7956.59	125.682	0.006	0.90	0.45	-20.77			1
F1+F3	8344.74	119.836	0.003	1.60	0.45	-0.36			1
F1-F2	1357.6	736.60		0.90		0.4			1
				G185-32					
F1	4635.3	215.74		1.93	0.07		1 or 2	0	2
F2	2701.2	370.21		1.62	0.07		1 or 2	0	2
F3	7048.8	141.87		1.43	0.07		3	0	2
F4	3317.8	301.41		1.13	0.07		1 or 2	0	2
F5	3335.6	299.79		0.95	0.07		1 or 2	0	2
F6	13784.9	72.54		0.93	0.07		1 or 2	0	2
2F3	14097.7	70.93		0.69	0.07	-0.1			2
F3-F6	6736.1	148.45		0.57	0.07	0.0			2

Note. − We have not included a complete list of eigenmodes for each star. Instead, we have only included eigenmodes relevant to this study. The ℓ and m identifications are from our analysis.

[a] Δf is the frequency difference between the calculated and observed combination frequency (i.e., $\Delta f = F1 + F2 - [F1 + F2]$).

References. − (1) Kepler et al. (1995b); (2) Castanheira et al. (2004).

at 142 s is the parent mode of a harmonic at 71 s. We use published measurements for G185-32 obtained from the WET campaign XCov 8 in 1992 September (Castanheira et al., 2004).

With the exception of the 142 s mode, Kepler et al. (2000b) identify all the other modes as either $\ell = 1$ or $\ell = 2$ based on HST data alone. Using independent temperature constraints they choose $\ell = 1$ for all of these modes. Under this identification, F1[9], at 215 s, is the highest amplitude $\ell = 1$ mode, and we use it to estimate the inclination. Castanheira et al. (2004) detect only one peak at 215 s, so we presume it to be the $m = 0$ component and use the neighboring noise limit to approximate the size of the $m = \pm 1$ peaks. The Pesnell (1985) method then yields $\Theta_0 = 13°$. If the inclination were greater than this, we would see the $m = \pm 1$ members of the multiplet above the noise. Our results are robust even if the ℓ identification is not; if F1 is actually an $\ell = 2$ mode, then the inclination of the star is less than 7°, and still in the range where our results are insensitive to the inclination (see Figure 2.3).

Figure 3.12 is a plot of the theoretically predicted combination frequency amplitude ratios for G185-32 (R_c with $\Theta_0 = 13°$) and the observed amplitudes of the detected combination frequencies for comparison. For clarity, the $\ell = 1, 1$ and $\ell = 2, 2$ lines are not included in Figure 3.12, but fall below the lowest line shown ($\ell = 1, 3$). Unlike the harmonics found in GD 66, GD 244, and G117-B15A, R_c for the harmonic of F3 in G185-32 is more than 50 times greater than the prediction for $\ell_i = \ell_j = 1$ and more than 15 times the prediction for $\ell_i = \ell_j = 2$. The best explanation for this is that F3 is a high ℓ mode, just as Thompson et al. (2004) claim for independent reasons. The value of ℓ that best explains our R_c is $\ell = 3$ rather than $\ell = 4$. However, in the case of high ℓ, our theory suffers from two problems. First, the geometric factor in the theory of Wu (2001) varies more

[9]Our nomenclature (see Table 3.6) does not follow Thompson et al. (2004), Castanheira et al. (2004), nor Kepler et al. (2000b). We have labeled the modes in order of highest amplitudes from the WET data.

rapidly with inclination for $\ell = 3$ and 4 (instead of the gradual changes for low ℓ shown in Figure 2.3, see Figure A.1 in Appendix A). We have accommodated this by including a range of inclinations about the 13° nominal value. We show this range as dotted lines in Figure 3.12, which indicate how R_c for $\ell_i = \ell_j = 3$ changes between $\Theta_0 = 0°$ and 20°. R_c for 2F3 falls within the prediction for $\ell_{F3} = 3$. The second problem is our use of a constant bolometric correction that is really only appropriate for $\ell = 1$. This is a limitation inherent to the analytic theory as Wu (2001) presented it, and could be addressed by employing numerical models, but this would be not be consistent with our objective of having a quick and easily applicable method for mode identification in large numbers of ZZ Ceti stars (see the discussion on error sensitivities in §2.3). We have calculated bolometric corrections for higher ℓ, and the differences are not large enough to change the $\ell = 3$ identification for F3. So the inconsistency of our $\ell = 3$ identification and the $\ell = 4$ identification of Thompson et al. (2004) remains a mystery. Fortunately, for seismological work it is useful to identify a mode as high ℓ, even if the exact value is unknown. The density of modes in the models at high ℓ is so large that they do not contribute seismological constraints because the radial overtone (k) is unknown, but misinterpreting a high ℓ mode as $\ell = 1$ or 2 would lead the models astray. So even if a mode identification method based on measurements of R_c alone cannot identify high ℓ modes precisely, it is still useful for its ability to discriminate between modes of high and low ℓ.

In addition to the identification of F3 as high ℓ, the limits on R_c for the harmonics of F1, F2, F4, F5, and F6 constrain that $\ell \leq 2$ for these modes, consistent with the tentative mode identifications of Castanheira et al. (2004). Our results are also consistent with the seismological analysis of Bradley (2006), including his high ℓ identification for F3, with the exception of his identification of F6 as high ℓ. Unfortunately, we are not able to definitively assign any ℓ values to these modes due to their intrinsically low amplitudes (see Clemens, 1994; Thompson et al., 2004). Likewise, the only detected cross term, which

is a combination with the high ℓ mode F3, is not able to narrow the choice of ℓ. Indeed, we are not even able to determine whether the mode we call F6 is a combination with F3 and a mode at 148 s or whether the latter is F3-F6. We have used the latter identification in Table 3.6, following Castanheira et al. (2004) and consistent with Bradley (2006).

3.2.2.2 Stars Without Detected Combinations

L19-2

McGraw (1977) discovered the variability of L19-2, a hot, low-amplitude ZZ Ceti star. O'Donoghue & Warner (1982) presented a comprehensive analysis of single site data, and were able to assign tentative values of ℓ to the pulsation modes. Bradley (2001) revised these identifications in light of theoretical improvements, finding three modes of $\ell = 1$ and two of $\ell = 2$. L19-2 was the subject of the WET campaign XCov 12 in 1995 April, on which Sullivan (1995) presented a preliminary paper. We have re-reduced and analyzed the archival WET data to search for combination frequencies, and found none detectable above the noise limit of the FT. We have included a sample lightcurve in Figure 3.13 and the FT of all of the L19-2 WET data in Figure 3.14.

As with GD 66, we used the prewhitening technique to measure pulsation frequencies in L19-2, and to reveal the multiplet structure in the highest amplitude modes. In Figure 3.15 we show the 192 s pulsation mode (F1) as a typical example. Figure 3.15a is the original FT in the region of F1. Figure 3.15b is the window function of the 192.61 s peak. The remaining panels show the results of our iterative fitting and removal of three pulsation frequencies. Note that there appears to be a significant residual near the $m = -1$ component. This is mysterious, but not unprecedented (Kawaler et al., 1995). We show the multiplet structure of the 113 s, 118 s, 350 s, and 143 s modes in Figures 3.16,

3.17, 3.18, and 3.19.[10] The identified periods of L19-2 are listed in Table 3.7 and presented visually in Figure 3.20. We do not detect any combination frequencies in L19-2. However, the noise level is sufficiently low, that the non-existence of combinations, particularly harmonics, constrains the ℓ values of the modes present.

Table 3.7: L19-2 Periods and Mode Identifications (WET Observations)

Mode Label	Frequency (μHz)	Period (sec)	σ_p (sec)	Amplitude (mma)	σ_{amp} (mma)	Δf^a (μHz)	ℓ	m^b
F1	5179.362	193.0740	0.0019	0.973	0.064	-12.433	1	-1
	5191.795	192.6116	0.0004	5.535	0.065		1	0
	5204.160	192.1540	0.0015	1.216	0.063	12.365	1	+1
F2	8789.054	113.7779	0.0004	1.766	0.067		1 or 2	0
	8828.619	113.2680	0.0024	0.271	0.067	39.565	1 or 2	+2
F3	8426.324	118.6757	0.0006	1.191	0.070	-11.109	1 or 2	-1
	8437.433	118.5195	0.0005	1.641	0.071		1 or 2	0
	8448.580	118.3631	0.0023	0.339	0.069	11.147	1 or 2	+1
F4	2855.785	350.1664	0.0073	0.918	0.068		1 or 2	0
	2868.023	348.6722	0.0192	0.347	0.068	12.238	1 or 2	+1
F5	6954.415	143.7935	0.0047	0.228	0.069	-18.112	≤ 3	-1?
	6972.527	143.4200	0.0030	0.354	0.070		≤ 3	0
	6991.176	143.0375	0.0031	0.341	0.069	18.649	≤ 3	+1

[a] Δf is the separation between the modes in the multiplets and the $m = 0$ member.
[b] The m identifications in the table are based on frequency splitting alone, not on the size of the combination peak limits.

We have used the multiplet structure at 192 s (F1) in Figure 3.15 to estimate the inclination of the pulsation axis of L19-2, finding an inclination of 16°. In Figure 3.21, we have plotted the theoretical predictions for combination frequency amplitudes in L19-2 (R_c with $\Theta_0 = 16°$). Instead of measured ratios for R_c, we have included the observed noise limit (indicated by the filled squares, crosses, open squares, and a star) at the frequencies where we expect combinations to be detected. The downward arrows indicate that all data points are limits on detections. The limit for the harmonic of F1 implies that mode is $\ell = 1$, which

[10] The deconstruction of F5 (143 s) is particularly interesting because of the confirmation of a peak at 143.79 s as predicted by O'Donoghue & Warner (1982).

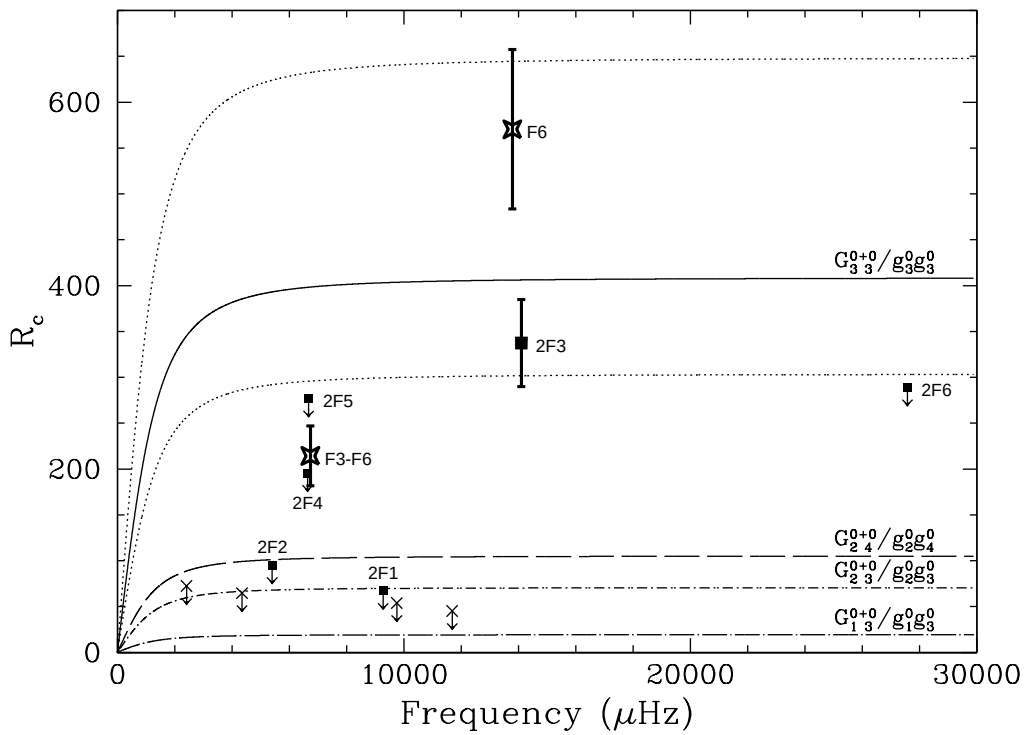

Figure 3.12: Ratio of combination to parent mode amplitudes (R_c) for G185-32. The lines are theoretical predictions for $G^{0+0}_{3\ 3}/g^0_3g^0_3(\Theta_0 = 13°)$ (solid line), $G^{0+0}_{2\ 4}/g^0_2g^0_4(\Theta_0 = 13°)$ (long-dashed line), $G^{0+0}_{2\ 3}/g^0_2g^0_3(\Theta_0 = 13°)$ (dot-dashed line), and $G^{0+0}_{1\ 3}/g^0_1g^0_3(\Theta_0 = 13°)$ (dot-long-dashed line). The data points are the detected harmonics or limits (filled squares), detected cross combination frequencies (stars), and limits for the cross combinations involving the F3 pulsation mode only (crosses). The downward arrows on the limits indicate that the points represent maximum values. The dotted lines on either side of the $\ell_i = \ell_j = 3$ line are the R_c predictions for extremum in inclination: $\Theta_0 = 20°$ (top) and $\Theta_0 = 0°$ (bottom). the predictions of Wu (2001) for $G^{0+0}_{4\ 4}/g^0_4g^0_4(\Theta_0 = 13°)$ are not shown because they reach values above $R_c \sim 3600$.

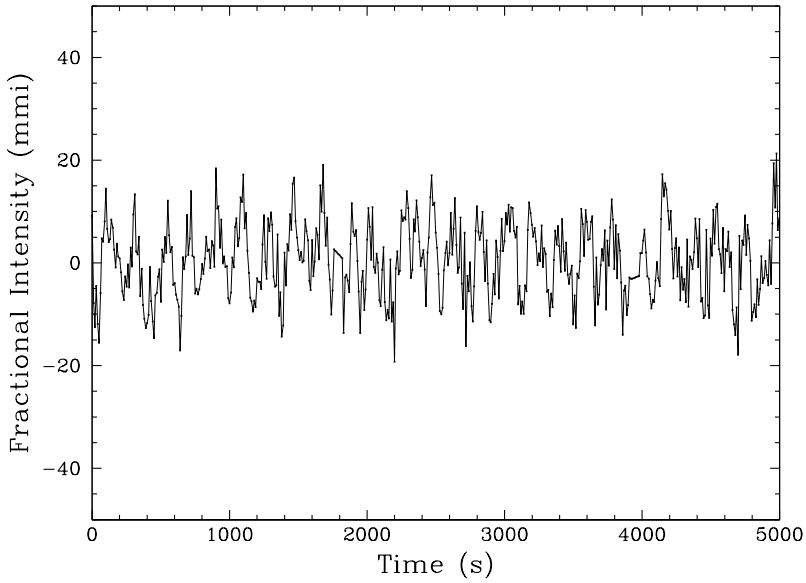

Figure 3.13: Lightcurve of L19-2 (WET observations). These data were acquired as part of the WET campaign XCov 12 in 1995 April with an exposure time of 10 s.

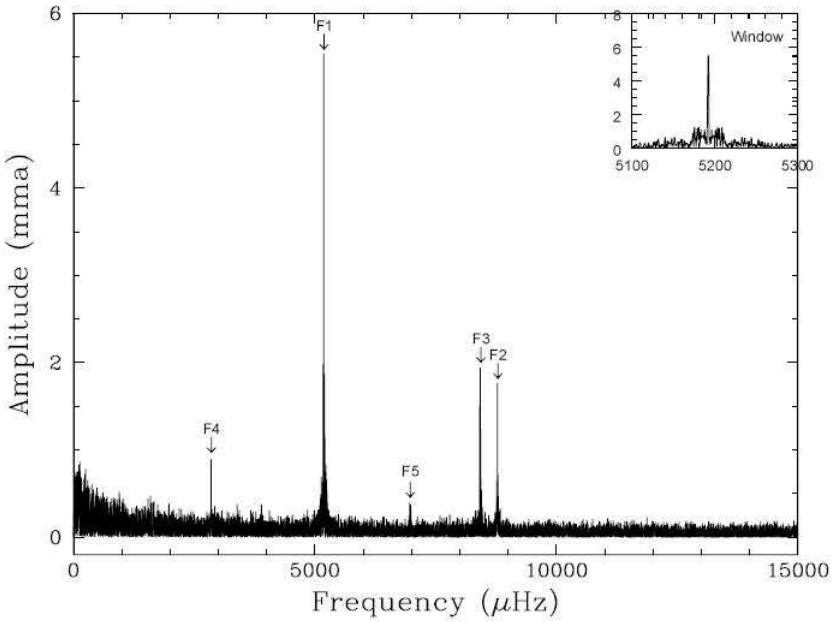

Figure 3.14: Fourier transform of L19-2 (WET observations). This FT includes all data listed in Table 3.2. We indicate the five pulsation modes that we reference in Table 3.7.

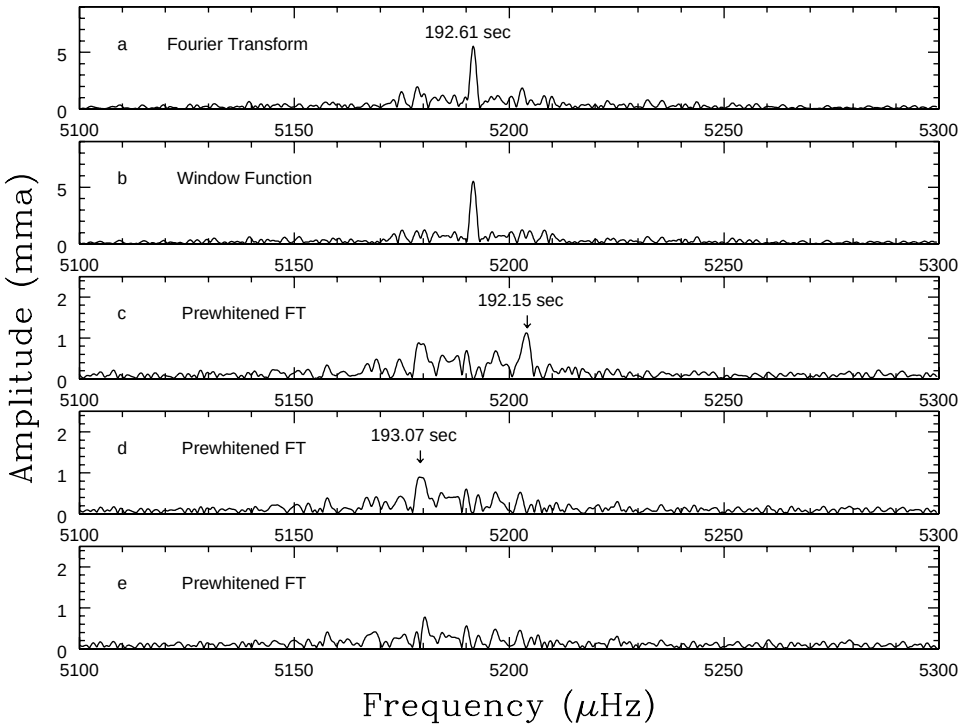

Figure 3.15: Deconstruction of F1 in L19-2. a: A Fourier transform of L19-2 near 192 s (F1). b: A window function obtained by taking an FT of a single sinusoid (with the same period and amplitude of the 192.61 s peak) that has been sampled in the same manner as the data. c: An FT near F1 with a period of 192.61 s removed. d: An FT near F1 with periods of 192.61 and 192.15 s removed. e: An FT near F1 with periods of 192.61, 192.15, and 193.08 s removed.

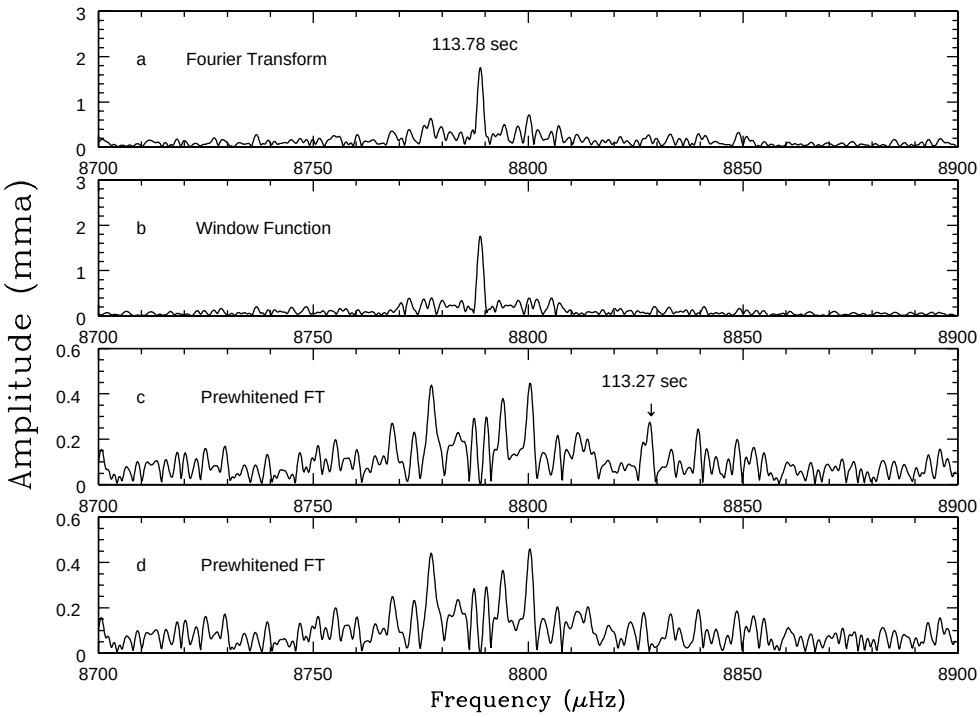

Figure 3.16: Deconstruction of F2 in L19-2. a: A Fourier transform of L19-2 near 113 s (F2). b: A window function obtained by taking an FT of a single sinusoid (with the same period and amplitude of the 113.78 s peak) that has been sampled in the same manner as the data. c: An FT near F2 with a period of 113.78 s removed. d: An FT near F2 with periods of 113.78 and 113.27 s removed. Note that the peak of 113.27 in panel c was not the highest amplitude peak remaining in the prewhitened FT. We chose this peak among the noise because of its pre-established presence in the FTs of O'Donoghue & Warner (1982).

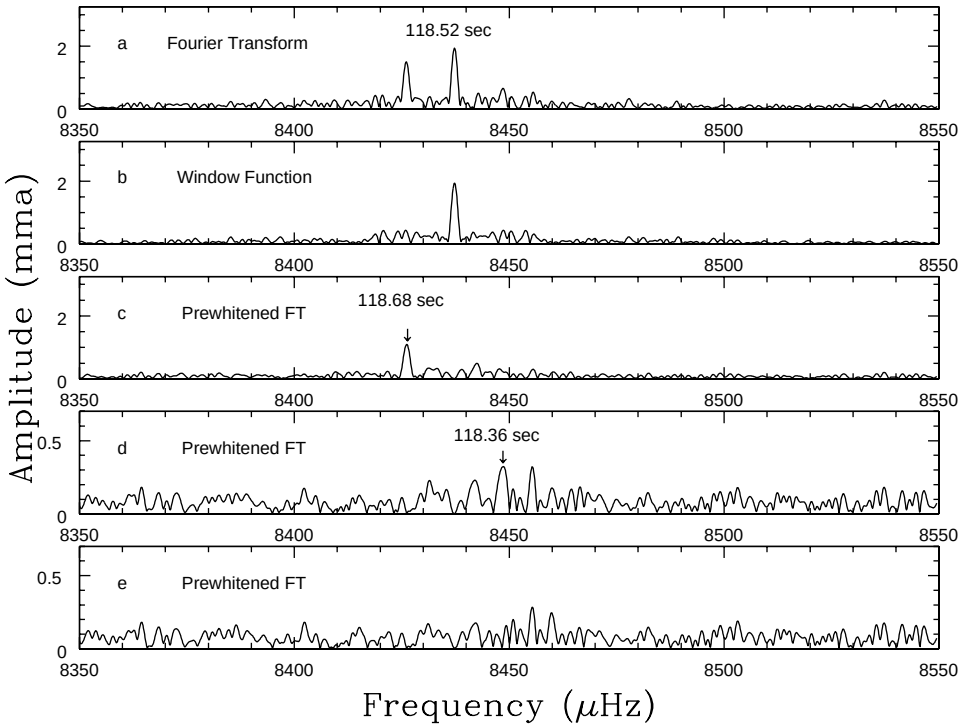

Figure 3.17: Deconstruction of F3 in L19-2. a: A Fourier transform of L19-2 near 118 s (F3). b: A window function obtained by taking an FT of a single sinusoid (with the same period and amplitude of the 118.52 s peak) that has been sampled in the same manner as the data. c: An FT near F3 with a period of 118.52 s removed. d: An FT near F3 with periods of 118.52 and 118.68 s removed. e: An FT near F3 with periods of 118.52, 118.68, and 118.36 s removed.

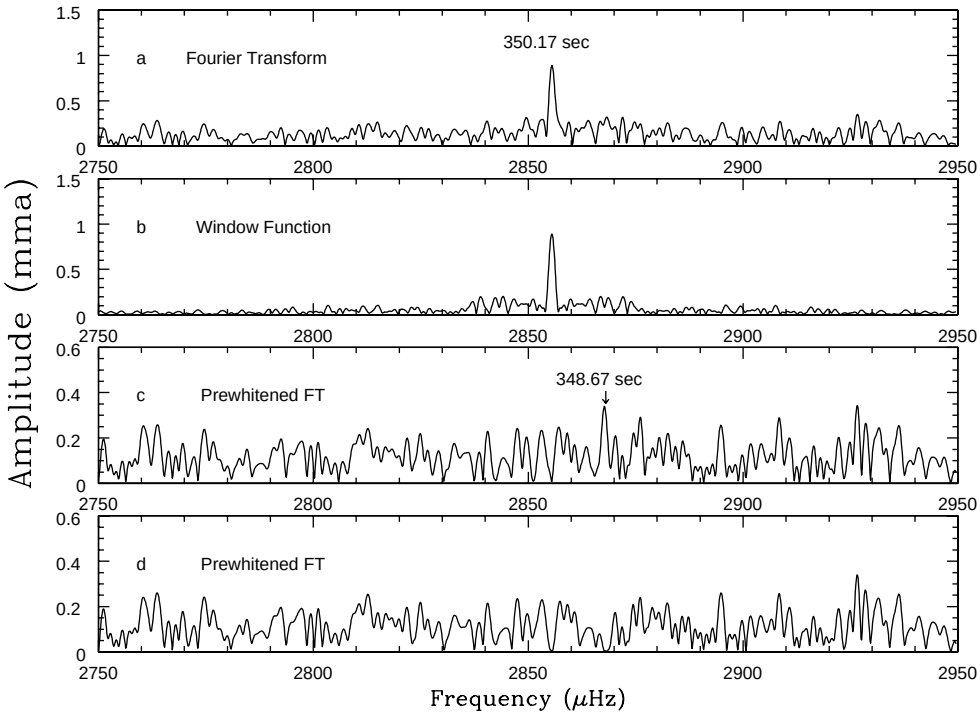

Figure 3.18: Deconstruction of F4 in L19-2. a: A Fourier transform of L19-2 near 350 s (F4). b: A window function obtained by taking an FT of a single sinusoid (with the same period and amplitude of the 350.17 s peak) that has been sampled in the same manner as the data. c: An FT near F4 with a period of 350.17 s removed. d: An FT near F4 with periods of 350.17 and 348.67 s removed.

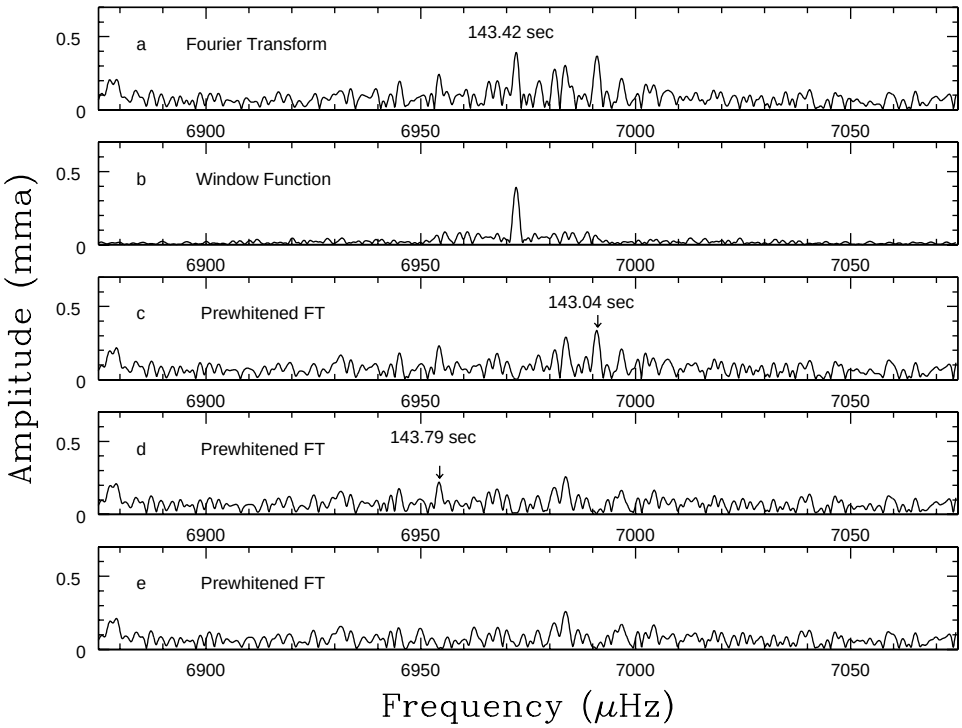

Figure 3.19: Deconstruction of F5 in L19-2. a: A Fourier transform of L19-2 near 143 s (F5). b: A window function obtained by taking an FT of a single sinusoid (with the same period and amplitude of the 143.42 s peak) that has been sampled in the same manner as the data. c: An FT near F5 with a period of 143.42 s removed. d: An FT near F5 with periods of 143.42 and 143.04 s removed. e: An FT near F5 with periods of 143.42, 143.04, and 143.79 s removed. This tentative identification of a peak at 143.79 s confirms predictions made by O'Donoghue & Warner (1982).

is consistent with how Bradley (2001) identified it based on its multiplet structure. The limits for F2, F3, and F4 imply that they are $\ell \leq 2$, again consistent with the multiplet structure that suggests F2 is $\ell = 2$ and F3 and F4 are $\ell = 1$ (Bradley, 2001). The limit for 2F5 constrains F5 to be $\ell \leq 3$.

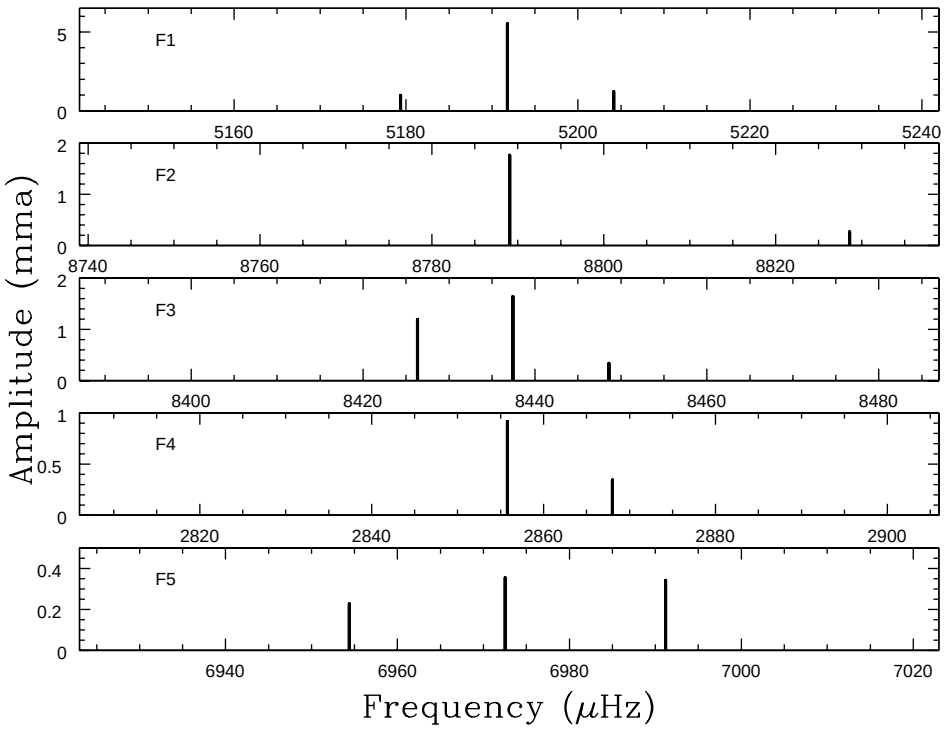

Figure 3.20: Prewhitened peaks in L19-2 Fourier transform (WET observations).

It is gratifying to find that non-detections of combination frequencies can provide useful seismological information, and that these corroborate independent methods in the case of L19-2. We note that the predictions of Wu (2001) suggest that the WET data are at the threshold of detecting the combination frequencies in L19-2. Larger telescope data on this star might be useful as a further test of the reliability of the theory of Wu (2001) for mode identification.

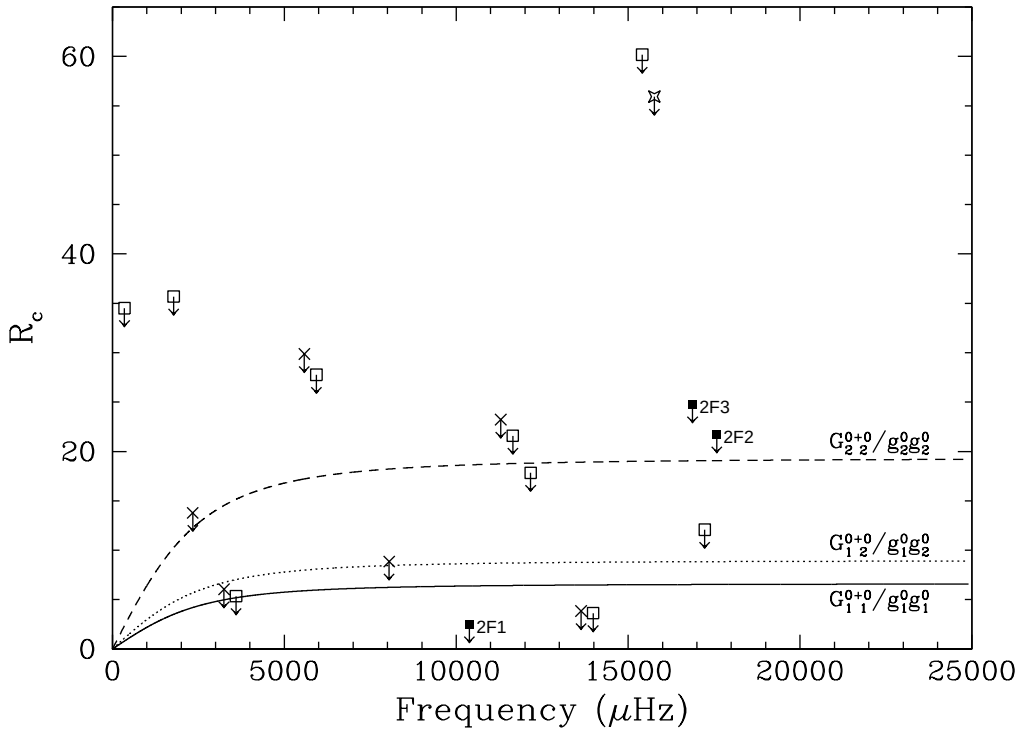

Figure 3.21: Ratio of combination to parent mode amplitudes (R_c) for L19-2 (WET observations). The lines are theoretical predictions for $G^{0+0}_{1\ 1}/g^0_1g^0_1(\Theta_0 = 16°)$ (solid line), $G^{0+0}_{1\ 2}/g^0_1g^0_2(\Theta_0 = 16°)$ (dotted line), and $G^{0+0}_{2\ 2}/g^0_2g^0_2(\Theta_0 = 16°)$ (dashed line). The data points are the limits on the harmonics (filled squares) and limits for the cross combinations for the presumed (Bradley, 2001) $\ell = 1, 1$ combinations (crosses), $\ell = 1, 2$ combinations (open squares), and an $\ell = 2, 2$ combination (star). The downward arrows on the limits indicate that the points represent maximum values.

GD 165

The pulsation pattern of GD 165 is very similar to that of L19-2. Both have their two primary pulsations near 120 and 193 s. Bergeron & McGraw (1990) discovered GD 165 to be a ZZ Ceti star as predicted by temperatures acquired from spectroscopic analysis placing it within the theoretical ZZ Ceti instability strip.

We included the data for GD 165 from WET observations (XCov 5, 1990 May) and from lightcurves obtained with the CFHT presented in an analysis by

Bergeron et al. (1993). The two primary pulsations of GD 165 have multiplet structure, to which we applied the Pesnell (1985) method and found 25° for the inclination.

Table 3.8: Periods and Mode Identifications for Published Data without Combination Frequencies

Mode Label	Frequency (μHz)	Period (sec)	σ_p (sec)	Amplitude (mma)	σ_{amp} (mma)	Δf^a (μHz)	ℓ	m^b	Ref.
				GD 165					
F1	8305.96	120.39543		1.76		-2.73	1?	-1	1
	8308.69	120.35585		4.79			1?	0	1
	8311.24	120.31905		1.36		2.55	1?	+1	1
F2	5187.02	192.78879		0.85		-2.98	1 or 2	-1	1
	5190.00	192.67841		2.35			1 or 2	0	1
	5192.82	192.57373		1.91		2.82	1 or 2	+1	1
F3[c]	3989.2	250.6797		0.6		-7.8	1 or 2	-1?	1
	3997.0	250.1864		1.0			1 or 2	0	1
				R548[d]					
F1	4691.915	213.1326		6.7			1	-1	2
	4699.946	212.7684		4.1		8.031	1	+1	2
F2	3639.348	274.7745		2.9			1	-1	2
	3646.297	274.2508		4.1		6.949	1	+1	2
F3	2997.25	333.639	0.001	1.03	0.13		1 or 2	0?	2
F4	3143.92	318.074	0.001	1.10	0.13		1 or 2	0?	2
F5	5339.43	187.286	0.001	0.43	0.12		1 or 2	0?	2
				G226-29					
F1	9134.7234	109.47239	0.00019	2.82	0.10	-16.2175	1	-1	3
	9150.9409	109.27838	0.00051	1.08	0.10		1	0	3
	9167.0187	109.08672	0.00022	2.49	0.10	16.0778	1	+1	3

Note. – The ℓ identifications are from our analysis.

[a]Δf is the separation between the modes in the multiplets and the $m = 0$ member.

[b]The m identifications for GD 165 are based on frequency splitting alone, not on the size of the combination peak limits.

[c]Bergeron et al. (1993) listed F3 from the WET data set, but not from the combined CFHT and WET data set. They identified the $m = -1$ member as questionable.

[d]The pulsation modes F3, F4, and F5 are those found in the 2001 data set of Mukadam et al. (2003).

References. – (1) Bergeron et al. (1993); (2) Mukadam et al. (2003); (3) Kepler et al. (1995a).

Bergeron et al. (1993) did not report finding any combination frequencies in the WET and CFHT combined data for GD 165. In Figure 3.22, we have plotted the theoretical predictions for GD 165 (R_c with $\Theta_0 = 25°$) along with the observed noise limits for putative combination peaks. Once again the limits

alone are sufficient to constrain F1 tentatively as $\ell = 1$, and the other modes to be $\ell \leq 2$, consistent with the $\ell = 1$ identifications for each mode determined by Bradley (2001) based on the multiplet structure. We list our mode identifications in Table 3.8.

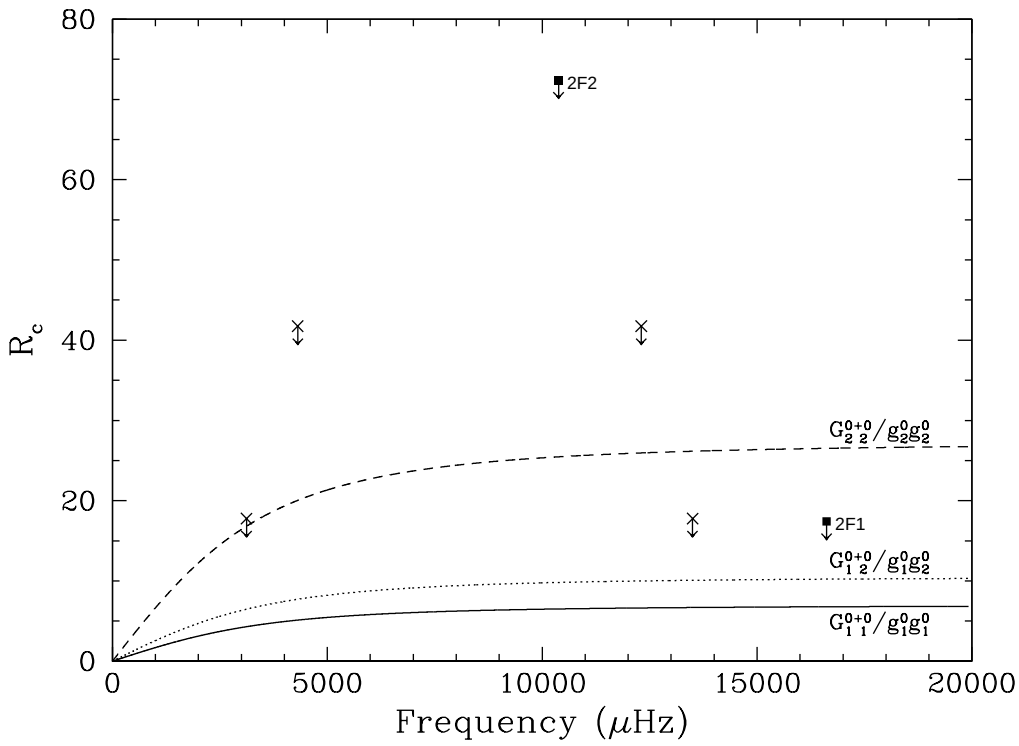

Figure 3.22: Ratio of combination to parent mode amplitudes (R_c) for GD 165. The lines are theoretical predictions for $G^{0+0}_{1\ 1}/g^0_1g^0_1(\Theta_0 = 25°)$ (solid line), $G^{0+0}_{1\ 2}/g^0_1g^0_2(\Theta_0 = 25°)$ (dotted line), and $G^{0+0}_{2\ 2}/g^0_2g^0_2(\Theta_0 = 25°)$ (dashed line). The data points are the limits on the harmonics (filled squares) and limits for the cross combinations (crosses). The downward arrows on the limits indicate that the points represent maximum values.

R548

R548, also called ZZ Ceti, is the prototype of this class of stars, and is one of the brightest and hottest. Lasker & Hesser (1971) discovered R548 to be variable. Its primary pulsation modes are doublets at 213 and 274 s. Like G117-B15A, R548 has a very stable pulsation mode at 213 s (Mukadam et al., 2003).

The data for R548 were gathered in the WET campaigns XCov 18 in 1999 November and XCov 20 in 2000 November, with additional data from the CFHT and the McDonald Observatory (Mukadam et al., 2003). The pulsation periods and amplitudes for R548 have been taken from Mukadam et al. (2003) and are listed in Table 3.8. As with our assumption for GD 244, Bradley (1998) suggests that the doublet structure in F1 and F2 results from viewing $\ell = 1$ modes at high inclination so that the third (central, $m = 0$) mode does not appear. Using the maximum amplitude of the prewhitened FT of F1, at 213 s, as an estimate on the amplitude of the $m = 0$ peak, we find the minimum possible inclination for R548 to be 79°. Unlike GD 244, another high inclination star, we do not detect combination frequencies in R548.

In Figure 3.23, we have plotted the predictions for R548 (R_c with $\Theta_0 = 79°$). We include the observed noise limit (indicated by the filled squares, crosses, open squares, and stars) at the frequencies where we expect combinations to be detected. The limits on the harmonics of F1 and F2 do not uniquely identify these modes, but only require that $\ell \leq 2$ for both. $2F1^-$ appears to constrain F1 to be $\ell = 1$, but the line below it at the bottom of the Figure is an $\ell = 2, 2$ combination for $m = 2$. However, the limits on the cross combination peaks at the sum of the $m = -1$ and $m = +1$ parent modes do require F1 and F2 to be $\ell = 1$ modes (see the circles in Figure 3.23), which agrees with the identifications of Bradley (1998). The limits for the harmonics of the F3, F4, and F5 singlets are sufficient to imply that they are $\ell \leq 2$ if $m = 0$, again consistent with the $\ell = 2$ identification of Bradley (1998). As with L19-2, the predictions of Wu (2001) suggest that these data are on the threshold of detecting the combination frequencies for the two dominant modes in R548.

G226-29

G226-29 is the brightest known ZZ Ceti star because of its proximity ($d = 11.0$ pc, $m_v = 12.22$; Kepler et al., 1995a). J. T. McGraw & G. Fontaine (1980,

unpublished results) discovered its variability, finding only one pulsation mode at 109 s that is rotationally split into a triplet. G226-29 is one of the hottest of the 105 known single-star system ZZ Ceti stars (see Kepler et al., 2005; Voss et al., 2006, and references therein), and Kepler et al. (2000b) suggest that we are observing G226-29 just as it enters the instability strip.

We included data for G226-29 from the WET campaign XCov 7 in 1992 February presented in Kepler et al. (1995a). We found the inclination to be 74° by assuming the evenly spaced triplet is an $\ell = 1$ mode. As discussed previously, our results do not depend sensitively on this assumption. Kepler et al. (1995a) did not detect combination frequencies in G226-29. In Figure 3.24, we have plotted the predictions for G226-29 (R_c with $\Theta_0 = 74°$). We include the observed noise limit (indicated by the filled squares, crosses, and an open square) at the frequencies where we expect combinations to be detected. The limits for the harmonics of each member of the triplet do not uniquely identify F1, but only require that $\ell \leq 2$. As with R548, another high inclination star with detected $m = \pm 1$ multiplet members, it is the limit on the cross combination peak at the sum of the $m = -1$ and $m = +1$ parent modes that require the G226-29 F1 mode to be $\ell = 1$. This result is consistent with the time-resolved UV spectroscopy data from HST presented in Kepler et al. (2000b). As with L19-2 and R548, the predictions of Wu (2001) suggest that these data are on the threshold of detecting the combination frequencies in G226-29.

3.3 Conclusions

The main result of our study is that combination frequencies, particularly harmonics, in the lightcurves of hot ZZ Ceti stars can be used along with the theory of Wu (2001) to constrain and in many cases to determine uniquely the spherical harmonic index (ℓ) of the modes that produced them. The first and easiest result to achieve with this method is to identify those modes with $\ell > 2$

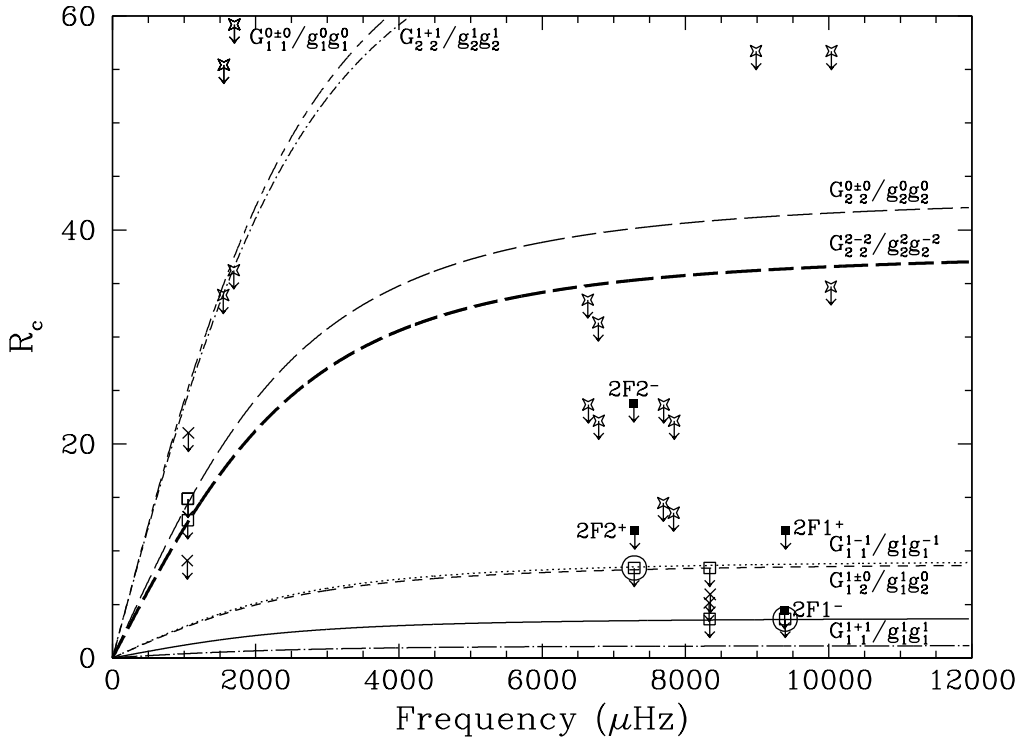

Figure 3.23: Ratio of combination to parent mode amplitudes (R_c) for R548. The lines are theoretical predictions for $G^{0\pm0}_{1\ 1}/g^0_1g^0_1(\Theta_0 = 79°)$ (long-short-dashed line), $G^{1+1}_{2\ 2}/g^1_2g^1_2(\Theta_0 = 79°)$ (dot-dashed line), $G^{0\pm0}_{2\ 2}/g^0_2g^0_2(\Theta_0 = 79°)$ (long-dashed line), $G^{2-2}_{2\ 2}/g^2_2g^{-2}_2(\Theta_0 = 79°)$ (bold long-dashed line), $G^{1-1}_{1\ 1}/g^1_1g^{-1}_1(\Theta_0 = 79°)$ (dotted line), $G^{1\pm0}_{1\ 2}/g^1_1g^0_2(\Theta_0 = 79°)$ (dashed line), $G^{1+1}_{1\ 1}/g^1_1g^1_1(\Theta_0 = 79°)$ (solid line), $G^{1\pm0}_{1\ 1}/g^1_1g^0_1(\Theta_0 = 79°)$ (solid line, not labeled because of space), and $G^{2+2}_{2\ 2}/g^2_2g^2_2(\Theta_0 = 79°)$ (dot-long-dashed line, not labeled). The data points are the limits on the harmonics (filled squares), limits for the same-m cross combinations (crosses), limits for the different-m cross combinations (open squares), and limits for the cross combinations between one of the doublet modes (F1 or F2) and one of the lower amplitude singlet modes (stars). The downward arrows on the limits indicate that the points represent maximum values. The open square limits for F1$^-$+F1$^+$ and F2$^-$+F2$^+$ are circled for easier identification.

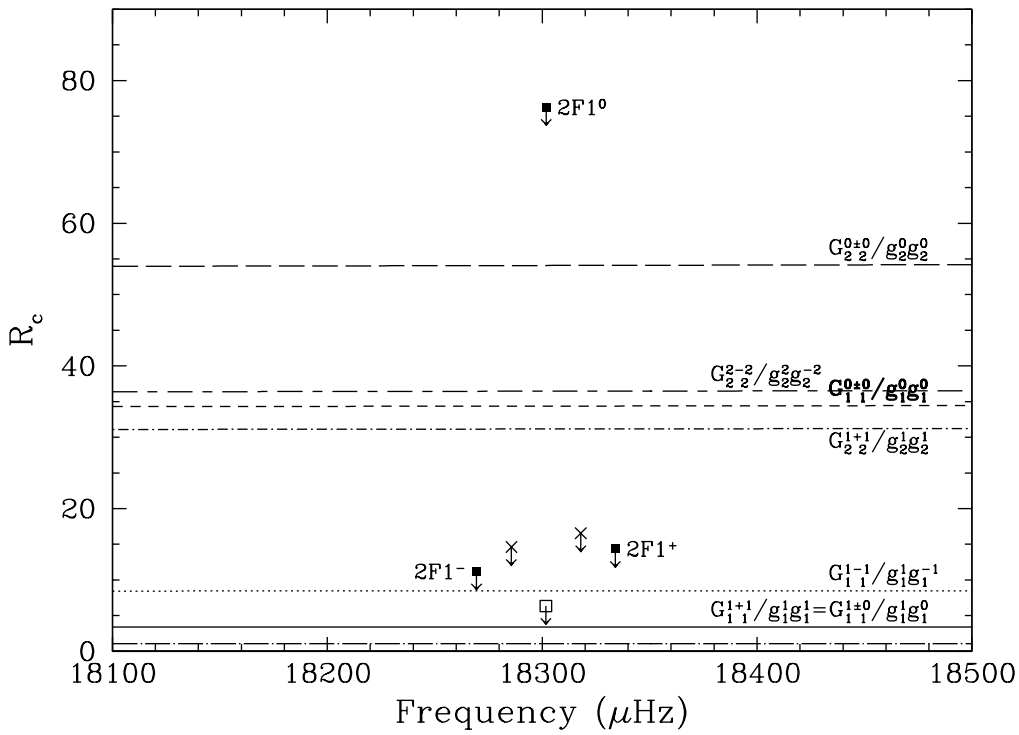

Figure 3.24: Ratio of combination to parent mode amplitudes (R_c) for G226-29. The lines are theoretical predictions for $G^{0\pm0}_{2\ 2}/g^0_2g^0_2(\Theta_0 = 74°)$ (long-dashed line), $G^{2-2}_{2\ 2}/g^2_2g^{-2}_2(\Theta_0 = 74°)$ (long-short-dashed line), $G^{0\pm0}_{1\ 1}/g^0_1g^0_1(\Theta_0 = 74°)$ (dashed line), $G^{1+1}_{2\ 2}/g^1_2g^1_2(\Theta_0 = 74°)$ (dot-dashed line), $G^{1-1}_{1\ 1}/g^1_1g^{-1}_1(\Theta_0 = 74°)$ (dotted line), $G^{1+1}_{1\ 1}/g^1_1g^1_1(\Theta_0 = 74°)$ (solid line), $G^{1\pm0}_{1\ 1}/g^1_1g^0_1(\Theta_0 = 74°)$ (solid line), and $G^{2+2}_{2\ 2}/g^2_2g^2_2(\Theta_0 = 74°)$ (dot-long-dashed line, not labeled because of space). Theoretical lines for $G^{2\pm0}_{2\ 2}/g^2_2g^0_2(\Theta_0 = 74°)$ and $G^{1\pm0}_{2\ 2}/g^1_2g^0_2(\Theta_0 = 74°)$ are not shown because they are very near to the predictions for $G^{1\pm0}_{1\ 1}/g^1_1g^0_1(\Theta_0 = 74°)$. The data points are the limits on the harmonics (filled squares), a limit for the nonzero different-m cross combination (open square), and limits for the cross combinations between the $m \neq 0$ modes and the central $m = 0$ mode (crosses). The downward arrows on the limits indicate that the points represent maximum values.

and those with $\ell \leq 2$. This alone is useful for significantly reducing the number of seismological models that need to be considered for a given star (Bradley, 1996). The theoretical mode spectrum at $\ell = 3$ and higher is so dense that there are many possible model fits to the typically sparse number of detected modes. By eliminating from consideration the high ℓ modes, the possibility of identifying a unique fit is improved. With the exception of a few small amplitude modes, in this chapter we have successfully eliminated $\ell > 2$ identification for all modes in seven of the eight stars in our study. The eighth star, G185-32, was previously thought to have a high ℓ mode (Thompson et al., 2004), and our method confirms this result (though we get $\ell = 3$ instead of $\ell = 4$).

For modes with sufficiently large amplitude, combination frequency amplitudes are further able to discriminate between $\ell = 1$ and $\ell = 2$, primarily through the use of harmonics. The harmonics are superior for this purpose because they are known to be same-ℓ combinations, and because same-ℓ combinations are well-separated in the theoretical plots of R_c. We were able to identify modes as $\ell = 1$ in six of the eight stars, and in every case our identifications agreed with any previous independent results.

The method we have used requires only time-series photometry and simple calculations as presented in Chapter 2. The essential part of these calculations is the evaluation of the geometric term in the theory of Wu (2001), which we have named $\mathcal{G}$. Calculating $\mathcal{G}$ requires the evaluation of integrals of spherical harmonics in the presence of a limb darkening law. To assist others in application of this technique, we have included tabulated matrices of combination frequency integrals for $\ell \leq 4$ in Appendix A. Applying these requires a straightforward estimation of the inclination, which we have done using multiplet amplitudes, where detected, and limits on the sizes of multiplet members where not detected. This has required that we assume that modes of every m are excited to the same amplitude in every mode, and that rotation always removes the frequency degeneracy of multiplet members. Fortunately, our results are not highly sensitive

to these assumptions.

In addition to our application of this method to eight stars, we have presented analyses of new data on GD 66 and GD 244 that will be useful for seismological study of these objects. We have not been able to definitively decompose the multiplet structure in these stars with single-site data, but the mode periods we have measured are given in Tables 3.4 and 3.5 for comparison to seismological models.

More important than the results for these individual stars is our verification of a quick and easy diagnostic tool that frequently yields definitive results. We hope the method will find broad and immediate application in the study of numerous ZZ Ceti stars being discovered with the SDSS (see Mukadam et al., 2004b; Mullally et al., 2005). Most of these are fainter than the objects we have measured, but photometry on a 4 m class telescope will be sufficient to reach useful detection limits. For example, if the V=15.56 mag star GD 66 were instead an 18th magnitude star, observations with a 4 m class telescope would reveal four of the combination frequency peaks that we identified, including the harmonics of the two highest amplitude peaks. Further study of the objects in this chapter will also be useful, both to secure definitive ℓ identifications of the smaller amplitude modes and to detect those combinations that hover just below the detection limits of the present data. We discuss observations using the 4.1 m SOAR Telescope in Chapter 4.

Chapter 4

Photometric Mode Identification for L19-2 with the SOAR Telescope

Dr. Peter Venkman: *Ray has gone bye-bye, Egon ... what've you got left?*

Dr. Egon Spengler: *Sorry, Venkman, I'm terrified beyond the capacity for rational thought.*

— Ghostbusters

4.1 Introduction

For nearly three decades, since its discovery by McGraw (1977), the hot, low-amplitude DAV (H atmosphere, variable) white dwarf star L19-2 has been the subject of study. O'Donoghue & Warner (1982, 1987) presented a comprehensive analysis of extensive single site data, and were able to assign tentative values of ℓ to the pulsation modes. Bradley (2001) revised these identifications in light of theoretical improvements, finding three modes of $\ell = 1$ and two of $\ell = 2$. In 1995 April, L19-2 was the subject of the WET campaign XCov 12, on which Sullivan

(1995) presented a preliminary paper. In Chapter 3, we re-reduced and analyzed the archival WET data to search for combination frequencies, and found none detectable above the noise limit of the Fourier transform (FT). In general, these combination frequencies, sum and difference frequencies and harmonics identified in FTs, result from the nonlinear behavior of pulse shapes. In this chapter, we apply our mode identification method that utilizes combination frequency amplitudes to the small amplitude DAV (ZZ Ceti) white dwarf star L19-2. Here, we present new data acquired in 2005 May from the 4.1 m SOAR Telescope.

L19-2 falls into the class of HDAV stars, which are low amplitude pulsators that have been shown to lie at the high temperature end of the instability strip and have short, stable pulsation periods (Winget & Fontaine, 1982; Clemens, 1994). The DAV stars are subdivided into the HDAV (hot) and CDAV (cool) groups, based on their pulsation property differences. Although the stars in the HDAV group exhibit fewer modes than those of the CDAV group, L19-2 has a comparably rich mode spectrum with five eigenmodes.

Although L19-2 did not exhibit detectable combination frequencies within the limits of the WET data discussed in Chapter 3, we showed that the limits of non-detected harmonics can constrain the identity of the modes. We found the highest amplitude mode at 192 s to be $\ell = 1$, constrained the three modes at 113, 118, and 350 s to be $\ell \leq 2$, and constrained the lowest amplitude mode at 143 s to be $\ell \leq 3$. These results are all consistent with the analysis of Bradley (2001).

The noise level of the L19-2 WET data set is low, very near the predicted detection limit for the harmonics of the two largest amplitude modes ($\sqrt{\langle P \rangle} \sim 0.1$ mma, where $\langle P \rangle$ is the average power of the FT in the region of the harmonics). In Chapter 3, we anticipated that observations with a 4 m class telescope would reveal previously undetected harmonics for L19-2, further constraining mode identifications for this star and justifying the theory of Wu (2001) as a reliable mode identification method. However, we are unable to detect new harmonics

for L19-2. Because of weather and time constraints, we were only able to acquire 8.13 hours of data for L19-2 with the SOAR Telescope. As a consequence, the noise level ($\sqrt{\langle P \rangle}$) for the SOAR data presented in this chapter is twice that of the WET data set considered in Chapter 3.

In §4.2 we present the new SOAR data for L19-2 and compare the theoretical predictions of Wu (2001) with these observations. In §4.3 we summarize our results and emphasize the need for future application of the technique to large samples of ZZ Ceti stars.

4.2 Data Reduction and Analysis

In §4.2.1, we present and describe our observations of L19-2 with the SOAR 4.1 m Telescope. In §4.2.2, we give a full description of the data reduction process. The purpose of this subsection is to extract mode frequencies and amplitudes via Fourier methods. Finally, in §4.2.3, we provide our analysis using the theory of Wu (2001) and present an updated evaluation of the modes in L19-2. We record the upper limit of the noise level ($\sqrt{\langle P \rangle}$) to compare the size of the harmonics and combination frequencies to the theory.

4.2.1 Observations

We obtained time-series photometry data on L19-2 in 2005 with the SOAR 4.1 m Telescope using the Goodman High Throughput Spectrograph in imaging mode with no filter (Clemens et al., 2004; Crain et al., 2004) and an Apogee AP10 CCD camera that we are temporarily using to commission the spectrograph (see López-Morales & Clemens, 2004, for camera characterization). At the time of our observations, the dewar and detector for the Goodman Spectrograph were not ready for use. We designed and built an attachment for the Apogee CCD camera allowing us to use it with the Goodman Spectrograph. We show drawings from our computer aided design in Figure 4.1. Figure 4.2 shows a photograph of

the CCD housed in the attachment.

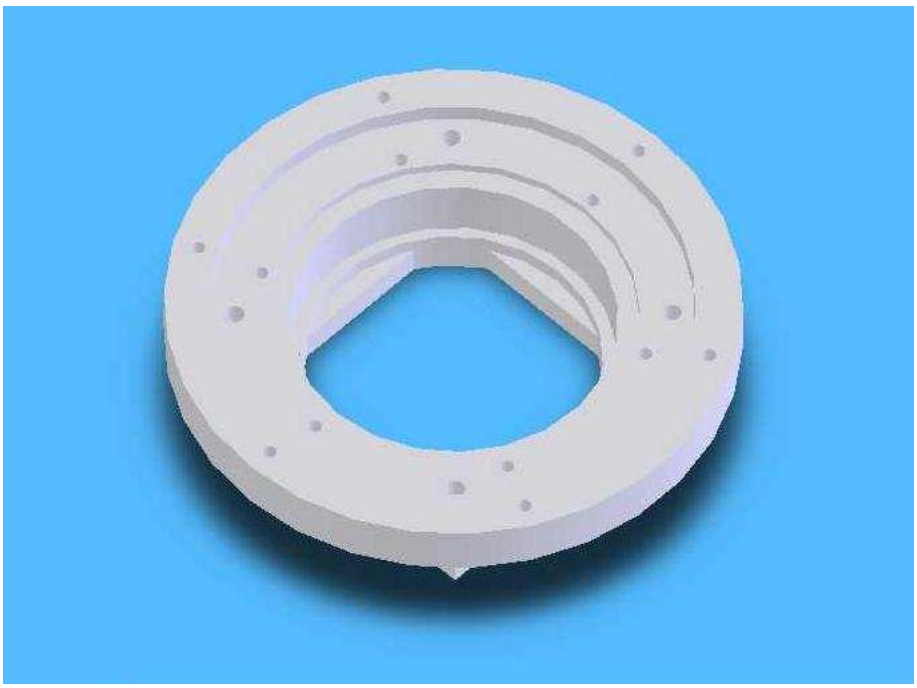

Figure 4.1: Drawing of attachment for Apogee CCD camera. We designed this attachment to house the CCD camera and fit against the Goodman Spectrograph temporarily.

We observed L19-2 on four consecutive nights totaling 29,270 s of data as indicated in the Journal of Observations, Table 4.1. We used an integration time of 10 s for the observations.

4.2.2 Data Reduction

We performed a complete reduction of the L19-2 data using the methods described by Mukadam et al. (2004b). We used weighted circular aperture photometry to create sky-subtracted lightcurves for each of the runs listed in Table 4.1. We then divided each lightcurve by the brightest comparison star (see Figure 4.3) and fitted a polynomial to each lightcurve to bring each run to the same fractional amplitude scale. We calculated the Barycentric Julian Ephemeris Date for the start-time of each run to convert the times to Barycentric Coordinated Time

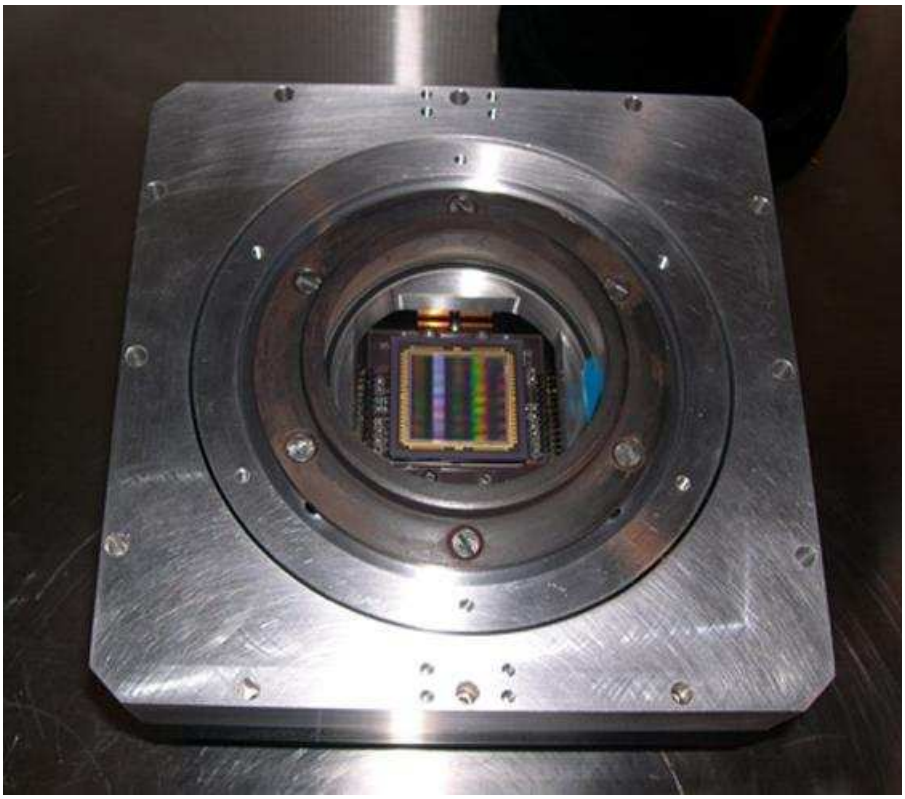

Figure 4.2: Photograph of attachment for Apogee CCD camera. The CCD can be seen in the center of the attachment.

Table 4.1: Journal of Observations for L19-2 (SOAR Telescope Observations)

Date (UT)	Start Time (UT)	Length (sec)	Integration Time (sec)
2005 May 19	07:31:59.7	7060	10
2005 May 20	09:01:58.7	3000	10
2005 May 21	02:23:28.7	16830	10
2005 May 22	07:41:30.0	2380	10

Note. − All observations were made with the SOAR 4.1 m Telescope.

(TCB). To identify the pulsation modes and possible combination frequencies of L19-2, we combined all of the lightcurves and computed a discrete FT. We have included a sample lightcurve in Figure 4.4 and the FT of all L19-2 data in Figure 4.5.

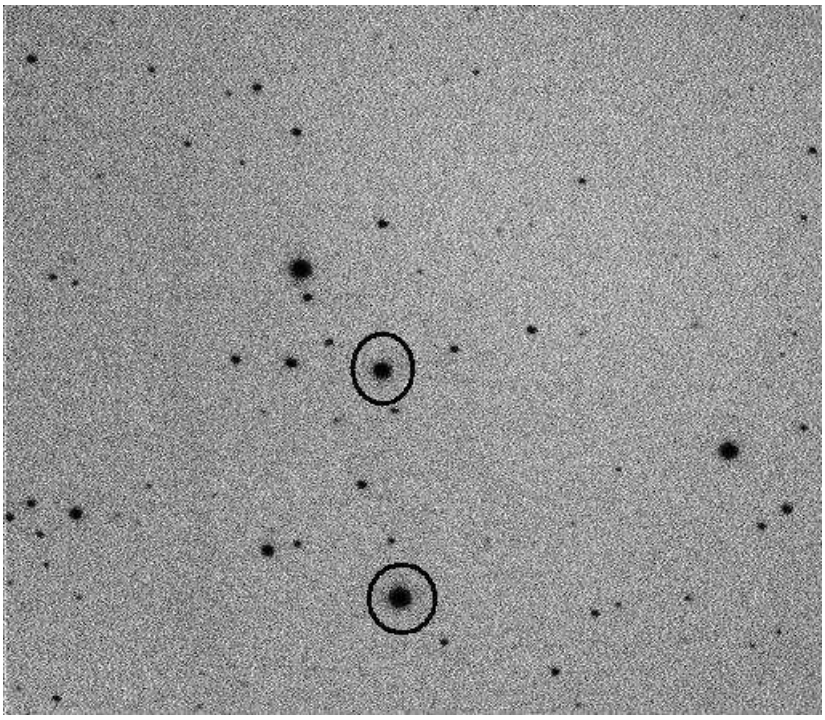

Figure 4.3: CCD image of L19-2. This CCD image was acquired with the Goodman Spectrograph on the 4.1 m SOAR Telescope on 21 May 2005 with an exposure time of 10 s. L19-2 (circled) is located near the center of the image. We divided each lightcurve by the brightest comparison star, which is circled in the bottom-center of the image.

To identify closely spaced modes in the regions of obvious excess power, we utilized a prewhitening technique similar to that of O'Donoghue & Warner (1982) using an iterative nonlinear least squares procedure. For each peak, we fitted the frequency, amplitude, and phase and then subtracted the fit from the original lightcurve. We then fitted a second frequency to the altered data, choosing in every case the largest remaining peak, and used the result of this fit to conduct a simultaneous least squares fit to the original data. Thus at each step in the

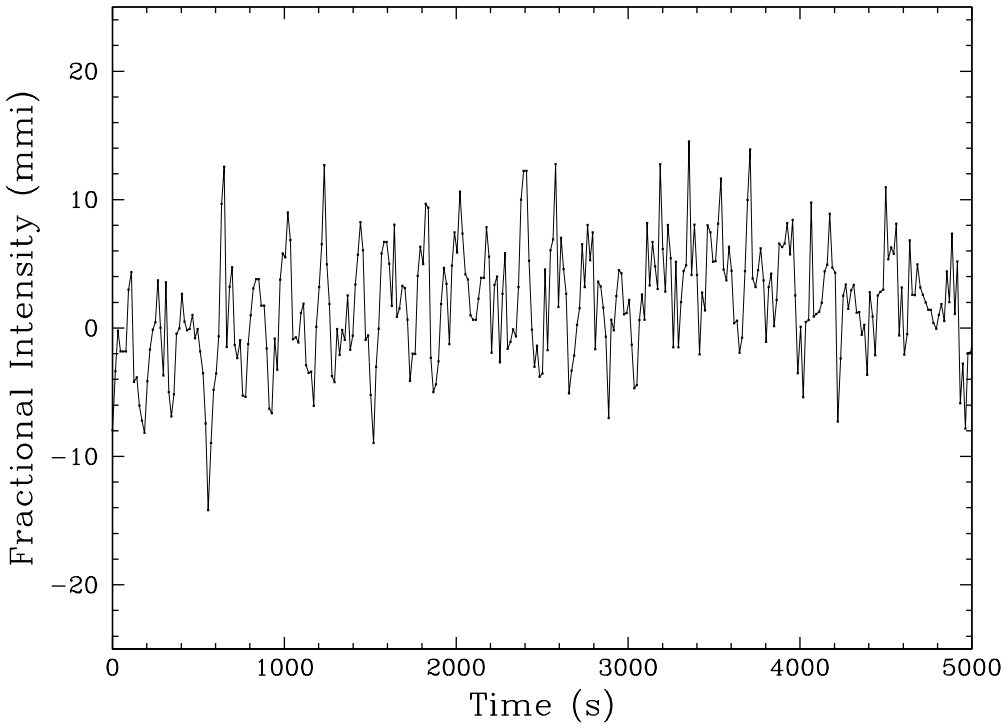

Figure 4.4: Lightcurve of L19-2 (SOAR Telescope observations). These data were acquired with the Goodman Spectrograph on the SOAR 4.1 m Telescope with an exposure time of 10 s.

prewhitening, the frequencies removed are from a simultaneous fit to the original data. Only two modes in the FT of these data actually show multiplet structure, F1 and F3. We did not detect harmonics and combination frequencies in these data. The five dominant pulsation modes (F1 - F5) and associated power derived from prewhitening are listed in Table 4.2 and presented visually in Figure 4.6. The four highest amplitude modes and associated multiplet structure are consistent to within 2 μHz of those found in both the WET data set in Table 3.7 and the modes found by O'Donoghue & Warner (1982).[11] Figure 4.6 shows clearly that the lowest amplitude mode, F5, is ~ 30 μHz from the expected frequency. However, the F5 mode is only two times as large as the background. The fre-

[11]However, O'Donoghue & Warner (1982) did not identify the $m = +1$ member of the F3 multiplet.

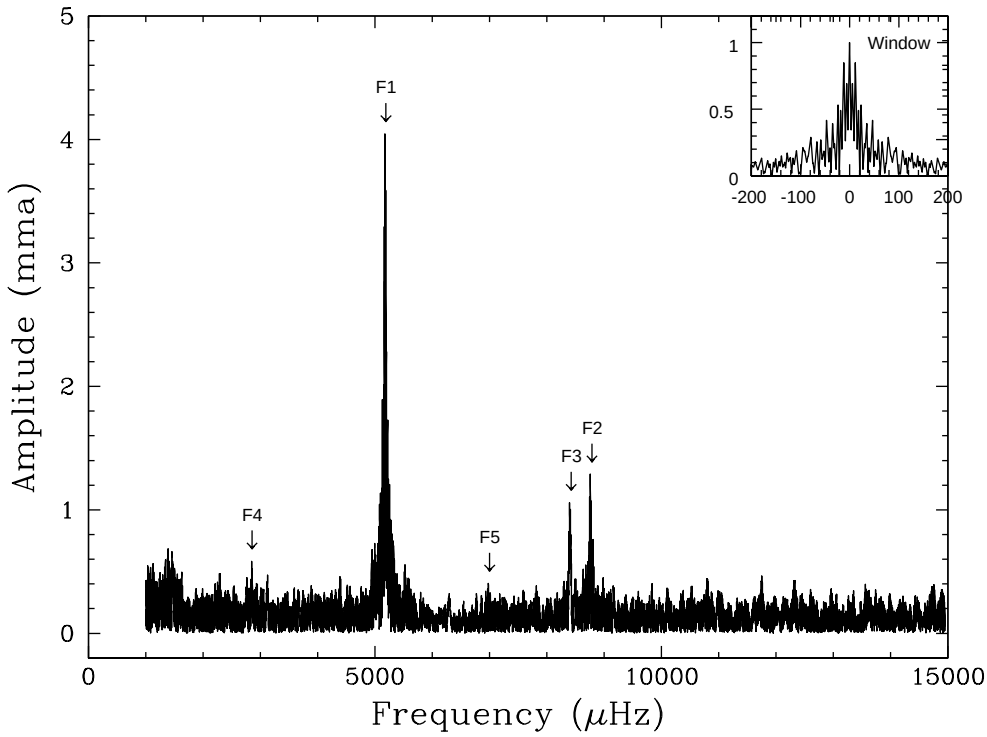

Figure 4.5: Fourier transform of L19-2 (SOAR Telescope observations). This FT includes all individual nights of the data that are listed in Table 4.1. We indicate the five pulsation modes that we reference in Table 4.2. The window function, in the top right of the figure, is the FT of a lightcurve of a sinusoid that has been sampled in the same manner as the original data.

quency of such a small signal is pulled by the presence of unresolved noise peaks.

4.2.3 Mode Identification

Measuring the limits for the harmonics and combination frequencies in L19-2 allows us to calculate the ratio of combination to parent mode amplitudes and compare it to the theoretical predictions (R_c, see equation 2.9). Figure 4.7 shows the observed limit of R_c for the harmonics and combination frequencies. We have plotted a limit equal to the 1 σ noise level in the FT. The observed R_c do not depend on any theory.

The theoretical calculations of R_c require that we supply an inclination esti-

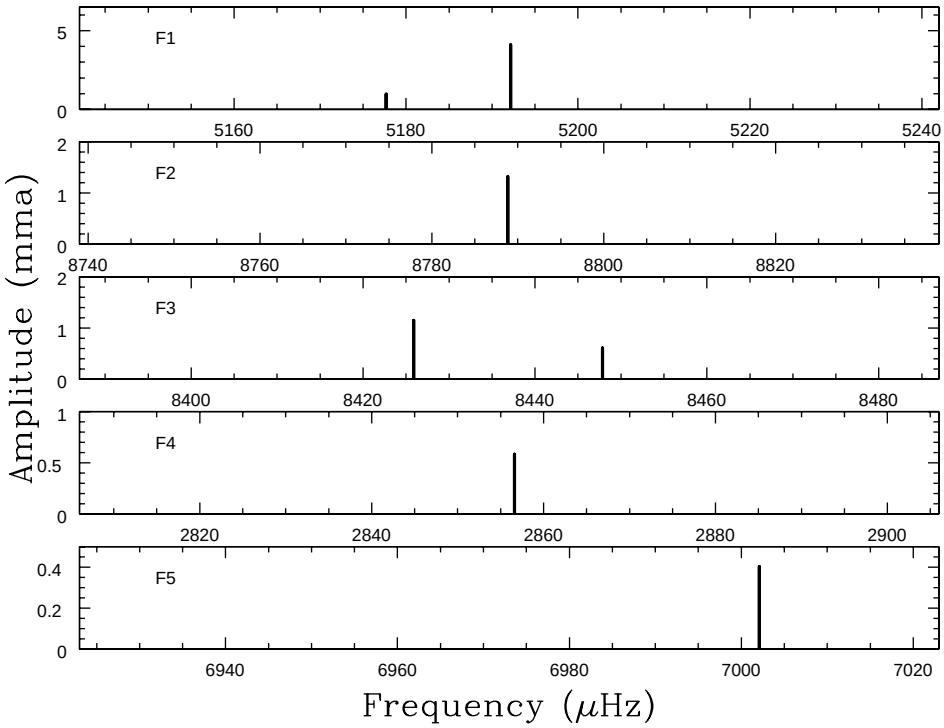

Figure 4.6: Prewhitened peaks in L19-2 Fourier transform (SOAR Telescope observations). The scale of this figure is the same as Figure 3.20 in Chapter 3 for ease in direct comparison between these data and the WET data.

mate, an estimate of τ_{c_0}, and a value for the parameter $2\beta + \gamma$. To be consistent with our previous analysis of L19-2, we have used $\Theta_0 = 16°$ for all of the theoretical calculations, which is the value determined in Chapter 3 using the technique of Pesnell (1985). The end result, R_c, is not very sensitive to this parameter as long as $\Theta_0 \leq 25°$ (see Figure 2.4). For τ_{c_0}, we have used the value of 350 s, which is the longest period mode in L19-2. This value only affects the location of the frequency roll-off, not the predicted combination frequency amplitudes in the high frequency limit. Finally, we use $2\beta + \gamma = -9.35$, which is the value that we found in Chapter 3 by normalizing the parameter for the hot, low-amplitude ZZ Ceti stars.

The theoretical lines for same-ℓ combinations are well-separated, suggesting that harmonics, which are same-ℓ by definition, are better able to constrain ℓ

Table 4.2: L19-2 Periods and Mode Identifications (SOAR Telescope Observations)

Mode Label	Frequency (μHz)	Period (sec)	σ_p (sec)	Amplitude (mma)	σ_{amp} (mma)	ℓ	m^a
F1	5177.694	193.1362	0.0180	0.97	0.15	1	-1
	5192.179	192.5973	0.0042	4.09	0.15	1	0
F2	8788.823	113.7809	0.0032	1.32	0.15	1 or 2	0
F3	8425.901	118.6817	0.0067	1.15	0.16	1 or 2	-1
	8447.857	118.3732	0.0126	0.61	0.16	1 or 2	+1
F4	2856.599	350.0666	0.0691	0.58	0.16	≤ 3	0
F5	7002.105	142.8142	0.0166	0.40	0.16	≤ 3	0

[a]The m identifications in the table are based on the frequency splitting alone, not on the size of the combination peaks.

when cross combinations cannot. The limit on the harmonic of F1 is only consistent with $\ell = 1$, while the limits for the harmonics of F2 and F3 are consistent with $\ell = 1$ or $\ell = 2$. These results are consistent with our analysis of the WET L19-2 data set in Chapter 3, and with how Bradley (2001) identified them based on the multiplet structure. The limits for the harmonics of F4 and F5 constrain these modes to be $\ell \leq 3$. The m identifications we assigned in Table 4.2 arise from frequency splitting only, and are not derived from combination frequency amplitudes.

4.3 Conclusions

We acquired 8.13 hours of time-series photometry data on L19-2 in 2005 May at the SOAR Telescope. We compared these data with the analytical predictions of Wu (2001) by calculating the ratio of combination frequency to parent mode amplitudes. These new data confirm conclusions from Chapter 3 that $\ell = 1$ for

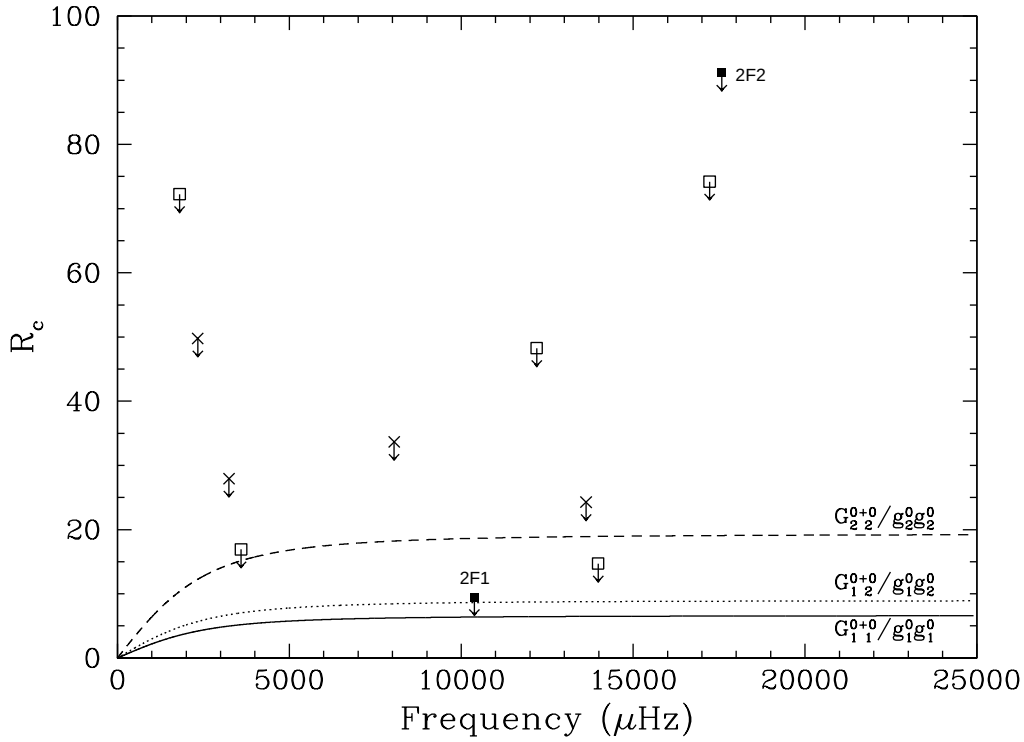

Figure 4.7: Ratio of combination to parent mode amplitudes (R_c) for L19-2 (SOAR Telescope observations). The lines are theoretical predictions for $G^{0+0}_{1\ 1}/g^0_1g^0_1(\Theta_0 = 16°)$ (solid line), $G^{0+0}_{1\ 2}/g^0_1g^0_2(\Theta_0 = 16°)$ (dotted line), and $G^{0+0}_{2\ 2}/g^0_2g^0_2(\Theta_0 = 16°)$ (dashed line). The data points are the limits on the harmonics (filled squares) and limits for the cross combinations for the presumed (Bradley, 2001) $\ell = 1, 1$ combinations (crosses) and $\ell = 1, 2$ combinations (open squares). The downward arrows on the limits indicate that the points represent maximum values.

F1 and $\ell = 1$ or $\ell = 2$ for F2 and F3, consistent with the previous seismological analysis of Bradley (2001).

It is unfortunate that we were not able to lower the L19-2 noise level with our 4 m class telescope. The signal to noise ratio (S/N) for the WET data from Chapter 3 is twice the S/N of the SOAR data presented in this chapter. Although the SOAR 4.1 m Telescope collects photons sixteen times faster than the WET 1 m class telescopes, we observed L19-2 for ~ 8 hours with the SOAR Telescope, which is insufficient to reduce the noise level when compared with the ~ 142 hours of data in the WET data set. The noise level goes down as the square root

of the number of data points, which is linearly related to the amount of time spanned by the observations. Increasing our observation time by four times (to 32 hours) would equate the noise level to the WET data set. Decreasing the WET noise level over the course of our five night observing run was an achievable goal, had the weather and other factors cooperated. However, the primary purpose of acquiring these data was to give the author further observational experience. Most importantly, we have accumulated the skills necessary to take raw data and extract useful information from it.

This chapter also verifies that this method for mode identification can be applied to pulsating white dwarf stars with relatively little effort as a first check on mode identifications. The first application of this method is to quickly discriminate between modes with $\ell > 2$ and those with $\ell \leq 2$. For modes with sufficiently high amplitude, the amplitudes of their harmonics allow further differentiation between $\ell = 1$ and $\ell = 2$ modes. Harmonics are known to be same-ℓ combinations, and the theoretical predictions for same-ℓ combinations are well separated in the theory of Wu (2001).

Chapter 5

Photometric Mode Identification for the DBV EC 20058-5234

Dr. Peter Venkman: *Ray, pretend for a moment that I don't know anything about metallurgy, engineering, or physics, and just tell me what is going on.*

Dr. Ray Stantz: *You never studied.*

— Ghostbusters

5.1 Introduction

EC 20058-5234 is one of the brightest members of the DBV group of pulsating stars. Koen et al. (1995) reported the discovery of the variability of EC 20058-5234 finding eight periodicities, including combination frequencies. EC 20058-5234 is a low-amplitude DBV with stable pulsation modes (Sullivan & Sullivan, 2000). Beauchamp et al. (1999) present optical spectra of EC 20058-5234, providing $T_{eff} \sim 28,000$ K and $\log g \sim 7.8$, though the errors are large due to instrumental problems with the detector used for the observations. In 1997 July, EC 20058-5234 was the secondary target star of the WET campaign XCov 15, on which Sullivan & Sullivan (2000) and Sullivan (2005) have presented pre-

liminary papers. The spectra of DB white dwarf stars are dominated by strong He I lines. The DBV instability strip is centered on 25,000 K and its existence was theoretically predicted by Winget et al. (1982a) before the discovery of the first DBV.

In this chapter, we will present our analysis of the pulsation modes using the combination frequencies amplitudes of the DBV EC 20058-5234. The theory of Wu (2001) provides approximate expressions for the size of combination frequencies that depend upon the frequency, amplitude, and spherical harmonic indices of the parent modes. We use the relative amplitudes of the combination frequencies to infer the spherical harmonic indices of their parent modes. In §5.2, we present the data. In §5.3, we describe our analysis and resultant mode identifications for EC 20058-5234. We summarize our results in §5.4.

5.2 Data

The data for EC 20058-5234 were obtained as the secondary target for the WET campaign XCov 15 in 1997 July (for further information see Sullivan, 2005). Table 5.1 include data from this WET run, as well as further observations acquired after 1997 as discussed in Sullivan (2005). In addition to interesting measurements of the plasmon neutrino flux, these data are being used for an asteroseismological analysis on this star. These data have been provided by D. Sullivan (2006, private communication) and we have performed our mode identification method to help facilitate the asteroseismology.

5.3 Mode Identification

Gathering the amplitudes for the harmonics and combination frequencies in EC 20058-5234 allows us to calculate the ratio of combination to parent mode amplitudes and compare it to the theoretical predictions (R_c, see Equation 2.9).

Table 5.1: EC 20058-5234 Periods and Mode Identifications

Mode Label[a]	Frequency (μHz)	Period (s)	Amplitude (mma)	Combination?	ℓ	R_c
f_1	1852.6	539.8	2.0		1 or 2	
f_2	1903.5	525.4	1.9		1 or 2	
f_3	2852.4	350.6	1.4		1 or 2	
f_4	2998.7	333.5	3.0		1 or 2	
f_5	3488.9	286.6	1.7			
f_6	3559.0	281.0	8.5		1	
f_7	3640.3	274.7	1.0			
f_8	3893.2	256.9	8.4		1?	
f_9	4887.8	204.6	2.7		1 or 2	
f_{10}	4902.2	204.0	1.7	f_2+f_4		149.12
f_{11}	5128.6	195.0	2.5		1 or 2	
f_{12}	6557.6	152.5	0.6	f_6+f_4		11.76
f_{13}	7452.2	134.2	1.7	f_6+f_8		11.90
f_{14}	9021.7	110.8	0.9	f_8+f_{11}		21.43
f_{15}	10030.7	99.7	0.7	$f_2+f_4+f_{11}$		
f_{16}	4816.8	207.6	0.7		≤ 3	
f_{17}	3924.2	254.8	0.5	?	≤ 3	
a	5462.5		$\sim$0.5	f_6+f_2		15.48
b	5745.8		$\sim$0.3	f_8+f_1		8.93
c	6745.6		$\sim$0.5	f_8+f_3		21.26
d	7118.0		$\sim$0.5	$2f_6$		6.92
e	7533.5		$\sim$0.4	f_8+f_7		23.81
f	8127.3		$\sim$0.5	f_4+f_{11}		33.33
g	8446.8		$\sim$0.5	f_6+f_9		10.89
h	8461.2		$\sim$0.6	$f_6+f_2+f_4$		
i	8781.0		0.6	f_8+f_9		13.23

Note. − These data are primarily from the WET campaign XCov 15 and are provided courtesy of D. Sullivan (2006, private communication).

[a]For simplicity, we have retained the mode labeling system of D. Sullivan (2006, private communication). Modes f_5, f_6, and f_7 are believed to be members of a rotationally split triplet centered on f_6.

Figure 5.1 shows the measured R_c for the harmonics and combination frequencies. For the non-detected harmonics, we have plotted a limit approximately equal to the 1 σ noise level in the FT. The observed R_c do not depend on any theory.

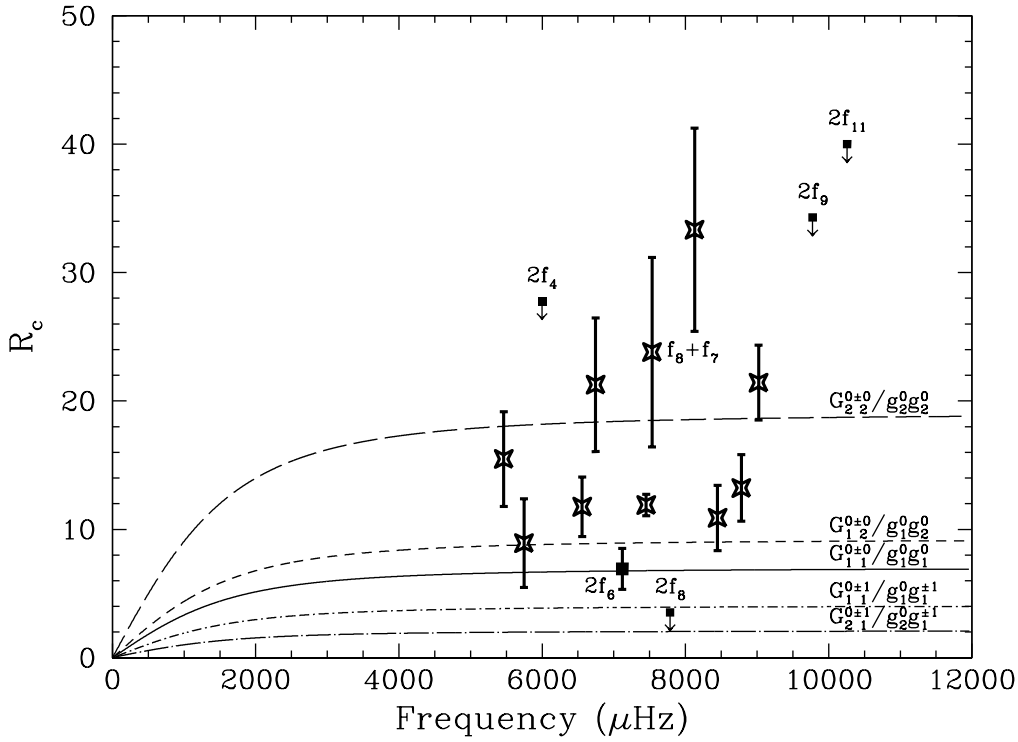

Figure 5.1: Ratio of combination to parent mode amplitudes (R_c) for EC 20058-5234. The lines are theoretical predictions for $G^{0\pm1}_{2\ 1}/g^0_2 g^{\pm1}_1(\Theta_0 = 13°)$ (dot-long-dashed line), $G^{0\pm1}_{1\ 1}/g^0_1 g^{\pm1}_1(\Theta_0 = 13°)$ (dot-dashed line), $G^{0\pm0}_{1\ 1}/g^0_1 g^0_1(\Theta_0 = 13°)$ (solid line), $G^{0\pm0}_{1\ 2}/g^0_1 g^0_2(\Theta_0 = 13°)$ (dashed line), and $G^{0\pm0}_{2\ 2}/g^0_2 g^0_2(\Theta_0 = 13°)$ (long-dashed line). The data points are the detected harmonics or limits (filled squares) and detected cross combination frequencies (stars). The downward arrows on the limits indicate that the points represent maximum values.

The theoretical calculations of R_c require that we supply an inclination estimate, an estimate of τ_{c0}, and a value for the parameter $2\beta + \gamma$. We have used $\Theta_0 = 13°$ for the inclination of this star for all of the theoretical calculations. We calculate this value by applying the technique of Pesnell (1985) to the rotationally split triplet f_5, f_6, and f_7 centered on f_6. The end result, R_c, is not very sensitive to this parameter as long as $\Theta_0 \leq 25°$ (see Figure 2.4). For τ_{c0}, we have

used the value of 539.8 s, which is the longest period mode in EC 20058-5234. This value only affects the location of the frequency roll-off, not the predicted combination frequency amplitudes in the high frequency limit. Finally, we use $2\beta + \gamma = -10$, which is the value that Wu (2001) uses for the DBV GD 358.

The theoretical lines for same-ℓ combinations are well-separated, suggesting that harmonics, which are same-ℓ by definition, are better able to constrain ℓ when cross combinations cannot. The harmonic of f_6 and the limit on the harmonic of f_8, the two highest amplitude modes, are only consistent with $\ell = 1$. However, two modes this closely space in period (only 24 s apart) are not expected to have the same ℓ. Indeed, Sullivan expects f_8 to be an $\ell = 2$ mode. We hoped that the combination of f_8 with f_7, the proposed $m = +1$ member of the f_6 triplet, would reveal more information about the ℓ of f_8, but it falls well above the predictions for an $\ell = 1$ or 2, $m = 0$ mode with an $\ell = 1$, $m = +1$ mode. However, all other detected cross combination frequencies involving f_8 are consistent with $\ell = 2$ for that mode. The limits on the harmonics of modes f_1, f_2, f_3, f_4, f_9, and f_{11} reveal that they are either $\ell = 1$ or 2 modes. After close inspection of Figure 5.1, one may be moved upon to say there is a distinct separation between combination frequencies with R_c clustered around the $\ell = 2, 2$ line and those clustered around the $\ell = 1, 1$ and $\ell = 1, 2$ lines. If this is genuine, f_2, f_3, f_4, and f_{11} may be further constrained to be $\ell = 2$ modes.

5.4 Conclusions

We have performed our mode identification method on the DBV EC 20058-5234. We have constrained the highest amplitude mode to be $\ell = 1$. We tentatively identify the second highest amplitude mode as $\ell = 1$, with some reservation. We constrain six other modes to be $\ell \leq 2$ based on the limits of their harmonics. Two low amplitude modes are found to be $\ell \leq 3$. These results will be valuable to the current asteroseismological analysis being performed on this

star.

The most important result of this chapter is the proof that this method serves as a quick and uncomplicated technique for mode identification for both DAV and DBV stars. The first application of this method is to quickly discriminate between modes with $\ell > 2$ and those with $\ell \leq 2$. For modes with sufficiently high amplitude, the amplitudes of their harmonics allow further differentiation between $\ell = 1$ and $\ell = 2$ modes. Harmonics are known to be same-ℓ combinations, and the theoretical predictions for same-ℓ combinations are well separated in the theory of Wu (2001).

Chapter 6

Summary and Conclusions

Dr. Ray Stantz: *Personally, I liked the university. They gave us money and facilities, we didn't have to produce anything! You've never been out of college! You don't know what it's like out there! I've* worked *in the private sector. They expect* results.
— Ghostbusters

Asteroseismology is a promising tool for using stellar pulsations to understand the interiors of white dwarf stars. In practice, we perform a normal-mode analysis by matching all observed frequencies to theoretical models for white dwarf interiors and determine which model best fits the observed periods. Because instability is believed to be an evolutionary stage for white dwarf stars (cf. Fontaine et al., 1982; Mukadam et al., 2004a), we apply the information gleaned from this normal-mode analysis to all white dwarf stars with the same mass, pulsating and non-pulsating white dwarf stars alike. Asteroseismology teaches us about the interiors of white dwarf stars and we apply this information to determine the age of the galaxy (both the disc and the halo), to formulate models for nuclear fusion, and to probe into the crystallization of white dwarf star cores as they cool. An accurate understanding for all of these interesting topics is only possible with correct asteroseismological analyses for pulsating white dwarf stars.

All of asteroseismology depends upon the accurate pulsation mode identification of the radial overtone number, k, and the spherical harmonic quantum numbers, ℓ and m, for each individual pulsation mode.

Historically, there are very few seismological studies on white dwarf stars. Without correct identification of ℓ for pulsation modes, there are too many theoretical models to fit to the observed period spectra of white dwarf stars. There are at least three observational methods for mode identification. The first two methods require either time-resolved spectroscopy with very large aperture optical telescopes (i.e., Keck, Clemens et al., 2000; Thompson et al., 2004) or time-series photometry in the optical and UV wavelengths with the HST (Robinson et al., 1995). These methods are time intensive and expensive. The intrinsically faint white dwarf stars require large aperture telescopes for these methods. However, the follow-up photometry of ZZ Ceti candidates from the Sloan Digital Sky Survey (SDSS) is finding large numbers of these pulsators that will be too faint for practical time-resolved spectroscopic methods (see Mukadam et al., 2004b; Mullally et al., 2005). We have determined a quick and inexpensive method for confidently assigning values of the spherical degree (ℓ) and azimuthal order (m) to individual eigenfrequencies. The method that we propose only requires time-series photometry on 4 m class telescopes for the faint SDSS ZZ Ceti stars. We use the size of the nonlinearities in the observed lightcurves to infer ℓ and m for the eigenmodes. The method that we discuss in this dissertation can be quickly applied to large samples of stars and provide the results necessary for asteroseismological analysis. We have demonstrated that the technique works on both DAV and DBV white dwarf stars and we have provided a routine for future application on objects.

The Fourier transforms (FTs) of DAV and DBV lightcurves generally show power at harmonics and at sum and difference frequencies. These "combination frequencies" are not in general the result of independent pulsation eigenmodes, but rather of frequency mixing between eigenmodes (Brickhill, 1992b; Goldreich

& Wu, 1999; Ising & Koester, 2001, BFW95). Wu (2001) was able to derive approximate expressions for the size of combination frequencies that depend upon the frequency, amplitude, and spherical harmonic indices of the parent modes, and upon the inclination of the star's pulsation axis to our line of sight. Her solutions yield physical insight into the problem, and make predictions for individual stars straightforward to calculate. The routine that we present for mode identification will significantly help asteroseismological analyses.

We have provided a detailed explanation of the analytical calculations of Wu (2001) in Chapter 2. We discussed our method for estimating the inclination of the stars' pulsation axes to the observer's line of sight. In Chapter 2, we lay out a framework for using the theory of Wu (2001) for mode identification. In Chapters 3 through 5, we have applied this theory to observations of pulsating white dwarf stars. We have presented the data for each star individually and compared the observed amplitudes with the predictions from the equations of Wu (2001), finding good correspondence between the observations and theory. In the following sections, we summarize the important achievements of this dissertation.

6.1 Harmonics Are the Key

The main result of this dissertation is that combination frequencies, particularly harmonics, in the lightcurves of hot ZZ Ceti stars can be used along with the theory of Wu (2001) to constrain and in many cases to determine uniquely the spherical harmonic index (ℓ) of the modes that produced them. The first and easiest result to achieve with this method is to identify those modes with $\ell > 2$ and those with $\ell \leq 2$. This alone is useful for significantly reducing the number of seismological models that need to be considered for a given star (Bradley, 1996). The theoretical mode spectrum at $\ell = 3$ and higher is so dense that there are many possible model fits to the typically sparse number of detected modes. By eliminating from consideration the high ℓ modes, the possibility of identifying

a unique fit is improved.

For modes with sufficiently large amplitude, combination frequency amplitudes are further able to discriminate between $\ell = 1$ and $\ell = 2$, primarily through the use of harmonics. The harmonics are superior for this purpose because they are known to be same-ℓ combinations, and because same-ℓ combinations are well-separated in the theoretical plots of R_c.

The method we have used requires only time-series photometry and simple calculations as presented in Chapter 2. The essential part of these calculations is the evaluation of the geometric term in the theory of Wu (2001), which we have named $\mathcal{G}$. Calculating $\mathcal{G}$ requires the evaluation of integrals of spherical harmonics in the presence of a limb darkening law. To assist others in application of this technique, we have included tabulated matrices of combination frequency integrals for $\ell \leq 4$ in Appendix A. Applying these requires a straightforward estimation of the inclination, which we have done using multiplet amplitudes, where detected, and limits on the sizes of multiplet members where not detected. This has required that we assume that modes of every m are excited to the same amplitude in every mode, and that rotation always removes the frequency degeneracy of multiplet members. Fortunately, our results are not highly sensitive to these assumptions.

For convenience, we summarize application of the method as follows:

1. Calculate the inclination with the Pesnell (1985) method using the ratio of the observed amplitudes in a given multiplet. Consult the sensitivity of $\mathcal{G}$ to inclination (see Figures 2.3, 2.4, and A.1) to ensure that R_c is changing slowly with inclination near this value.

2. Calculate the theoretical R_c for both $\ell = 1$ and 2 by approximating τ_{c_0} with the longest period mode and using the bolometric correction $\alpha_\lambda = 0.4$. We use $2\beta + \gamma = -9.35$ for hot, low-amplitude DA stars, while Wu (2001) uses $2\beta + \gamma = -10$ for the cool DA star G29-38.

3. Compare the calculated R_c with the measured value obtained with the am-

plitudes of the combinations and their parents.

6.2 Verification of the Theory of Yanqin Wu

Through our analysis, we have shown that the theory of Wu (2001) provides the only available analytical predictions for combination frequencies that are consistent with the amplitudes we measure. An entirely different model for explaining combination frequencies was proposed by BFW95. The BFW95 theory invokes the nonlinear response of the radiative atmosphere, ignoring the changes to the surface convection zone. We have shown that, in general, even for the low amplitude pulsators, the BFW95 theory underestimates the sizes of combination frequencies in *most* ZZ Ceti stars by an order of magnitude or more and that they will be smaller than in the theory of Wu (2001) (for the same ℓ). Moreover, without very precise temperature measurements, the temperature sensitivity of the BFW95 theory makes mode identification problematic if the BFW95 theory is correct. In addition, the BFW95 theory predicts that the size of the individual combination frequencies is independent of the pulsation frequency in any single star, unlike the theory of Wu (2001), so, contrary to observational evidence, low frequency difference modes are not suppressed in the BFW95 theory.

Moreover, the theory of Goldreich & Wu (1999) (founded on the theory of Brickhill (1992b)) implicitly contains a mode driving mechanism different from that originally proposed for the DAV stars. Verification of the analytical predictions of Wu (2001) supports the convective driving mechanism as the source of pulsations in DAV stars.

6.3 New Fourier Transforms for GD 66, GD 244, and L19-2

In Chapter 3, we presented independent analyses of new data on the DAV white dwarf stars GD 66 and GD 244 that will be useful for seismological study of these objects. There are few published lightcurves and FTs for these two stars and their period spectra were previously uncertain. The mode periods we have measured and published are given in Tables 3.4 and 3.5 for comparison to seismological models. Additionally, we have identified the ℓ values for each mode to facilitate the seismological analyses. This is important because without correct identification of ℓ for pulsation modes, there are too many theoretical models to fit the observed period spectra of white dwarf stars. By identifying the ℓ for each mode, we have helped to preemptively exclude incorrect seismological models.

We identified five independent pulsations modes and nine combination frequencies for GD 66. We found that the four highest amplitude modes are only consistent with a mode identification of $\ell = 1$. We constrained the lowest amplitude mode to be $\ell \leq 2$. We identified four independent pulsation modes and six combination frequencies for GD 244. The three highest amplitude pulsation modes are consistent with $\ell = 1$ and the lowest amplitude mode has $\ell \leq 3$.

We have presented new reductions for archival Whole Earth Telescope (WET) data for L19-2, summarized in Table 3.7. The complete reduction for these data are previously unpublished (for preliminary results, see Sullivan, 1995), though Bradley (2001) has conducted a seismological analysis on these data. Our mode identification results are consistent with how Bradley (2001) identified the L19-2 modes based on their multiplet structure. We identified five independent pulsation modes and did not detect combination frequencies in L19-2. Because we were unable to use measured amplitudes of combination frequencies for our analysis, we included the observed noise limit as an upper bound for comparison to theory. We found the highest amplitude mode to be $\ell = 1$, the three intermedi-

ate amplitude modes to be $\ell \leq 2$, and the lowest amplitude mode to be $\ell \leq 3$. It is gratifying to find that non-detections of combination frequencies can provide useful seismological information, and that these corroborate independent methods in the case of L19-2.

6.4 Mode Identification for Published Data

In Chapter 3, we identified modes for five DAV white dwarf stars using published data. G117-B15A and G185-32 have detectable combination frequencies, while GD 165, R548, and G226-29 do not. We were able to identify modes as $\ell = 1$ in four of the five stars, and in every case our identifications agreed with any previous independent results, making those ℓ identifications certain. With the exception of a few small amplitude modes, we have successfully eliminated $\ell > 2$ identification for all modes in four of the five stars. The fifth star, G185-32, was previously thought to have a high ℓ mode (Thompson et al., 2004), and our method confirms this result (though we get $\ell = 3$ instead of $\ell = 4$). The details of the mode identification for these published data are found in Tables 3.6 and 3.8.

6.5 An Expedition to Cerro Pachon

We acquired 8.13 hours of time-series photometry data on L19-2 in 2005 May at the SOAR Telescope using the Goodman Spectrograph and presented this information in Chapter 4. These new data confirm conclusions from Chapter 3 that $\ell = 1$ for the highest amplitude mode and $\ell = 1$ or $\ell = 2$ for the next two highest amplitude modes (the full results are listed in Table 4.2). This chapter verified that this mode identification method can be applied to pulsating white dwarf stars with relatively little effort as a first check on mode identifications. These observations have paved the way for further mode identification investigations at

the SOAR Telescope.

At the time of our observations, the dewar and detector for the Goodman Spectrograph were not ready for use. We designed and built an attachment for a temporary Apogee AP10 CCD camera allowing us to use it with the Goodman Spectrograph. We designed and built this attachment to house the CCD camera and mate with the Goodman Spectrograph.

6.6 Applicable to DAV and DBV Stars

In Chapter 5, we included an analysis of the DBV star EC 20058-5234 to demonstrate that the method is widely and easily applicable to all pulsating white dwarf stars. We constrained the two highest amplitude modes to be $\ell = 1$ and six other modes to be $\ell = 1$ or 2 (see Table 5.1). These mode identifications will be useful for an ongoing seismological analysis of this star.

6.7 Future Application

The pulsations of white dwarf stars equip us with a means of delving in to the unseen interiors of white dwarf stars, similar to the seismologists who use earthquakes to understand the internal layers of the Earth. This dissertation describes an important step forward for asteroseismologists, presenting a simplified method for identifying individual pulsation modes in these stars that utilizes the size of the nonlinearities present in the lightcurves of pulsating white dwarf stars. Without identifying ℓ for each individual pulsation mode, we are unable to unlock the secrets of the white dwarf stellar interiors.

We have presented a quick and inexpensive method for confidently assigning values of ℓ and m to individual eigenfrequencies in pulsating white dwarf stars using straightforward calculations. This method can be quickly applied to large samples of stars. The follow-up photometry from the SDSS is providing large

numbers of ZZ Ceti stars that are simply too faint for practical time-resolved spectroscopic mode identification analysis. Fortunately, these new ZZ Ceti stars are an immediate source for further application of our new mode identification method, easily applied with 4 m telescopes. This will provide an order of magnitude increase of stars for immediate seismological analyses.

Appendix A

Selected Solutions for $G_{\ell_i\ \ell_j}^{m_i \pm m_j} / g_{\ell_i}^{m_i} g_{\ell_j}^{m_j}(\Theta_\circ)$

The following tables contain solutions for $G_{\ell_i\ \ell_j}^{m_i \pm m_j} / g_{\ell_i}^{m_i} g_{\ell_j}^{m_j}(\Theta_\circ)$ (see equations 2.4, 2.5, and 2.9) for the values of ℓ and m that are potentially useful for mode identification with photometry using the theory of Wu (2001).[12] Table A.1 contains solutions for $\ell_i = \ell_j = 1$. Tables A.2 and A.3 contain solutions for $\ell_i = 1$, $\ell_j = 2$ and $\ell_i = \ell_j = 2$. Finally, Table A.4 contains solutions for $\ell_i = 3$ or 4 and $\ell_j \leq 4$ with $m_i = m_j = 0$. For comparison with Figures 2.3 and 2.4, we include a plot of the variations of $\mathcal{G}$ with inclination for $\ell = 3, 3$ and $\ell = 4, 4$ in Figure A.1.

[12]This appendix was originally published as Appendix A of Yeates et al. (2005) and is reproduced by permission of the AAS.

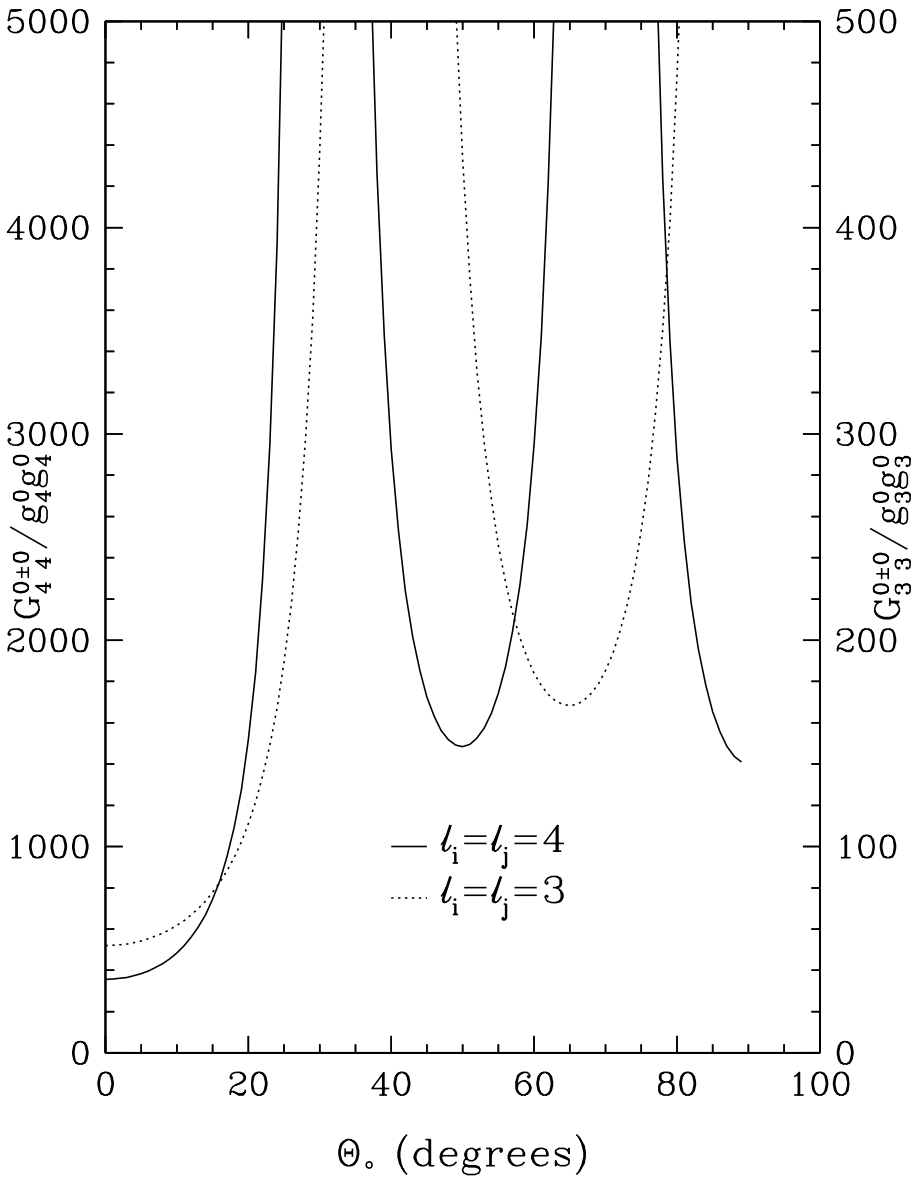

Figure A.1: $\mathcal{G}$ with $m_i = m_j = 0$ (see equation 2.9) plotted as a function of inclination angle ($\Theta_\circ$). The scale of $\mathcal{G}$ for $\ell_i = \ell_j = 4$ (solid line) is a factor of ten larger than the scale of $\mathcal{G}$ for $\ell_i = \ell_j = 3$ (dotted line). The predicted amplitudes of the combination frequencies show a dramatic increase for inclinations greater than 20°, and the predictions less than 20° increase more rapidly than the cases for $\ell = 1$ and 2 (see Figures 2.3 and 2.4).

Table A.1: Values of $G_{1\ 1}^{m_i+m_j}/g_1^{m_i}g_1^{m_j}(\Theta_\circ)$

$m_i \backslash m_j$	-1	0	+1
-1	0.65	0.65	$-0.65 - \frac{0.90}{\sin^2(\Theta_\circ)}$
0	0.65	$0.65 + \frac{0.45}{\cos^2(\Theta_\circ)}$	-0.65
+1	$-0.65 - \frac{0.90}{\sin^2(\Theta_\circ)}$	-0.65	0.65

Note. − For values of $G_{1\ 1}^{m_i-m_j}/g_1^{m_i}g_1^{m_j}(\Theta_\circ)$, reverse the sign of m_j.

Table A.2: Values of $G_{1\ 2}^{m_i+m_j}/g_1^{m_i}g_2^{m_j}(\Theta_\circ)$

$m_i \backslash m_j$	-2	-1	0	+1	+2
-1	0.27	0.27	$\frac{-0.81\sin^2(\Theta_\circ)-0.58}{3\cos^2(\Theta_\circ)-1}$	$-0.27-\frac{1.12}{\sin^2(\Theta_\circ)}$	$0.27+\frac{2.24}{\sin^2(\Theta_\circ)}$
0	0.27	$0.27+\frac{0.56}{\cos^2(\Theta_\circ)}$	$\frac{0.81\cos^2(\Theta_\circ)+1.97}{3\cos^2(\Theta_\circ)-1}$	$-0.27-\frac{0.56}{\cos^2(\Theta_\circ)}$	0.27
+1	$-0.27-\frac{2.24}{\sin^2(\Theta_\circ)}$	$-0.27-\frac{1.12}{\sin^2(\Theta_\circ)}$	$\frac{0.81\sin^2(\Theta_\circ)+0.58}{3\cos^2(\Theta_\circ)-1}$	0.27	-0.27

Note. − For values of $G_{1\ 2}^{m_i-m_j}/g_1^{m_i}g_2^{m_j}(\Theta_\circ)$, reverse the sign of m_j.

Table A.3: Values of $G_{2\ 2}^{m_i+m_j}/g_2^{m_i}g_2^{m_j}(\Theta_\circ)$

$m_i \backslash m_j$	-2	-1	0	+1	+2
-2	-0.20	-0.20	$\frac{0.59\cos^4(\Theta_\circ)+1.08\cos^2(\Theta_\circ)-1.67}{\sin^2(\Theta_\circ)(3\cos^2(\Theta_\circ)-1)}$	$0.20-\frac{1.87}{\sin^2(\Theta_\circ)}$	$\frac{-0.20\sin^4(\Theta_\circ)+3.74\sin^2(\Theta_\circ)+2.66}{\sin^4(\Theta_\circ)}$
-1	-0.20	$\frac{0.20\cos^4(\Theta_\circ)-0.66\cos^2(\Theta_\circ)+0.47}{\cos^2(\Theta_\circ)\sin^2(\Theta_\circ)}$	$\frac{-0.59\cos^2(\Theta_\circ)+1.13}{3\cos^2(\Theta_\circ)-1}$	$-\frac{0.20\cos^4(\Theta_\circ)+0.27\cos^2(\Theta_\circ)+1.13}{\cos^2(\Theta_\circ)\sin^2(\Theta_\circ)}$	$-0.20+\frac{1.87}{\sin^2(\Theta_\circ)}$
0	$\frac{0.59\cos^4(\Theta_\circ)+1.08\cos^2(\Theta_\circ)-1.67}{\sin^2(\Theta_\circ)(3\cos^2(\Theta_\circ)-1)}$	$\frac{-0.59\cos^2(\Theta_\circ)+1.13}{3\cos^2(\Theta_\circ)-1}$	$\frac{-1.78\cos^4(\Theta_\circ)+6.80\cos^2(\Theta_\circ)+5.66}{(3\cos^2(\Theta_\circ)-1)^2}$	$\frac{0.59\cos^2(\Theta_\circ)-1.13}{3\cos^2(\Theta_\circ)-1}$	$\frac{0.59\cos^4(\Theta_\circ)+1.08\cos^2(\Theta_\circ)-1.67}{\sin^2(\Theta_\circ)(3\cos^2(\Theta_\circ)-1)}$
+1	$0.20-\frac{1.87}{\sin^2(\Theta_\circ)}$	$-\frac{0.20\cos^4(\Theta_\circ)+0.27\cos^2(\Theta_\circ)+1.13}{\cos^2(\Theta_\circ)\sin^2(\Theta_\circ)}$	$\frac{0.59\cos^2(\Theta_\circ)-1.13}{3\cos^2(\Theta_\circ)-1}$	$\frac{0.20\cos^4(\Theta_\circ)-0.66\cos^2(\Theta_\circ)+0.47}{\cos^2(\Theta_\circ)\sin^2(\Theta_\circ)}$	0.20
+2	$\frac{-0.20\sin^4(\Theta_\circ)+3.74\sin^2(\Theta_\circ)+2.66}{\sin^4(\Theta_\circ)}$	$-0.20+\frac{1.87}{\sin^2(\Theta_\circ)}$	$\frac{0.59\cos^4(\Theta_\circ)+1.08\cos^2(\Theta_\circ)-1.67}{\sin^2(\Theta_\circ)(3\cos^2(\Theta_\circ)-1)}$	0.20	-0.20

Note − For values of $G_{2\ 2}^{m_i-m_j}/g_2^{m_i}g_2^{m_j}(\Theta_\circ)$, reverse the sign of m_j.

Table A.4: Values of $G^{0\pm0}_{\ell_i\ \ell_j}/g^0_{\ell_i}g^0_{\ell_j}(\Theta_\circ)$

$\ell_i \backslash \ell_j$	3	4
1	$\frac{-0.78\cos^4(\Theta_\circ)+3.82\cos^2(\Theta_\circ)-1.12}{1.67\cos^4(\Theta_\circ)-\cos^2(\Theta_\circ)}$	$\frac{-6.18\cos^4(\Theta_\circ)+19.41\cos^2(\Theta_\circ)-9}{-11.67\cos^4(\Theta_\circ)+10\cos^2(\Theta_\circ)-1}$
2	$\frac{-1.92\cos^4(\Theta_\circ)+4.87\cos^2(\Theta_\circ)+9.86}{(3\cos^2(\Theta_\circ)-1)(1.67\cos^2(\Theta_\circ)-1)}$	$\frac{40.38\cos^6(\Theta_\circ)-73.72\cos^4(\Theta_\circ)+144.05\cos^2(\Theta_\circ)-39.04}{(3\cos^2(\Theta_\circ)-1)(-11.67\cos^4(\Theta_\circ)+10\cos^2(\Theta_\circ)-1)}$
3	$\frac{5.56\cos^6(\Theta_\circ)-10\cos^4(\Theta_\circ)+15.17\cos^2(\Theta_\circ)+12.40}{(1.67\cos^3(\Theta_\circ)-\cos(\Theta_\circ))^2}$	$\frac{35\cos^6(\Theta_\circ)-75\cos^4(\Theta_\circ)+85\cos^2(\Theta_\circ)+153.69}{(1.67\cos^2(\Theta_\circ)-1)(-11.67\cos^4(\Theta_\circ)+10\cos^2(\Theta_\circ)-1)}$
4	$\frac{35\cos^6(\Theta_\circ)-75\cos^4(\Theta_\circ)+85\cos^2(\Theta_\circ)+153.69}{(1.67\cos^2(\Theta_\circ)-1)(-11.67\cos^4(\Theta_\circ)+10\cos^2(\Theta_\circ)-1)}$	$\frac{-1225\cos^8(\Theta_\circ)+2660\cos^6(\Theta_\circ)-2070\cos^4(\Theta_\circ)+1769.26\cos^2(\Theta_\circ)+1400.80}{(-11.67\cos^4(\Theta_\circ)+10\cos^2(\Theta_\circ)-1)^2}$

REFERENCES

Beauchamp, A., Wesemael, F., Bergeron, P., Fontaine, G., Saffer, R. A., Liebert, J., & Brassard, P. 1999, The Astrophysical Journal, 516, 887

Bergeron, P., Fontaine, G., Billères, M., Boudreault, S., & Green, E. M. 2004, The Astrophysical Journal, 600, 404

Bergeron, P., & McGraw, J. T. 1990, The Astrophysical Journal, Letters to the Editor, 352, L45

Bergeron, P., Saffer, R. A., & Liebert, J. 1992, The Astrophysical Journal, 394, 228

Bergeron, P. et al. 1993, The Astronomical Journal, 106, 1987

Bradley, P. A. 1996, The Astrophysical Journal, 468, 350

—. 1998, The Astrophysical Journal, Supplement Series, 116, 307

—. 2001, The Astrophysical Journal, 552, 326

—. 2006, Memorie della Societa Astronomica Italiana, 77, 437

Brassard, P., Fontaine, G., & Wesemael, F. 1995, The Astrophysical Journal, Supplement Series, 96, 545

Brassard, P., Fontaine, G., Wesemael, F., & Talon, A. 1993, in NATO ASIC Proc. 403: White Dwarfs: Advances in Observation and Theory, ed. M. A. Barstow, (Dordrecht: Kluwer Academic Publishers), 485

Brickhill, A. J. 1983, Monthly Notices of the RAS, 204, 537

—. 1990, Monthly Notices of the RAS, 246, 510

—. 1991a, Monthly Notices of the RAS, 251, 673

—. 1991b, Monthly Notices of the RAS, 252, 334

—. 1992a, Monthly Notices of the RAS, 259, 519

—. 1992b, Monthly Notices of the RAS, 259, 529

Castanheira, B. G. et al. 2004, Astronomy and Astrophysics, 413, 623

Chandrasekhar, S. 1931, The Astrophysical Journal, 74, 81

—. 1934a, The Observatory, 57, 93

—. 1934b, The Observatory, 57, 373

Christensen-Dalsgaard, J. 2002, Reviews of Modern Physics, 74, 1073

Clemens, J. C. 1994, Ph.D. Thesis, Univ. Texas, Austin

Clemens, J. C., Crain, J. A., & Anderson, R. 2004, in Proceedings of the SPIE, 5492: Ground-based Instrumentation for Astronomy, ed. A. F. M. Moorwood & M. Iye, (The International Society for Optical Engineering), 331

Clemens, J. C., van Kerkwijk, M. H., & Wu, Y. 2000, Monthly Notices of the RAS, 314, 220

Crain, J. A., Clemens, J. C., & Bayliss, M. 2004, in Proceedings of the SPIE, 5496: Optical, Infrared, and Millimeter Space Telescopes, ed. H. Lewis & G. Raffi, (The International Society for Optical Engineering), 455

D'Antona, F. 1989, LNP Vol. 328: IAU Colloq. 114: White Dwarfs, 328, (New York: Springer Verlag), 44

Dolez, N., & Vauclair, G. 1981, Astronomy and Astrophysics, 102, 375

Dolez, N., Vauclair, G., & Chevreton, M. 1983, Astronomy and Astrophysics, 121, L23

Dziembowski, W., & Koester, D. 1981, Astronomy and Astrophysics, 97, 16

Finley, D. S., Koester, D., & Basri, G. 1997, The Astrophysical Journal, 488, 375

Fontaine, G., Bergeron, P., Brassard, P., Billères, M., & Charpinet, S. 2001, The Astrophysical Journal, 557, 792

Fontaine, G., McGraw, J. T., Dearborn, D. S. P., Gustafson, J., & Lacombe, P. 1982, The Astrophysical Journal, 258, 651

Fontaine, G., Wesemael, F., Bergeron, P., Lacombe, P., Lamontagne, R., & Saumon, D. 1985, The Astrophysical Journal, 294, 339

Fowler, R. H. 1926, Monthly Notices of the RAS, 87, 114

Goldreich, P., & Wu, Y. 1999, The Astrophysical Journal, 511, 904

Grauer, A. D., & Bond, H. E. 1984, The Astrophysical Journal, 277, 211

Greenstein, J. L. 1976, The Astronomical Journal, 81, 323

—. 1982, The Astrophysical Journal, 258, 661

Holberg, J. B., Barstow, M. A., Bruhweiler, F. C., Cruise, A. M., & Penny, A. J. 1998, The Astrophysical Journal, 497, 935

Horne, J. H., & Baliunas, S. L. 1986, The Astrophysical Journal, 302, 757

Isern, J., García-Berro, E., Hernanz, M., & Mochkovitch, R. 1998, Journal of the Physics of Condensed Matter, 10, 11263

Ising, J., & Koester, D. 2001, Astronomy and Astrophysics, 374, 116

Kawaler, S. D. et al. 1995, The Astrophysical Journal, 450, 350

Kepler, S. O. 1984, The Astrophysical Journal, 286, 314

—. 1993, Baltic Astronomy, 2, 515

Kepler, S. O., Castanheira, B. G., Saraiva, M. F. O., Nitta, A., Kleinman, S. J., Mullally, F., Winget, D. E., & Eisenstein, D. J. 2005, Astronomy and Astrophysics, 442, 629

Kepler, S. O., Mukadam, A., Winget, D. E., Nather, R. E., Metcalfe, T. S., Reed, M. D., Kawaler, S. D., & Bradley, P. A. 2000a, The Astrophysical Journal, Letters to the Editor, 534, L185

Kepler, S. O., Robinson, E. L., Koester, D., Clemens, J. C., Nather, R. E., & Jiang, X. J. 2000b, The Astrophysical Journal, 539, 379

Kepler, S. O., Robinson, E. L., Nather, R. E., & McGraw, J. T. 1982, The Astrophysical Journal, 254, 676

Kepler, S. O. et al. 1995a, The Astrophysical Journal, 447, 874

Kepler, S. O. et al. 1995b, Baltic Astronomy, 4, 221

Kleinman, S. J. 1995, Ph.D. Thesis, Univ. Texas, Austin

Kleinman, S. J. et al. 1998, The Astrophysical Journal, 495, 424

Koen, C., O'Donoghue, D., Stobie, R. S., Kilkenny, D., & Ashley, R. 1995, Monthly Notices of the RAS, 277, 913

Koester, D., Schulz, H., & Weidemann, V. 1979, Astronomy and Astrophysics, 76, 262

Lasker, B. M., & Hesser, J. E. 1971, The Astrophysical Journal, Letters to the Editor, 163, L89+

López-Morales, M., & Clemens, J. C. 2004, Publications of the ASP, 116, 22

Mazzitelli, I., & D'Antona, F. 1986, The Astrophysical Journal, 308, 706

McGraw, J. T. 1977, The Astrophysical Journal, Letters to the Editor, 214, L123

—. 1980, Space Science Reviews, 27, 601

McGraw, J. T., Fontaine, G., Dearborn, D. S. P., Gustafson, J., Starrfield, S. G., & Lacombe, P. 1981, The Astrophysical Journal, 250, 349

McGraw, J. T., & Robinson, E. L. 1976, The Astrophysical Journal, Letters to the Editor, 205, L155

Mestel, L. 1952, Monthly Notices of the RAS, 112, 583

Mukadam, A. S., Winget, D. E., von Hippel, T., Montgomery, M. H., Kepler, S. O., & Costa, A. F. M. 2004a, The Astrophysical Journal, 612, 1052

Mukadam, A. S. et al. 2003, The Astrophysical Journal, 594, 961

—. 2004b, The Astrophysical Journal, 607, 982

Mullally, F., Thompson, S. E., Castanheira, B. G., Winget, D. E., Kepler, S. O., Eisenstein, D. J., Kleinman, S. J., & Nitta, A. 2005, The Astrophysical Journal, 625, 966

Nather, R. E., & Mukadam, A. S. 2004, The Astrophysical Journal, 605, 846

Nather, R. E., Winget, D. E., Clemens, J. C., Hansen, C. J., & Hine, B. P. 1990, The Astrophysical Journal, 361, 309

O'Donoghue, D. E., & Warner, B. 1982, Monthly Notices of the RAS, 200, 563

—. 1987, Monthly Notices of the RAS, 228, 949

Pesnell, W. D. 1985, The Astrophysical Journal, 292, 238

—. 1987, The Astrophysical Journal, 314, 598

Robinson, E. L., Kepler, S. O., & Nather, R. E. 1982, The Astrophysical Journal, 259, 219

Robinson, E. L. et al. 1995, The Astrophysical Journal, 438, 908

Sullivan, D. J. 1995, Baltic Astronomy, 4, 261

—. 2005, in ASP Conf. Ser. 334: 14th European Workshop on White Dwarfs, ed. D. Koester & S. Moehler, (Provo: Astronomical Society of the Pacific), 495

Sullivan, D. J., & Sullivan, T. 2000, Baltic Astronomy, 9, 81

Thompson, S. E., Clemens, J. C., van Kerkwijk, M. H., O'Brien, M. S., & Koester, D. 2004, The Astrophysical Journal, 610, 1001

van Kerkwijk, M. H., Clemens, J. C., & Wu, Y. 2000, Monthly Notices of the RAS, 314, 209

Vauclair, G., Belmonte, J. A., Pfeiffer, B., Chevreton, M., Dolez, N., Motch, C., Werner, K., & Pakull, M. W. 1993, Astronomy and Astrophysics, 267, L35

Vauclair, G. et al. 2002, Astronomy and Astrophysics, 381, 122

Voss, B., Koester, D., Østensen, R., Kepler, S. O., Napiwotzki, R., Homeier, D., & Reimers, D. 2006, Astronomy and Astrophysics, 450, 1061

Vuille, F., & Brassard, P. 2000, Monthly Notices of the RAS, 313, 185

Winget, D. E. 1998, The Journal of the Physics of Condensed Matter, 10, 11247

Winget, D. E., & Fontaine, G. 1982, in Pulsations in Classical and Cataclysmic Variable Stars, ed. J. P. Cox & C. J. Hansen, (Boulder: Univ. Colorado), 46

Winget, D. E., Robinson, E. L., Nather, R. E., & Fontaine, G. 1982b, The Astrophysical Journal, Letters to the Editor, 262, L11

Winget, D. E., van Horn, H. M., & Hansen, C. J. 1981, The Astrophysical Journal, Letters to the Editor, 245, L33

Winget, D. E., van Horn, H. M., Tassoul, M., Hansen, C. J., Fontaine, G., & Carroll, B. W. 1982a, The Astrophysical Journal, Letters to the Editor, 252, L65

Winget, D. E. et al. 1991, The Astrophysical Journal, 378, 326

Wood, M. A. 1990, The Journal of the RAS of Canada, 84, 150

Wu, Y. 2001, Monthly Notices of the RAS, 323, 248

Wu, Y., & Goldreich, P. 1999, The Astrophysical Journal, 519, 783

Yeates, C. M., Clemens, J. C., Thompson, S. E., & Mullally, F. 2005, The Astrophysical Journal, 635, 1239